Master Thesis in Geosciences

Age and origin of the Mesoproterozoic basement of the Nesodden Peninsula, SE Norway

A geochronological and isotopic study

Edina Pózer Bue

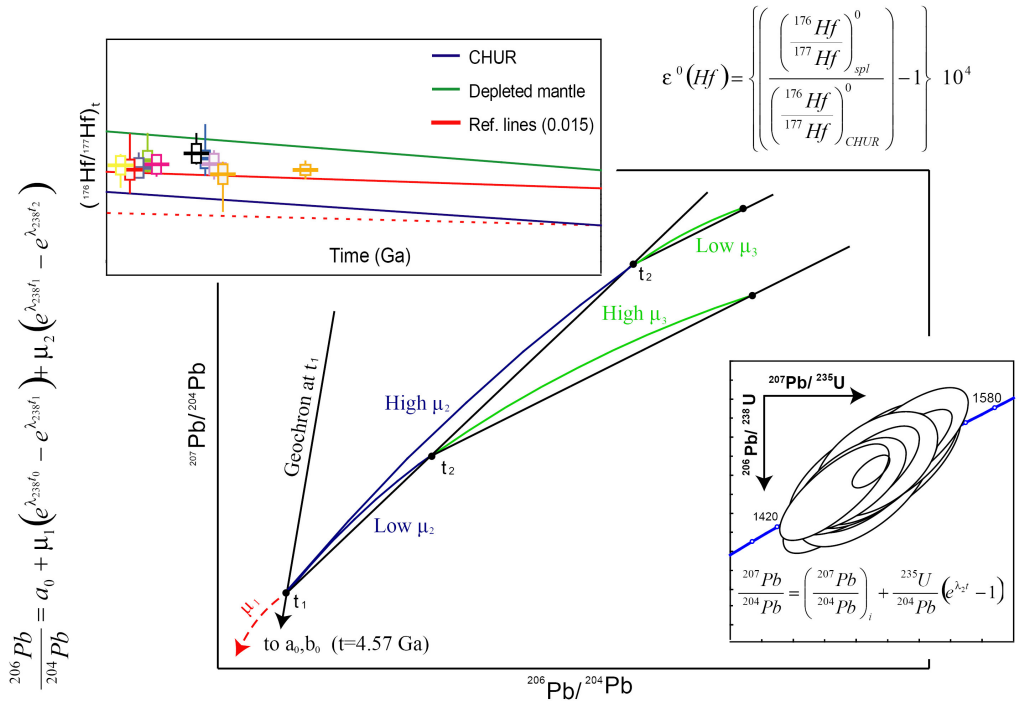

UNIVERSITY OF OSLO

FACULTY OF MATHEMATICS AND NATURAL SCIENCES

Age and origin of the Mesoproterozoic basement of the Nesodden Peninsula, SE Norway

A geochronological and isotopic study

Edina Pózer Bue

Master Thesis in Geosciences
Discipline: Tectonics, petrology and geochemistry
Department of Geosciences
Faculty of Mathematics and Natural Sciences

UNIVERSITY OF OSLO

March 3, 2008

Tutor(s): Tom Andersen

This work is published digitally through DUO – Digitale Utgivelser ved UiO

http://www.duo.uio.no

It is also catalogued in BIBSYS (http://www.bibsys.no/english)

Cover design by A.M. Lundmark & soon to be M.Sc. E. Pózer Bue

Acknowledgements

Writing a Masters thesis is a major undertaking (I know!), and without the support of numerous people it wouldn't have been possible to finish this project. First of all I would like to thank my supervisor Professor Tom Andersen, who has been inspiring and supportive of me since my bachelor years (and that's how I ended up choosing this particular field as my specialty!). He's taught me as much isotope geology as my head can hold, he has been helpful and patient and his door was/is always open when help is needed.

Siri Lene Simonsen has helped me with all the lab work, but she has also been a friend who has always cheered me up at the lab and helped me keep a positive attitude. Thank you, Siri!

Dr Stuart Graham is no longer working here in Norway, but he introduced me to both the mysterious workings of the mass spectrometer and to Australian humour: since the machine doesn't have a brain, I'll try to use my own Stuart, promise!

Numerous dedicated people have helped me with my lab work, special thanks to the ever so helpful Gunborg Bye Fjeld, who has helped me crush so many rocks and gave many useful tips over the years, Berit Løken Berg who has probably imaged more zircons than anyone else on this planet, and still isn't tired of helping out with CL and BSE on the SEM, Tulio Benites has helped me with thinsections, as have Salahalldin Akhavan when I was in desperate need in the final days of my thesis. I thank Jarkko T. Lamminen, Mofak Said Naoroz, Dr Rune S. Selbekk and the Natural History Museum, Oslo, for providing geological material.

I must also thank my dear friends at the institute, Marie Berstad (M.Sc.), who is the kindest person and best friend anyone could ever wish for, helping me out any time with anything (and of course Endre!), Marianne who has made me a coffein addict for real and who would always help out with library problems, and all the other students who kindly diverted my attention from writing by offering good companionship.

Finally, I would like to thank my own Dr Lundmark for always being there for me, encouraging, criticising, and not least of all feeding me during my work with this thesis. Various IT problems, English language problems and sample carrying would have proved far more challenging without your ever present support. Thank you so very much! You are truly inspiring…

Abstract

The Nesodden study area is part of the complex Southwest Scandinavian Domain in the Baltic Shield. To investigate its magmatic/metamorphic evolution, and to constrain magma sources, 482 *in situ* LA-MC-ICPMS U-Pb and Lu-Hf analyses were performed on zircon grains from granitic to tonalitic gneisses, granitoids, and a granitic pegmatite. The U-Pb data yield ages at 1.54-1.53 Ga for foliated granites and granitic gneisses, and 1.50-1.49 Ga for a second group of granitic and tonalitic rocks, whereas the pegmatite gave an age of 1.05 Ga. The present day $^{176}Hf/^{177}Hf$ ratios mainly range from 0.28191 to 0.28207; however, a smaller group (mainly zircons from the Sveconorwegian pegmatite) have higher $^{176}Hf/^{177}Hf$ ratios of 0.28208 and 0.2822. The time-corrected initial Hf isotopic composition of zircons in 6 analysed rocks has a range of 5-6 εHf–units, whereas zircons in the remaining 3 samples have a much larger range of 9-11 εHf–units. The ranges indicate that the magmas were heterogeneous, with contributions from isotopically distinct sources, including depleted mantle (ε_{Hf} = ca. +10) and Paleoproterozoic crustal rocks corresponding in age and composition to the granitoids of the Transscandinavian Igneous Belt (TIB) which have ε_{Hf} = -1 to -2. Whole-rock Pb isotope compositions of the samples were determined by solution MC-ICPMS analysis. The present day $^{206}Pb/^{204}Pb$, $^{207}Pb/^{204}Pb$ and $^{208}Pb/^{204}Pb$ ratios vary widely, from 17.282 to 29.586, from 15.487 to 16.414 and from 36.901 to 45.912, respectively. A three-stage model of Pb isotopic evolution can reproduce the present-day compositions: (1) A mantle stage ending at ca. 2.1 Ga; (2) extraction and emplacement of the crustal precursor at ca. 1.5 Ga, and; (3) anatexis and metamorphism at ca. 1.05 Ga. The data confirm previously inferred Mesoproterozoic younging to the west in the south-western part of the Baltic Shield, and support a model of westwards growth of the Shield along a long-lived active continental margin. The effect of Sveconorwegian metamorphism is reflected in discordant U-Pb data from the gneisses, and confirmed by Pb-Pb modelling. Influence of Permian magmatic activity in the Oslo Rift area at ca. 290 Ma is also reflected in the U-Pb data. Three-stage Pb-Pb modelling agrees with the crustal residence time obtained by the Hf analyses. Data from inherited zircons further indicate that the crustal component detected in the rocks does not derive exclusively from TIB equivalents, but also reflects some recycling of marginally older, calc-alkaline gneiss complexes in the region.

1 Introduction

1.1 Purpose of study

The Precambrian supracrustal gneisses and various granitic (*sensu lato*) gneisses that make up the study area are situated at the eastern edge of the Phanerozoic Oslo Rift, forming part of the Kongsberg-Marstrand block (Andersen 2005) in the Southwest Scandinavian Domain of the Baltic Shield or Fennoscandia (SSD; Figure 1 and 2). The granitic gneisses are structural markers that constrain the minimum age for the deposition of the supracrustal rocks in the area, and the maximum age for regional deformation and metamorphism, ages that at present are not well known. The three-fold purpose of this study is to:

a) characterise the age relations between the granitic gneisses by U-Pb *in situ* zircon dating
b) to find out if Paleoproterozoic rocks are present at depth by zircon Lu-Hf isotope analysis and by Pb-Pb analyses on whole rock samples
c) to attempt to constrain the relationships, if any, between the Kongsberg-Marstrand block granitic gneisses and other rock provinces that make up the south-western Baltic Shield

1.2 Geological setting

The field area is situated on the western shore of the Nesodden Peninsula in the Oslo fjord, in south-eastern Norway. The area extends from Spro southward to Fagerstrand and covers ca. 8 km^2 (Figure 3). Most of the area is suburban, but it also includes farmland, lakes and forests. In the Pleistocene, glaciations eroded and sculpted the landscape, and today the topography is gentle, stretching from sea-level up to ca. 200 m above sea level. However, the crystalline basement exposed on Nesodden is bounded by steeply dipping Permocarboniferous faults; in fact, the entire peninsula forms a horst surrounded by graben structures related to the formation of the ca. 290 Ma Oslo rift (Sundvoll et al. 1990). Movements along the faults have been estimated to up to 1000 metres (Swensson 1986). The western fault zone makes up the western boundary of the field area. To the east and west of the Nesodden crystalline basement, folded Cambro-Silurian sedimentary rocks have been preserved in the graben structures and are exposed on the numerous islands in the fjord. To the north, Permocarboniferous (typically alkaline) plutonic and volcanic rocks dominate. On Nesodden, these are represented by numerous dolerite dykes that cross-cut all other structures. The Precambrian bedrock has received less attention than the neighbouring Oslo rift rocks and

fossiliferous Palaeozoic strata. Although the area was mapped in some detail by Brock (1927) and Gleditsch (1952), the precise nature of the relations between the Precambrian rock types remain uncertain, doubtlessly due to the mostly tectonic nature of the contacts.

2 Regional geology

2.1 Introduction

The Baltic Shield is situated in the northern part of the East European Craton and is one of the best known Precambrian shields in the world (Figure 1). It extends across Norway, Sweden, Finland and north-western Russia. The Baltic Shield grew by multiple subduction-related magmatic events and accretion of micro-continents onto an Archaean core in the late Archaean and the Proterozoic (Gaál and Gorbatschev 1987). The north-eastern parts of the Baltic Shield represent the core of the craton; from here it gets progressively younger towards the southwest. This geochronological zonation roughly corresponds to crustal growth during the 3.1-2.9 Ga Saamian orogeny, the 2.9-2.6 Ga Lopian orogeny, the 2.0-1.75 Ga Svecofennian orogeny and the 1.75-1.5 Ga Gothian orogeny (Gaál and Gorbatschev 1987). Later events mainly led to reworking and fracturing of the existing basement, and include the 1.25-0.9 Ga Sveconorwegian orogeny and the 0.6-0.4 Caledonian orogeny along with rifting and continental igneous activity (sometimes referred to as anororogenic) (Gaál and Gorbatschev 1987). Hence, the Precambrian Baltic Shield is divided into three domains from the northeast to the southwest, the Archaean Domain, dominated by Saamian and Lopian rocks, the Svecofennian Domain, and the Southwest Scandinavian Domain, which is the part of the Baltic Shield that was reworked in Sveconorwegian time.

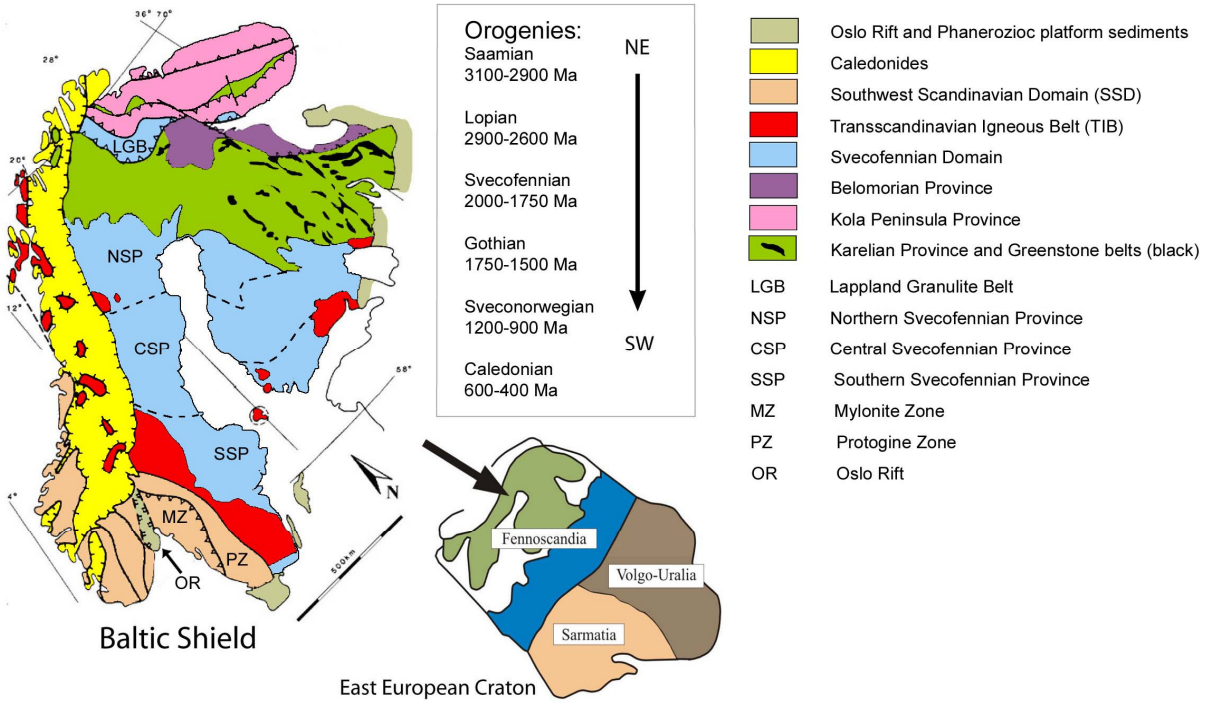

Figure 1. The Baltic Shield – major tectono-stratigraphic units. Modified after Gaàl and Gorbatschev (1987) and GeoGuide Online.

2.2 The Archaean Domain

The Archaean core of the Baltic Shield was formed between 3.51 and 2.5 Ga ago as a result of multiple events of subduction, accretion, collisional events and mantle-plume activity (Mutanen and Huhma 2003, Slabunov et al. 2006). It is divided into three crustal provinces separated by Proterozoic thrust faults: the Karelian Province in the south, the Belomorian Province in the central part and the Kola Peninsula Province in the northeast (Figure 1).

The oldest parts of the Archaean Domain are found in the Karelian Province, which includes the relatively poorly known 3.1-2.9 Ga Saamian rocks and the 2.9-2.6 Ga Lopian rocks, along with rare occurrences of up to 3.5 Ga old rocks, including the oldest European rock, the Siurua gneiss (Gaál and Gorbatschev 1987, Mutanen and Huhma 2003). These typically tonalitic-trondhjemitic-granodioritic (TTG) gneisses represent the oldest preserved continental crust in the Baltic Shield, providing information about the earliest evolution of the crust (Gaál and Gorbatschev 1987 and references therein). Dating by U-Pb, Rb-Sr and Sm-Nd methods, together with REE studies, show that the up to 3.1 Ga old Saamian plutonic rocks consist of material that have a previous crustal residence time of 250 to 500 Ma (Jahn et al. 1984). The Lopian of the Karelian Province includes more than 20 major and several minor komatiite bearing greenstone belts intruded by granites, and surrounded by Archaean TTG gneisses (Gaál and Gorbatschev 1987). The Lopian rocks provide evidence for late Archaean

plate tectonics, and most of the Archaean rocks were formed in this time period (Gaál and Gorbatschev 1987).

The mainly 2.9-2.7 Ga Belomorian Province consists predominantly of medium- to high-grade paragneisses (including f. ex. banded iron quartzites, metapelites and amphibolites) related to subduction along the margin of the Karelian Protocraton (Bibikova et al. 2001). The Karelian and the Belomorian Province are separated by a 30-50 km wide "junction zone" marked by greenstone belts, interpreted to outline a Neoarchaean collisional front (Bibikova et al. 2001 and references therein).

The Kola Peninsula Province consists mainly of metapelites and quartzites that were deposited at ca. 2.9-2.7 Ga and later deformed, metamorphosed and affected by granitic magmatism at ca. 2.7-2.6 Ga (Gaál and Gorbatschev 1987 and references therein). The Kola Peninsula gneisses are poly-deformed and poly-metamorphic and the primary Neoarchaean relationships between the different terranes are therefore only partly preserved (Bibikova et al. 2001 and references therein).

At the beginning of the Proterozoic, the development of several rift systems led to the break-up of the Archaean protocraton, possibly as the result of mantle plume activity (Bibikova et al. 2001 and references therein). The final break up of the Archaean craton occurred at ca. 1.95 Ga ago and an ocean basin was formed (Nironen 1997). The break-up was followed by the 1.95-1.80 Ga Lapland-Kola orogen, involving the reassembling of the previously rifted fragments and leading to the formation of the Lapland Granulite Belt along the collisional front (Bibikova et al. 2001 and references therein). In general, Proterozoic reworking of the Archaean Domain was most intense in the Belomorian and the Kola Province (both extensively reworked during the Lapland-Kola orogeny). In the Karelian Province the reworking was less intense (Bibikova et al. 2001 and references therein) although both rifting (Samsonov et al. 2005 and references therein) and granitoid and mafic magmatism took place (Käpyaho et al. 2006 and references therein). A second collisional zone, the Svecofennian, is coeval with the Lapland-Kola collisional orogen and will be discussed further in the following chapter.

2.3 The Svecofennian Domain

In the Paleoproterozoic, a passive continental margin developed along the western edge of the Archaean craton. Metasediments originally deposited as turbidites and conglomerates indicate a shelf, or near-shelf environment at the time of deposition (Nironen 1997). Also, some

metaturbidites along the eastern part of the Svecofennian Province were deposited on an unconformity, testifying to erosion prior to the sedimentation (Gaál and Gorbatschev 1987). With the start of the Svecofennian orogen, large scale formation of juvenile continental crust took place, focused primarily to a short period lasting from 1.93 to 1.87 Ga (Gaál and Gorbatschev 1987). The large amounts of igneous rocks produced within a short time period is particular to the Svecofennian, setting it distinctly apart from the Archaean and the Phanerozoic.

The Svecofennian Domain is divided into three major provinces: the Northern, the Central and the Southern Svecofennian Province. The Northern and the Southern Provinces are volcanic belts dominated by mainly dacitic and rhyolitic calc-alkaline volcanic suites. These two volcanic belts have many similarities, both of them are thought to be remnants of island arcs, and both are underlain by thick basal greywackies that suggest a continental margin environment (Gaál and Gorbatschev 1987 and references therein). Both the Northern and Southern Provinces' volcanic rocks were formed during a short time interval between 1.90-1.87 Ga ago (Gaál and Gorbatschev 1987 and references therein).

The two volcanic belts form a U-shaped arc that envelops the Central Province from the north, east and south. The Central Province consists mainly of metagreywackies and metapelites, originally deposited in a sedimentary basin often referred to as the Bothnian basin (Lundquist 1979 and references therein). Most of the Svecofennian Domain is intruded by granitoids, representing early-, late- and post-orogenic magmatism, making it difficult to recognise the stratigraphic relationships in the Bothnian basin.

The early, I-type granitoid intrusions make up the bulk of the Svecofennian continental crust. They form large plutonic complexes of differentiated suits of calcic and calc-alkaline rocks, e.g., gabbros, diorites, granites, granodiorites and, most commonly, tonalities (Gaál and Gorbatschev 1987 and references therein). The early Svecofennian plutonism took place between 1.9-1.87 Ga ago and was followed by local magmatism until ca. 1.85 Ga ago (Huhma 1986, Gaál and Gorbatschev 1987 and references therein).

By 1.87 Ga most of the Svecofennian crust was consolidated enough to allow rifting of the continental crust, associated with emplacement of dolorite dyke swarms (later metamorphosed to amphibolites) between 1.87-1.83 Ga ago. The ca. 1.83–1.77 Ga late granitoids are mainly granitic S-type rocks of crustal origin, undifferentiated and associated with migmatites and pegmatites (Gaál and Gorbatschev 1987 and references therein).

The post-orogenic granite plutonism started with minor granite intrusions as early as 1.80 Ga ago (Patchett and Kouvo 1986, Gaál and Gorbatschev 1987 and references therein). It

was followed by bimodal, intracratonic, gabbro/anorthosite/rapakivi granite magmatism 1.70-1.54 Ga ago (Gaál and Gorbatschev 1987 and references therein).

2.4 The Transscandinavian Igneous Belt

From ca. 1.85 to 1.65 Ga the Svecofennian crust was intruded by voluminous granitic batholiths and rhyolitic porphyries, forming the Transscandinavian Igneous Belt (TIB). It stretches from the coast of central Norway to southeast Sweden, and locally crops out in basement windows in the Caledonides (Andersen 2005 and references therein). The TIB is ca. 1600 km long, up to 150 km wide and approximately north-south trending (Gaál and Gorbatschev 1987, Andersen et al. 2002a).

The TIB rocks can be divided into three different generations. The ca. 1.85-1.83 Ga TIB-0 rocks reperesent the earliest TIB magmatism. The second generation consist of the 1.81-1.76 Ga TIB-1 rocks, partly overlapping in age with the waning stage of late Svecofennian magmatism. The third generation includes the 1.71-1.65 Ga TIB-2 and TIB-3 groups, where TIB-3 shows a temporal overlap with the beginning of the Gothian orogeny (Andersson and Wikström 2004 and references therein). However, in contrast to the late Svecofennian S-type magmatism and the generally tonalitic and calc-alkaline Gothian magmatism (see below), the TIB rocks are typically I- and A-type (monzo-) granitoids, frequently alkali-calcic (though some are calc-alkaline), and have a coarse grained texture with K-feldspar megacrysts (Gorbatschev 2004 and references therein).

The TIB rocks generally have low initial $^{87}Sr/^{86}Sr$ ratios, which together with Nd-isotope studies suggest that the intrusives are derivatives of the mantle or of the lower crust (Gaál and Gorbatschev 1987 and references therein). Different tectonic settings have been proposed for the formation of the TIB, envisaging either crustal extension along the Svecofennian margin, or an active continental margin, or post-extensional collapse following over-thickening of the crust (Andersson et al. 2004 and references therein). However, Andersson et al. (2004) argued that given the lack of evidence for either large scale extension (e.g., extensional shear zones or dyke swarms), or medium- to high-pressure metamorphism associated with collisional tectonics, and given the geochemical signatures of mafic TIB rocks, a subduction setting along the Svecofennian margin is the more likely of the proposed models.

The TIB magmatism was followed by extension related 1.65-1.51 Ga rapakivi granite magmatism along pre-existing week zones in the crust (Nironen 1997).

2.5 The Southwest Scandinavian Domain

At least three different nomenclature systems have been proposed for the internal division of the Southwest Scandinavian Domain (SSD) (Andersen 2005). The tectonostratigraphic terrane systems of Åhäll and Gower (1997) and Bingen et al. (2005) have been criticised by (Andersen 2005) since the terraine status of several of the segments/sectors in the SSD remains uncertain and/or debated. In the present study the segment/sector nomenclature of Berthelsen (1980) and Gaàl and Gorbatschev (1987) will be used.

The SSD extends across the western rim of the Baltic Shield (Figure 2). It consists mainly of Gothian rocks (1.75-1.5 Ga) and re-worked TIB equivalents. The Gothian rocks formed during mid-Proterozoic westwards growth of the craton, suggested to represent a 200-250 Ma long period of Andean type subduction along the Baltic Shield (Andersen 2005 and references therein). The Gothian crust is typically more felsic in the east, changing from calcic/calc-alkaline in the west to more alkali-calcic/alkaline, roughly coeval rocks in the east. Also, Gothian rocks of sedimentary origin were deposited in a shallow marine water environment in the east, and in a deep marine water environment in the west (Gaál and Gorbatschev 1987 and references therein).

The SSD was subsequently reworked during three major geological events; the Hallandian (1.5-1.4 Ga), the Sveconorwegian (1.25-0.9 Ga) and the Caledonian (0.6-0.4 Ga) orogenies. Although substantial volumes of granitic rocks were emplaced in the Sveconorwegian, and the Caledonian nappes cover a considerable area, these are still minor additions compared to the crustal material added during the Gothian orogeny (Gaál and Gorbatschev 1987).

During the Sveconorwegian orogeny, the SSD was deformed, metamorphosed and intruded by several generations of magmatic rocks (Bingen et al. 2005, Andersen et al. 2007b and references therein). The influence of Sveconorwegian reworking decreases towards the east, and ends with the Sveconorwegian Frontal Deformation Zone (SFDZ; Söderlund et al. 2002 and references therein) and the Protogine Zone (PZ; Gaál and Gorbatschev 1987). The faulting along the Protogine Zone started shortly after the formation of the TIB and lasted until the end of the Sveconorwegian orogeny ca. 0.9 Ga ago (Gaál and Gorbatschev 1987).

Other Sveconorwegian crustal scale shear zones, typically north-south trending, divides the SSD into sectors (e.g., Stephens et al. 1996) that may have been displaced southwards along the edge of the Baltic Shield during the orogeny (Haas et al. 1999, Bingen et al. 2001).

Some of the major shear zones were reactivated in Phanerozoic time (Swensson 1986). Below follows a brief description of the different sectors.

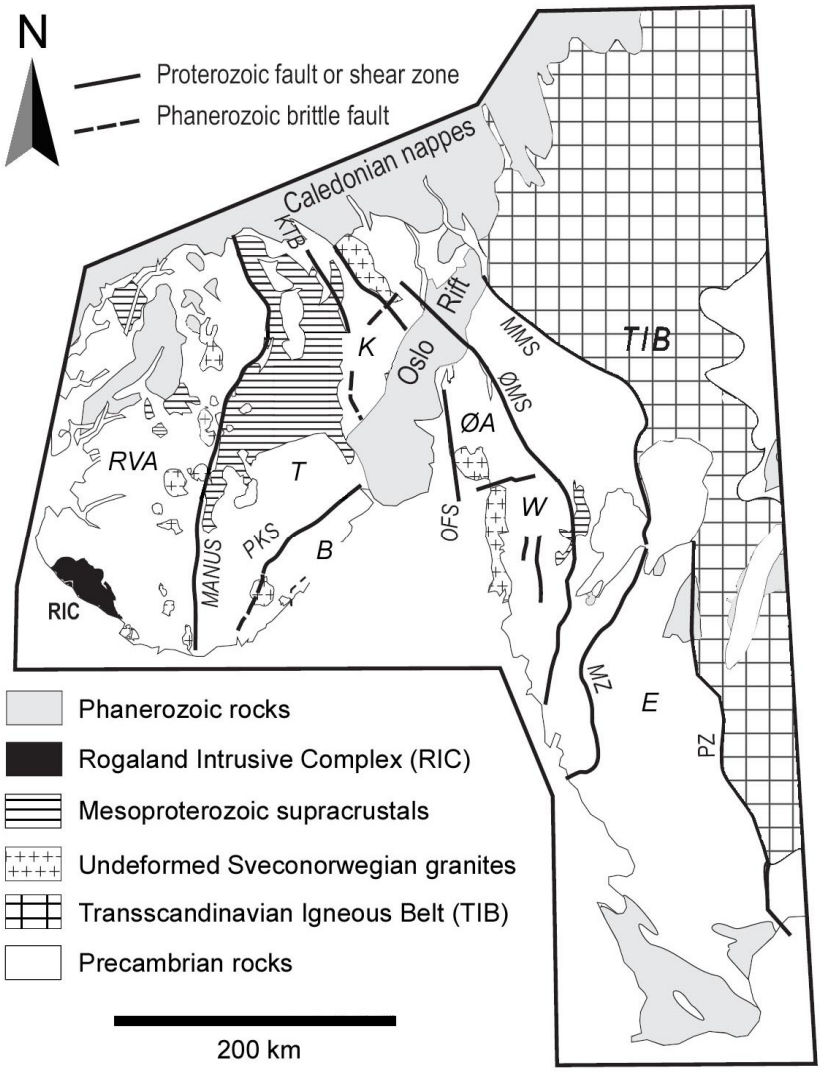

Figure 2. Simplified geological map of the Southwest Scandinavian Domain (SSD), modified after Andersen et al. 2007b. Regional units: RVA: Rogaland-Vest Agder sector, T: Telemark sector, B: Bamble sector, K: Kongsberg sector, ØA: Østfold-Akershus sector, W: Western segment, E: Eastern segment, TIB: Transscandinavian Igneous Belt. Shear zones: MANUS: Mandal-Ustaoset shear zone, PKS: Porsgrunn-Kristiansand shear zone, OFS: Oslofjord shear zone, ØMS: Ørje Mylonite shear zone, MMS/MZ: Mjøsa-Magnor shear zone/Mylonite Zone, PZ: Protogine Zone. RIC: Rogaland Igneous Complex

2.6 The study area and surrounding parts of the SSD

The Rogaland-Vest Agder (RVA) sector makes up the south-western Precambrian continental crust of Norway (Figure 2) and is bounded to the northwest by the present-day Caledonian thrust front and to the east by the Mandal-Ustaoset shear zone (MANUS), which separates it from the Telemark sector. The MANUS is a major crustal lineament that may be >1120 Ma (Sigmond 1985). The RVA sector is mainly made up of tonalitic to granitic gneiss, but also includes minor amounts of meta-sedimentary rocks. Several Sveconorwegian granitic

intrusions have been recognized in southern Norway and one of them can be found in the RVA sector, the ca. 1.05 Ga deformed granitic Feda suite, which is likely subduction related (Bingen and Bremen 1998). The RVA sector also contains the large, ca. 930 Ma anorogenic Rogaland Igneous Complex (or Egersund complex; Andersen et al. 2001a, 2002a and references therein) in its south-western part, consisting of anorthosites and related hypersthene bearing and mafic intrusions.

The neighbouring Telemark sector is separated from the Kongsberg sector in the east-northeast by a Precambrian ductile shear zone often referred to as the Kongsberg-boundary or the Kongsberg-Telemark boundary; to the east it also has a boundary to the late-Palaeozoic Oslo Rift and to the southeast it is separated from the Bamble sector by the Porsgrunn-Kristiansand shear zone (PKS). The PKS is a Precambrian ductile shear zone interpreted as a major Sveconorwegian thrust (Mulch 2003). The Telemark sector contains low-grade (green-schist to lower amphibolite facies) supracrustal rocks in the north (the Telemark supracrustals), consisting partly of the ca. 1.5 Ga Rjukan group meta-rhyolites and meta-basalts (Dahlgren et al. 1990). This bimodal sequence is believed to have been deposited during Mesoproterozoic continental rifting that created extensional basins (Sigmond et al. 1997a, 1997b, Sigmond 1998). South of the Rjukan group a younger, ca. 1.15 Ga supracrustal sequence crops out. This sequence contains quartzites, the Bandak and the Heddal groups, which are mixed volcanic and sedimentary sequences (Andersen et al. 2002a). Further south, granitic gneisses of uncertain origin and late Sveconorwegian granites are the characteristic rock types (Andersen et al. 2001a). Andersen et al. (2007b) found that some of the gneisses are early Sveconorwegian magmatic rocks.

The Bamble sector contains meta-sedimentary gneisses, quartzites and amphibolites that were intruded by Sveconorwegian gabbros, granites and charnockites. Upper amphibolite to granulite facies metamorphism was dated to ca. 1100 Ma (Kullerud and Dahlgren 1993). There are also minor ca. 1.5 Ga granodioritic to tonalitic gneisses in the area, such as the 1.56 Ga Gjerstadvatn and 1.55 Ga Justøy tonalities, and the 1.52 Ga Jomås granodiorite (Andersen et al. 2004a). The Bamble sector also includes the Tromøy gneiss complex, which is made up of low-potassium calc-alkaline rocks and is recognised as an island arc fragment that formed at ca. 1.2 Ga (Knudsen and Andersen 1999). Sveconorwegian granitic intrusions in this sector are the 0.9 Ga Herefoss granite (Andersen 1997) on the boundary to the Telemark sector, and to the east of the intrusion is the ca. 0.98 Ga Grimstad granite (Kullerud and Machado 1991).

The Kongsberg sector is separated from the Bamble sector by the south-western corner of the Oslo Rift. In the southern part of the Kongsberg sector granodioritic and tonalitic

gneisses are much more abundant than in the Bamble sector, including the 1.53 Ga Snarum granodiorite (Andersen et al. 2004a and references therein). Poorly known meta- and ortho-gneisses, possibly >1.6 Ga, are common in the north-eastern part of the sector (Nordgulen 1999). The Flå granite in the north-western part of the sector is a large Sveconorwegian (0.92 Ga) intrusion (Andersen et al. 2002b and references therein). The Kongsberg sector is separated from the Østold-Akershus sector to the south-east by the Oslo Rift.

The Østold-Akershus sector (ØA) is the northward continuation of the Western segment of SW Sweden, and may be continous across the Oslo Rift with the Kongsberg-sector. The Solør complex (SC) is situated in the northern part of the ØA sector and consists of 1.67 Ga and older TIB equivalent potassic granites and supracrustal gneisses (Andersen et al. 2002a) and younger mafic intrusions (Andersen 2005). The boundary between the SC and the Romerike complex (RC) to the south is the Sveconorwegian Mjøsa-Magnor shear zone (MMS; Andersen 2005) which is known as the Mylonite Zone (MZ; Gaál and Gorbatschev 1987) on the Swedish side. The RC mainly contains mid-Proterozoic migmatitic gneisses, possibly of supracrustal origin, which were later intruded by calc-alkaline granitoids (Berthelsen et al. 1996). The RC is part of the Median segment. The southern boundary of the RC is the Ørje Mylonite Zone (ØMS, Berthelsen et al. 1996), known as the Dalsland Boundary Thrust in Sweden, which separates the RC from the Østfold complex (ØC). The ØC consists mainly of meta-supracrustal gneisses, several generations of granitic to tonalitic orthogneisses (Graversen 1984) and amphibolites, meta-rhyolites and meta-sedimentary gneisses, which likely corresponds to the ca. 1.60-1.59 Ga supracrustals in the Stora Le-Marstrand belt of south-western Sweden (e.g. Åhäll and Connelly 2008). The ØC is part of the Western segment of SW Sweden (Söderlund et al. 1999 and references therein) and it includes the Nesodden Peninsula in the west. At ca. 925 Ma the ØC was intruded by the Østfold-Bohus granite (Eliasson and Schöberg 1991).

The basement rocks of the ØA sector mainly consists of 1.7-1.3 Ga old supracrustal gneisses and granitic to tonalitic orthogneisses (Andersen et al. 2001a). Calc-alkaline gneisses from Feiring, Sørmarka, Midtskog, Bjørkelangen and Tistedalen have been dated by Andersen et al. (2004a) to 1.57 Ga, 1.52 Ga, 1.57 Ga, 1.58 Ga and 1.6 Ga, respectively. The ØA sector includes the 1.6 Ga old Slemmestad meta-rhyolite, which is situated on the western shore of the Oslo fjord (Andersen et al. 2004a).

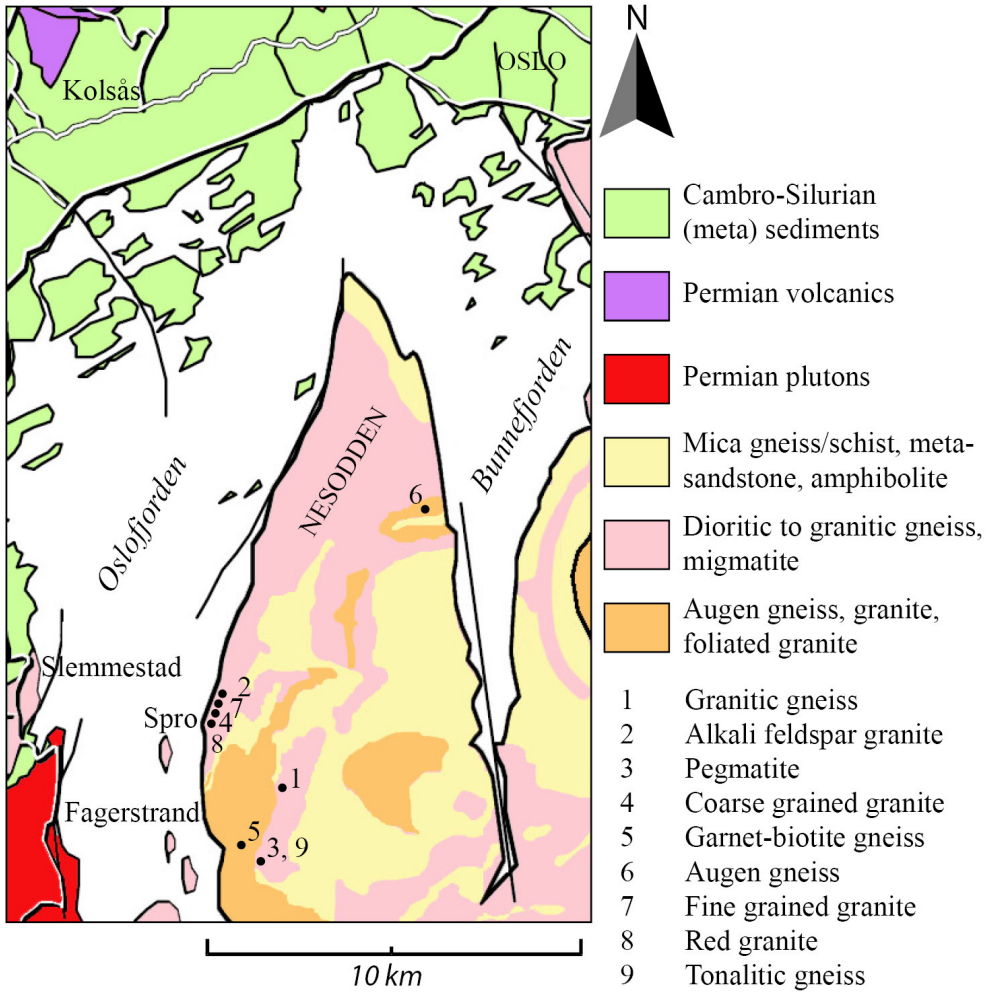

Figure 3. Simplified geological map of the Nesodden Peninsula with sample localities. Modified after Naterstad et al. (1990).

The Western segment, or Idefjorden 'terrane' (Åhäll and Connelly 2008 and references therein), in south-western Sweden continues further to the east and south, containing mainly deformed supracrustals and intrusive rocks such as the ca. 1.66 Ga meta-supracrustals and granitic intrusions of the Horred formation, the 1.63-1.59 Ga Åmål formation comprising volcanic, volcanoclastic and sedimentary rocks, and the 1.63-1.59 Göteborg and 1.59-1.52 Hisingen granitoid intrusions (Åhäll and Connelly 2008). The Hisingen suit consists of intermediate granitoid intrusions characteristic of continental arc magmatism (Åhäll and Connelly 2008). The Western segment is separated from the Eastern segment by the Mylonite Zone (Gaál and Gorbatschev 1987). The Eastern segment of the SSD is bounded by the TIB to the east and by the SFDZ. The Eastern segment includes 1.70-1.66 Ga granitoid gneisses that were intruded by 1.62-0.90 Ga rocks (Åhäll and Connelly 2008 and references therein). The eastern boundary of the Eastern segment includes the Protogine Zone of Gaál and

Gorbaschev (1987) as well, which includes intrusions of syanites, granites and mafic dykes (Gaál and Gorbatschev 1987).

Andersen et al. (2004a) concluded that the above described areas in southeast Norway were part of a cordillera-type continental margin with characteristic intermediate to felsic calc-alkaline magmatism and that the central parts of southern Norway were part of the Baltic continental margin prior to 1.6 Ga, and possibly well before that. Calc-alkaline magmatism was likely continuous from ca. 1.66 to 1.50 Ga along the south-western margin of the Baltic Shield, and parts of magmatic island arcs are preserved as calc-alkaline gneisses. Rocks from this age-interval, especially the last 100 Ma, can be found across southern Norway on both sides of the Oslo rift and there are no particular age-differences or changes in geochemical character between the different rocks, not even across major Precambrian shear zones in the area. Zircon U-Pb and Lu-Hf isotope data indicates that sedimentary basins along the margin of the Baltic Shield received the clastic input from young arc-related sources as well as from older sources that originated within the Shield itself. The best candidate for the older source is TIB related 1.8-1.7 Ga granites or other mafic rocks (Andersen et al. 2004a).

3 Analytical methods

3.1 Introduction

Isotopes of an element have identical chemical properties since they have the same number of protons and electrons, but their masses differ (e.g. ^{235}U and ^{238}U), as they have different numbers of neutrons. Some isotopes are unstable, also called radionuclides, and will decay to stable isotopes, or stable nuclides, by different modes of radioactive decay. The stable nucleides formed are called (radiogenic) daughters, and the unstable nucleides are called parents. Some radionuclides occur naturally since they have very slow decay rates, and have not yet totally decayed to stable daughter isotopes, other, more short-lived radionuclides (e.g., ^{218}Rn which has a half-life of 35 ms) exist because they are continuously produced as part of decay chains of longer-lived isotopes. The rate of decay of an unstable nucleide is controlled only by the instability of the radioactive nucleus, and will not change with time or with changes in the environment. The parent and the daughter nucleides (and the intermediate daughters of the decay chains as well) have different chemical and physical properties, and will therefore respond differently to changes in their environment, e.g. melting, fluid activity etc. This forms the basis of isotope geochemistry. By analysing the isotopic compositions of single minerals or whole rock samples, it is possible to constrain the different processes that

led to their formation, and, under some circumstances, to date these processes. In this chapter the theoretical background for the geochemical analyses used in this study are described, along with sample preparations, and analytical methods used.

3.2 Zircon

Zircon ($ZrSiO_4$) is one of the most widely used minerals for U-Pb and Lu-Hf isotopic measurements in geosciences. It is widespread in igneous, sedimentary and metamorphic rocks, and can be a versatile indicator of the geological and petrological history of its host rock. Since it is resistant to both physical weathering and chemical alteration, it can survive several cycles of erosion and deposition. Furthermore, its ability to remain a closed system at temperatures close to 900˚C (i.e., its high blocking temperature; Ireland and Williams 2003), makes it possible for the mineral to survive partial melting of its host rock and transportation in a magma, or high grade metamorphism, and still preserve information of past geological processes.

Zircon has a tendency to substitute zirconium (Zr) in its crystal structure with uranium (U) and thorium (Th), which have similar ionic radii and the same ionic charge as Zr. During crystallisation it can incorporate relatively large amounts of U and Th, which decay to lead (Pb). While Pb does not fit in the crystal structure of zircon, and is thus not typically incorporated in the crystal as it forms, the zircon will under most circumstances hold on to the radiogenic lead formed in the zircon from the decay of U and Th. Thus, zircon has a U-Th-Pb geochronometer that can be used for dating the geological processes that formed it. In general, a mineral suited for U-Pb dating has to be a closed isotopic system, meaning no gain or loss of U or Pb; it should contain a sufficient amount of U and Pb for the isotopic measurements and it should not have initial lead in its crystal structure. Zircon more or less meets all three criteria and is thus very well suited for U-Pb dating.

Zircon also has a tendency to substitute Zr with hafnium (Hf) in its crystal structure, along with smaller amounts of lutetium (Lu). Since Lu decays to Hf, the initial daughter is much more abundant than the parent, the opposite of the U-Th-Pb system. While this makes the Lu-Hf system less than ideal for dating, it can give us valuable information on the petrogenesis of the rock. The ratio of the two isotopes will essentially mirror that of the magma from which the zircon formed, which in turn will reflect the nature of the magma source, i.e. primitive (mantle) or evolved (crust).

3.3 Theoretical background

3.3.1 The U-Th-Pb system

U and Th decay to stable isotopes of Pb. The three naturally occurring radioactive isotopes of U are ^{238}U, ^{235}U and ^{234}U. Together with the naturally occurring long-lived radioactive ^{232}Th there are five other radioactive Th isotopes that are intermediate daughters in the decay series of ^{238}U, ^{235}U and of ^{232}Th. All three decay series are branched. The decay of ^{238}U, ^{235}U and ^{232}Th are summarized in the following equations, where Q represents the total decay energy emitted during the decay:

$$^{238}U \rightarrow {}^{206}Pb + 8\,{}^{4}He + 6\beta^{-} + Q \quad (1)$$

$$^{235}U \rightarrow {}^{207}Pb + 7\,{}^{4}He + 4\beta^{-} + Q \quad (2)$$

$$^{232}Th \rightarrow {}^{208}Pb + 6\,{}^{4}He + 4\beta^{-} + Q \quad (3)$$

Uranium and Th are incompatible elements, and are incorporated into the liquid phase during partial melting of the mantle, making the silica rich continental crust enriched in U and Th compared to rocks of the upper mantle. Granitic rocks, for instance, therefore have higher U and Th contents than basaltic rocks. In granitic rocks the Th content is generally higher than the U, possibly because U is a mobile element (soluble in water) under oxidizing conditions, and so may have been removed from the system in aqueous solution as uranyl ions. U and Th concentrations in common rock-forming silicate minerals are evenly low. These elements are instead incorporated into U and/or Th bearing accessory minerals such as zircon, apatite, monazite etc.

The U-Th-Pb system provides one of the most accurate and precise age determination methods for terrestrial rocks. The equations for age determinations are:

$$\frac{^{206}Pb}{^{204}Pb} = \left(\frac{^{206}Pb}{^{204}Pb}\right)_i + \frac{^{238}U}{^{204}Pb}\left(e^{\lambda_1 t} - 1\right) \quad (4)$$

$$\frac{^{207}Pb}{^{204}Pb} = \left(\frac{^{207}Pb}{^{204}Pb}\right)_i + \frac{^{235}U}{^{204}Pb}\left(e^{\lambda_2 t} - 1\right) \quad (5)$$

$$\frac{^{208}Pb}{^{204}Pb} = \left(\frac{^{208}Pb}{^{204}Pb}\right)_i + \frac{^{232}Th}{^{204}Pb}\left(e^{\lambda_3 t} - 1\right) \quad (6)$$

where subscript *i* denotes initial values and λ_1, λ_2 and λ_3 are the decay constants of ^{238}U, ^{235}U and ^{232}Th, respectively (Table 1). $^{238}U/^{204}Pb$, $^{235}U/^{204}Pb$ and $^{232}Th/^{204}Pb$ are isotope ratios calculated from the measured concentrations of U, Th and Pb values.

Table 1. Abundances, half-lives and decay constants of naturally occurring U and Th isotopes

Isotope	Abundance (%)	Half-live (years)	Decay Constant (y^{-1})
^{238}U	99.2743	4.468×10^{9}	1.55125×10^{-10}
^{235}U	0.72	0.7038×10^{9}	9.8485×10^{-10}
^{232}Th	100	14.010×10^{9}	4.9475×10^{-11}

Reference: (Steiger and Jäger 1977)

Equations 4, 5 and 6 are written in terms of the atomic $^{206}Pb/^{204}Pb$, $^{207}Pb/^{204}Pb$ and $^{208}Pb/^{204}Pb$ ratios. Since the only stable non-radiogenic Pb isotope is ^{204}Pb, its amount reflects the initial lead present in the mineral. Using the isotope abundance of common lead, the U-Pb and Th-Pb ages can be calculated by equations 4-6. To achieve concordant U-Pb and Th-Pb dates (i.e., the different isotopic clocks gives the same ages) the samples must satisfy the requirements for dating. The mineral must remain a closed system to U, Th, Pb and to all the intermediate daughters; correct initial Pb isotope ratios must be used (normally approximated by common lead); the decay constants for ^{238}U, ^{235}U and ^{232}Th must be known; the U isotopic composition is normal and has not been modified in any way, and all the analytical results are accurate (no systematic errors). In reality, the closed system assumption is rarely satisfied since U is a mobile element under oxidizing conditions, thus some U loss is common during chemical weathering in addition to Pb loss. Also, the crystal structures of U-bearing minerals are often damaged by radiation, which again can result in lead loss or the loss of intermediate daughters in the decay chain. Thus, most U-Pb and Th-Pb dates are discordant.

In addition to zircon, which is the most commonly used mineral for U-Th-Pb dating, a number of minerals incorporate U and/or Th in their crystal structures. Some of the most commonly used for dating are titanite (sphene), monazite and badeleyite. These minerals are present in different rock types, and also exhibit different blocking temperatures and form during different conditions, extending the range of datable rocks and conditions/processes that may be dated.

3.3.2 The Lu-Hf system

Lutetium and Hf are lithophile elements and are mainly concentrated in silicate minerals. Lutetium has two naturally occurring isotopes: ^{175}Lu and ^{176}Lu. Hafnium has six naturally occurring isotopes, one of which is the radiogenic ^{176}Hf, formed by decay of ^{176}Lu to ^{176}Hf by β-emission. The decay of ^{176}Lu has a half-life of $35.7*10^9$ years (Faure and Mensing 2005 and references therein) and is summarized in equation 7, where $\bar{\nu}$ is the complementary antineutrino and Q represents the total decay energy emitted during the decay:

$$^{176}Lu \rightarrow {}^{176}Hf + \beta^- + \bar{\nu} + Q \qquad (7)$$

This part of the branched decay of ^{176}Lu is the basis for the Lu-Hf isochron dating method, which is not in widespread use. The other part of the branched decay is the decay to ^{176}Yb by electron capture, which only makes up 3 ± 1% of all ^{176}Lu decay. The isotopic composition of Hf can be used to investigate the origin of igneous rocks. Since Hf is more incompatible than Lu in the presence of a melt phase, mantle melts, and therefore ultimately the continental crust, has a lower Lu/Hf ratio than the residual, depleted mantle (DM).

Lutetium and Hf do not normally form their own minerals (Hafnon, (Hf, Zr)SiO_4 is one of the few) in geological environments, but are incorporated into other minerals. Lutetium is a heavy rare earth element (HREE), and has a similar ionic radius to calcium (Ca) and will therefore substitute for Ca in crystal structures. Hafnium has approximately the same ionic radius as Zr, thus Hf is incorporated into Zr bearing minerals, e.g. zircon or badeleyite. The average Hf concentration in zircon is as high as 15200 ppm. The Lu concentrations are also typically elevated in zircons (in zircon typically 20-70 ppm), but the resulting Lu/Hf ratio in zircon is generally very low (Faure and Mensing 2005). Given this, it is evident that the isotopic composition of Hf in zircon changes very slowly with time.

In order to get information on the source-characteristics of granitic igneous rocks it is useful to look at Hf isotope variations in zircon grains instead of whole rock samples. This is because zircon, as a highly resistant mineral, typically preserves the isotopes better than the whole rock. Secondly, the zircon acts as a time keeper in its own right, and a combination of U-Pb dating and Lu-Hf analysis on the same grain (or parts thereof) will yield a superior time resolution compared to whole rock data (and may in fact allow the geologist to investigate earlier rock forming cycles by analysing inherited zircons). Variations in abundance of ^{176}Hf are expressed with respect to the naturally occurring stable ^{177}Hf of constant absolute

abundance. The initial $^{176}Hf/^{177}Hf$ ratios of single zircon grains record the composition of the magma at the time of zircon crystallisation. Variations in Hf isotope composition during magma evolution may be recorded in individual crystals in different growth zones, e.g., if incomplete magma mixing took place (e.g. Griffin et al. 2002).

To estimate the original Lu/Hf ratio of the Earth, the Chondritic Uniform Reservoir (CHUR) model is used. It is based on the composition of chondritic meteorites and the assumption that these meteorites represent the total composition of the Earth, i.e., that Earth was formed from the same source as the chondritic meteorites (DePaolo and Wasserburg 1976). There is also an underlying assumption that the isotopic evolution of Hf in the undifferentiated Bulk Silicate Earth (BSE) and CHUR has been parallel through time.

The $^{176}Hf/^{177}Hf$ ratio of a rock or mineral can be compared to that of the CHUR, as expressed by the ε-value that is defined by the following equation:

$$\varepsilon^0(Hf) = \left\{ \left(\frac{\left(\frac{^{176}Hf}{^{177}Hf} \right)^0_{spl}}{\left(\frac{^{176}Hf}{^{177}Hf} \right)^0_{CHUR}} \right) - 1 \right\} 10^4 \qquad (8)$$

where

$(^{176}Hf/^{177}Hf)^0_{spl}$ = $^{176}Hf/^{177}Hf$ ratio of a rock or mineral at present (t = 0) (spl = sample)

$(^{176}Hf/^{177}Hf)^0_{CHUR}$ = $^{176}Hf/^{177}Hf$ ratio of CHUR at present (t = 0), equal to 0.28286 (Faure and Mensing 2005)

Positive and negative ε-values mean that the sample is enriched in, respectively depleted in time-corrected $^{176}Hf/^{177}Hf$ compared to the chondritic reservoir. A positive ε-value indicates derivation from a magma source with higher Lu/Hf ratios than the CHUR and BSE, such a magma source is the depleted mantle reservoir (since Lu is less incompatible than Hf in the presence of silicate melts). Negative ε-values, on the other hand, indicate a magma source with lower Lu/Hf ratios over time than CHUR and BSE, such as crustal rocks. Mixing of material from different reservoirs, such as depleted mantle and continental crust, yields rocks with intermediate ε-values.

Isotopic evolution of Hf in a sample can be examined by plotting the time-corrected $^{176}Hf/^{177}Hf$, i.e., the initial ratio (henceforth referred to as Hf_i), of the sample against the time t

(Ga) ($^{207}Pb/^{206}Pb$ ages for zircons older then 600 Ma), which in the present study is determined by U-Pb *in situ* zircon dating (Figure 19). The graphs representing CHUR and DM isotopic evolution are also shown in the plot, together with a reference line for the sample that indicates its hypothetical isotopic evolution given a known Lu/Hf ratio. In the diagrams Hf_i ratios were chosen instead of ε_{Hf}-values, because zircon defines an almost horizontal growth curve in the Hf_i vs. time diagram, whereas in a ε_{Hf} vs. time diagram it forms a steeply dipping line, which is more difficoult to work with. For further explanation and Figures see section 4.3.

3.3.3 The Pb-Pb system

Lead is a chalcophile element that behaves as a large-ion lithophile element (LILE) in silicate systems. As described in section 3.3.1, the stable Pb isotopes occurring in nature are ^{206}Pb, ^{207}Pb and ^{208}Pb, which are the radiogenic daughters of ^{238}U, ^{235}U and ^{232}Th, respectively, along with the non-radiogenic isotope ^{204}Pb (that is generally regarded as stable because of its long half-life). Lead tends to form its own minerals, such as galena or cerrusite, but it often substitutes for potassium (K) in silicates such as K-feldspar, since they have similar ionic radius. Thus, K-feldspar bearing rocks like granites and pegmatites often have considerable amounts of Pb, which includes both radiogenic Pb and non-radiogenic Pb that was incorporated into minerals when the rock was formed.

The three decay systems described in section 3.3.1 gives three potential isochron systems as follows:

$$\frac{^{206}Pb}{^{204}Pb} = \left(\frac{^{206}Pb}{^{204}Pb}\right)_0 + \frac{^{238}U}{^{204}Pb}\left(e^{\lambda_{238}t} - 1\right) \tag{9}$$

$$\frac{^{207}Pb}{^{204}Pb} = \left(\frac{^{207}Pb}{^{204}Pb}\right)_0 + \frac{^{235}U}{^{204}Pb}\left(e^{\lambda_{235}t} - 1\right) \tag{10}$$

$$\frac{^{208}Pb}{^{204}Pb} = \left(\frac{^{208}Pb}{^{204}Pb}\right)_0 + \frac{^{232}Th}{^{204}Pb}\left(e^{\lambda_{232}t} - 1\right) \tag{11}$$

where subscript 0 denotes the initial isotopic ratio of Pb in a rock or mineral and λ_{238}, λ_{235} and λ_{232} are the decay constants of ^{238}U, ^{235}U and ^{232}Th, respectively (Table 1). However, because of late U loss the data points in a simple U-Pb isochron diagram almost always plot above and

to the left of the relevant isochron. Reformulating and dividing equations 9 and 10 give the following equation:

$$\frac{\left(^{207}Pb/^{204}Pb - \left(^{207}Pb/^{204}Pb\right)_0\right)}{\left(^{206}Pb/^{204}Pb - \left(^{206}Pb/^{204}Pb\right)_0\right)} = \frac{1}{137.88} \cdot \frac{e^{\lambda_{235}t} - 1}{e^{\lambda_{238}t} - 1} \tag{12}$$

This equation defines a straight line in a $^{207}Pb/^{204}Pb$ vs. $^{206}Pb/^{204}Pb$ diagram that passes through the point: $[(^{206}Pb/^{204}Pb)_0,(^{207}Pb/^{204}Pb)_0]$ and has a slope of 1/137.88 $[(e^{\lambda 235t} - 1) / (e^{\lambda 238t} - 1)]$ giving the basis for the lead-lead isochron method. The age of the isochron line can be determined from its slope by a process of iteration.

The Pb-Pb isochron method was one of the first dating methods ever used, but is not a much used dating method today. However, the Pb-Pb system is a powerful petrogenetic tracer. When working with rocks with complex evolution histories Pb-Pb modelling has proved to be a useful tool providing information about the source regions of the rock (Stacey and Kramers 1975, Taylor et al. 1980, Andersen et al. 1994, Faure and Mensing 2005), and can be used as a complementary method with other isotope systems like Lu-Hf.

The $^{238}U/^{204}Pb$ ratio is denoted with the Greek letter μ, giving the following relationship: $^{235}U/^{204}Pb = \mu/137.88$. The present day Pb isotopic composition in a mineral or rock reflects: (1) its age, i.e. the time that has past since the last isotopic homogenization of Pb, (2) the proportions of its U-, Th- and Pb-isotopes and (3) the history and composition of its source. Assuming that Pb evolution started from the initial meteoritic lead composition determined by Tatsumoto et al. (1973, Canyon Diablo troilite) at $t_0 = 4.57$ Ga (the age of the Earth) and has evolved in a closed system until t_1; the composition of this lead is given by:

$$\frac{^{206}Pb}{^{204}Pb} = a_0 + \mu_1\left(e^{\lambda_{238}t_0} - e^{\lambda_{238}t_1}\right) \tag{13}$$

$$\frac{^{207}Pb}{^{204}Pb} = b_0 + \left(\frac{\mu_1}{137.88}\right)\left(e^{\lambda_{235}t_0} - e^{\lambda_{235}t_1}\right) \tag{14}$$

$$\frac{^{208}Pb}{^{204}Pb} = c_0 + \omega\left(e^{\lambda_{232}t_0} - e^{\lambda_{232}t_1}\right) \tag{15}$$

where $a_0 = 9.307$, $b_0 = 10.294$ and $c_0 = 29.476$ are the initial lead compositions. If the Pb evolution were to continue from t_1 to t_2 in a second reservoir with a different μ-value (μ_2) then the lead isotope ratio is given by:

$$\frac{^{206}Pb}{^{204}Pb} = a_0 + \mu_1\left(e^{\lambda_{238}t_0} - e^{\lambda_{238}t_1}\right) + \mu_2\left(e^{\lambda_{238}t_1} - e^{\lambda_{238}t_2}\right) \quad (16)$$

Similar equations can be written for the other two parent-daughter systems as well. It describes the two-stage evolution of Pb, which is shown in Figure 4. Lead that evolved in a reservoir with the same μ_1 will plot on the same t_1 isochron and the position of the analysed sample on this isochron depends on the value of μ_2. For each μ-value a separate growth curve can be constructed. Growth curves in a Pb-Pb isochron diagram are non-linear curves leading from [($^{206}Pb/^{204}Pb)_0$, ($^{207}Pb/^{204}Pb)_0$] (initial lead ratios) to points on the isochron line where the samples plot. The initial Pb composition at t_1 is given by the intersection of the t_1 isochron and the geochron at t_1. The Pb isochron is defined by the isotope ratios of single-stage leads that were separated from a U-Pb reservoir at a specific date, obtaining different μ-values at separation. The geochron is an isochron defined by samples that separated from the primordial reservoir at t = 0, i.e. lead samples that have resided in their reservoirs for 4.57 Ga, or has been separated from their respective reservoirs just recently. A sample will plot on a paleoisochron with an age of t_1 if its Pb composition has remained unchanged since t_1, in which case the position of t_1 will depend on the value of μ_2. This only occurs in U-free systems such as K-feldspar formed at t_1, which incorporates Pb and excludes U in its crystal structure.

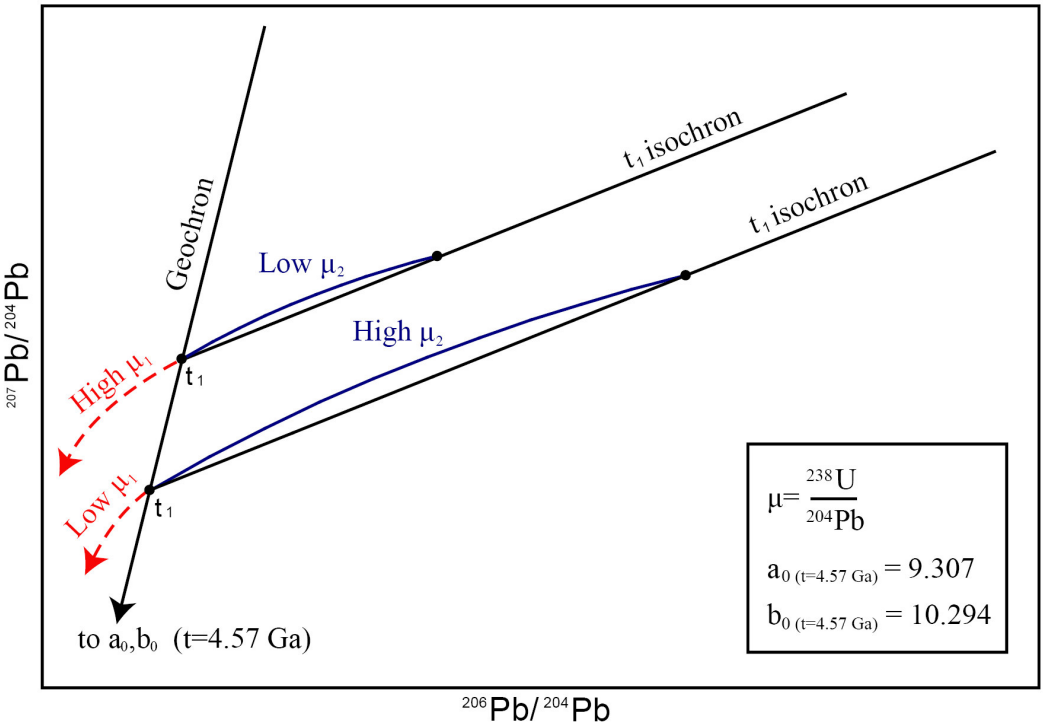

Figure 4. Schematic figure illustrating two-stage model for isotopic Pb evolution. Modified after Simonsen (1997 and references therein)

The Pb isotope system in rocks and minerals has typically evolved through multi-stage processes, i.e. the Pb isotopic evolution has taken place in more than two reservoirs. This can be accounted for by expanding equation 16 for additional stages with separate μ-values, and can be done for the other two parent-daughter systems as well. The most commonly used model assumes three stages of successive U-Th-Pb evolution in three different reservoirs, each characterised by a constant $^{238}U/^{204}Pb$ ratio (i.e. μ_1, μ_2 and μ_3) and $^{232}Th/^{204}Pb$ ratio (i.e. κ_1, κ_2 and κ_3) (Figure 5). The first stage of evolution corresponds to the time the Pb resided in the mantle reservoir with a time integrated μ_1-value. Thus, t_1 reflects the date when the Pb was separated from the mantle reservoir, i.e., the age of the continental protolith. The second stage reflects the evolution of the protolith until t_2, representing the age of final isotopic homogenization during magmatism or metamorphism. The third stage represents the evolution until the present in a third reservoir. The μ_1 is determined by the meteoritic Pb value (Tatsumoto et al. 1973), and by constraining t_1 and t_2 using Lu-Hf and U-Pb data respectively, the μ_2, μ_3 can be determined graphically from the PBI Excel program (Andersen 1998). The Pb-Pb evolution model can be used as a sensitive indicator of multi-stage processes, visually illustrating how a present day Pb composition of a suite of rock or mineral relates to a model reservoir as a function of time.

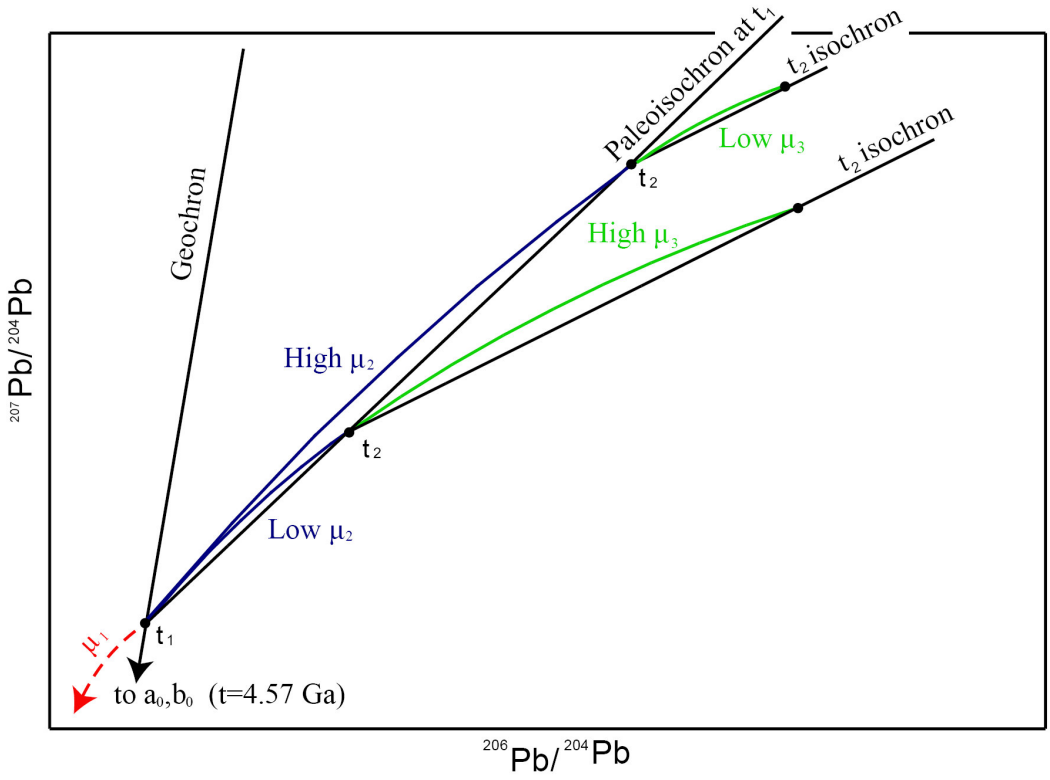

Figure 5. Schematic figure illustrating three-stage model for isotopic Pb evolution. Modified after Simonsen (1997 and references therein)

3.4 Sample preparation

All analytical work, including sample preparation, chemistry and isotope measurements were performed at the Department of Geosciences, University of Oslo, Norway.

Samples weighing 3-5 kg were washed in water, first with a steel brush, then in an ultrasonic bath for 15 minutes and finally dried in an oven over night at 45˚C. The samples were then crushed to coarse grains (<1cm) in a jaw crusher, and sieved through a splitter. A small amount was put aside for whole rock analyses. The remaining part was then crushed to ca. 0.5 mm using a Retsch percussion mill crusher. Zircons were separated using a Wilfley-table and heavy liquid (Sodium Heteropolytungstates ρ = 2.80 +/- 0.02 g/mL). Zircons for analyses were hand-picked under a binocular microscope. About 80 to 110 zircon crystals from each sample were mounted in epoxy and then polished to expose the mineral grains for U-Pb and Hf analyses. These were then carbon coated and examined by backscatter electron imaging (BSE). The zircons were finally polished with diamond abrasive powder to remove the carbon coating and then washed in HNO_3 in an ultrasonic bath for 15 minutes and finally rinsed with MilliQ water. The analyses were performed on a NU Plasma HR multi collector

ICPMS and a New Wave/Merchantek LUV-213 laser microprobe (LA-MC-ICPMS) at the Department of Geosciences at the University of Oslo, Norway.

For Pb-Pb whole rock analyses: the parts preserved after the splitting procedure were further pulverized to powder using a mill. After homogenization the samples were weighed (Table 2 in Appendix) on an analytical balance type of scale. The samples were then dissolved and by following the lead separation protocols (see Appendix) the desired elemental fractions were collected for further LA-MC-ICPMS analyses.

3.5 LA-MC-ICPMS (Laser Ablation Multi-collector Inductively Coupled Plasma Mass Spectrometry)

Inductively coupled plasma mass spectrometry (ICPMS) has become a widely used tool in geochemistry over the past few decades, since it allows precise measurements of small amounts of isotopes. Coupled with laser ablation (LA), it can be used to analyse parts of minerals, giving the further advantages of high spatial resolution (the laser beam is typically a few tens of micrometer wide), and it only uses a small amount of the sample, making further analyses possible.

An ICPMS comprises a high-temperature inductively coupled plasma (ICP) source and a mass spectrometer (MS). The MC-ICPMS is a high precision isotope ratio mass-spectrometer where the ICPMS utilizes the ionizing capabilities of a plasma to generate ions. The material to be analyzed is transported to the torch as an aerosol in an argon (Ar) or helium (He), or mixed, gas flow. The aerosol can be generated in two ways: (1) By aspiring a dilute solution through a nebulizer (applied in section 3.5.3), or (2) By ablating a solid sample with a focussed laser beam (applied in section 3.5.1 and 3.5.2). Using He instead of Ar to transport the sample minimizes ablated material deposition around the laser pit, which in turn improves sample transport efficiency. It also yields a more stable signal and higher reproducibility of the U-Pb fractionation. Almost anything will ionize in the plasma, thus the load of ions generated are impure/mixed both in terms of mass and energy, although there are typically few molecular ions compared to Secondary Ionisation Mass Spectrometry (SIMS). An electrostatic analyser (ESA) is needed to filter away the unwanted energies to make the magnetic sector work as a mass analyser. The magnetic sector of the instrument separates the ions that enter the MS by their mass-to-charge ratios, and after separation these are counted in a suitable detector, Faraday cups or in ion counters. A detector counts the number of ions striking it and then translates it into an electrical signal that can be measured and related to the

number of atoms of the element by using calibration standards (Košler and Sylvester 2003, Wolf 2005). The MC-ICPMS at the Department of Geosciences (University of Oslo, Norway) is a NU Plasma HR multi collector ICPMS or HR-ICPMS. This type of instrument was specifically developed for high-precision isotope ratio analyses. With the multi-collector system it is usually possible to determine the isotopes of a single element simultaneously, increasing the precision of the measurements.

Compared to other techniques, like Isotope Dilution Thermal Ionisation Mass Spectrometry (ID-TIMS) and SIMS, LA-MC-ICPMS has both distinct advantages and drawbacks.

The LA-MC-ICPMS is gaining on both TIMS and SIMS by (1) low cost, (2) easier and less time consuming sample preparation, (3) short analysis time and (4) high ionisation efficiency, which is required e.g. for Hf and osmium (Os) analysis (Kinny et al. 1991). Compared to TIMS the LA-MC-ICPMS has better spatial resolution and is less destructive of the sample (*in situ* method), however, it does not achieve the high precision of the TIMS. Compared to SIMS the LA-MC-ICPMS has lower precision, not as good spatial resolution and is slightly more destructive of the sample. Given these trade-offs, a geologist should thoroughly consider the problem he or she wants to address in relation to the strengths and weaknesses of these methods.

3.5.1 U-Pb

The *in situ* LA-MC-ICPMS U-Pb analyses were performed on carefully chosen zircon grains. For each sample ca. 20 to 40 zircons were analysed, giving a total of 260 analyses. The ICPMS detector system is specifically constructed for U-Pb analysis, and can simultaneously analyse ^{204}Pb, ^{206}Pb and ^{207}Pb in secondary electron multiplier ion counters, along with ^{235}U and ^{238}U which are measured in Faraday cups. The ^{235}U signal is typically too week to be measured with high precision and ^{235}U is therefore determined from the natural atomic ratio of ^{235}U/^{238}U, i.e., 137.88.

Each analysis starts with a 30 seconds on-mass background measurement (laser off), followed by 60 seconds ablation of the sample. The instrument includes a microscope that provides a visual image of the sample, which is necessary for in situ LAM-ICPMS work. The laser used is a New Wave/Merchantek LUV-213 Nd:YAG solid state laser microprobe that provides UV laser with 213 nm wave length. The laser conditions during ablation were: laser beam diameter 40µm, pulse frequency 10 Hz, and beam energy density $\leq$ 0.1 J/m^2. With

constant ablation conditions, the U-Pb elemental fractionation and mass discrimination of the Pb isotopes during ablation and in the plasma can be corrected for by using isotopically homogenous reference zircons with known age (Jackson et al. 2004). These standards are mounted on a separate epoxy disk and the U/Pb ratios are measured on the standards before and after the analyses of the unknown samples. Three different types of standards were used for U-Pb age determinations (Table 3).

Table 3. Standards used for U-Pb and Lu-Hf analyses

			Present day				Initial		
Reference sample		N	$^{176}Yb/^{177}Hf$	$^{176}Lu/^{177}Hf$	$^{176}Hf/^{177}Hf$	$^{178}Hf/^{177}Hf$	t (Ma)	$(^{176}Hf/^{177}Hf)_t$	References for U-Pb ages
91500		129	0.0120	0.0003	0.282301	1.46728	1061	0.282294	(e.g. Jackson et al. 2004)
	2SD		0.0043	0.00005	0.000080	0.00018		0.000079	
Mud Tank		509	0.0015	0.00003	0.282509	1.46727	732	0.282509	(T. Andersen, pers. comm.)
	2SD		0.0010	0.00002	0.000050	0.00010		0.000050	
Temora 2		172	0.0399	0.0011	0.282699	1.46727	418	0.282690	(e.g. Kamo et al. 2004)
	2SD		0.0281	0.0007	0.000065	0.00010		0.000063	
GJ-1		115	0.0096	0.00028	0.282018	1.46727	608	0.282015	(e.g. Jackson et al. 2004)
	2SD		0.0024	0.00002	0.000062	0.00012		0.000062	
A382 *(not used for Hf analyses)*							1876 ± 5		H. Huhma, pers. comm. to T. Andersen*

*This age is in agreement with the age obtained by Patchett & Kouvo (1996).

Analytical routines are described in detail in Andersen et al. (2004b) and Jackson et al. (2004) and adapted for multi collector instrument as described by Andersen et al. (2007b) and Røhr et al. (2008).

The laser ablation dating technique does not usually require large common lead corrections; however, for some zircons a common lead correction is necessary. In most cases where the LA-ICPMS method is applied, the common lead originates from the zircon itself, and by using the right protocols it is possible to correct for the ^{206}Pb and ^{207}Pb that forms part of the common lead (Košler and Sylvester 2003). When common lead is high, it should in principle be possible to measure it and correct the radiogenic lead accordingly. However, the ^{204}Pb shares its mass and charge with ^{204}Hg, a contaminant that likely stems from the argon flow, and hence must be corrected for. The correction is done by the background measuring routine described above. Standard measurements on three different standards were done at the start and finish of every analytical session, and two different standards were analysed during the sessions at one hour intervals. The standardisation procedure used in this study is described in detail by Røhr et al. (2008).

Data reductions were done using a spreadsheet written in Visual Basic for Microsoft Excel®. This includes procedures for interactive selection of the acquisition range to be integrated, and corrections for U-Pb fractionation and drift in the ion-counters. The standards are used to calculate corrections for elemental fractionation of U and Pb during ablation and in the plasma, mass-spectrometer mass bias and instrumental drift, extrapolating correction factors between standard runs. The standard runs also allow the precision of the instrument over time to be calculated. The precision is presently (> 3 years of data) less than or equal to one per cent for $^{206}Pb/^{238}U$ and $^{207}Pb/^{206}Pb$ ratios, and less than or equal to 1.4% for $^{207}Pb/^{235}U$ (2σ). Concordia ages and intercept ages were calculated using IsoplotEx 3.00 (Ludwig 2003).

3.5.2 Lu-Hf

The *in situ* LA-MC-ICPMS Lu-Hf analyses were performed on grains previously analysed for U-Pb (sections 4.2). A total of 222 zircons were analysed, ca. 15 to 30 for each sample. During the Lu-Hf analyses masses 172 to 180 were measured for each zircon in Faraday cup collectors, using the U-Pb collector block described above. For each analysis the required ablation time was longer then that of the U-Pb analyses in order to obtain an internal precision of ≤ 0.000040 (2σ). Thus, after the on-mass 30 seconds background measurement the ablation time generally lasted 120-150 seconds. Ablation conditions were: beam diameter 55 µm in aperture imaging mode, pulse frequency 5 Hz, and beam energy density ca. 1 J/m^2.

The isotopic ratios were calculated from the raw data by using the Nu Plasma time-resolved analysis software. The mass discrimination factor used for Hf was determined assuming $^{179}Hf/^{177}Hf = 0.7325$ and the raw data were corrected for mass discrimination using an exponential law. Correction for isobaric interferences on ^{176}Hf, ^{176}Lu and ^{176}Yb is discussed by Røhr et al. (2008). The established correction procedure used shows a good long-term stability, determined by data from reference zircons run as unknowns. Correlation between the corrected $^{176}Hf/^{177}Hf$ and $^{176}Yb/^{177}Hf$ has not been found, which indicates that systematic bias was not incurred by under- or over-correcting the interferences at $^{176}Yb/^{177}Hf \leq 0.1$ (Røhr et al. 2008).

The decay constant (λ) of ^{176}Lu used in all calculations was set to 1.867×10^{-11} a^{-1} (Söderlund et al. 2004) that is consistent with the results obtained by Scherer et al. (2001). To calculate the ε_{Hf}-values present-day chondritic $^{176}Hf/^{177}Hf = 0.282802$ and $^{176}Lu/^{177}Hf = 0.0337$ were used (Bouvier et al. 2007) and an adaption of the DM model of Griffin et al. (2000) has been adopted, with a $(^{176}Hf/^{177}Hf)_{DM}$ of 0.28325 ($\varepsilon_{Hf} = +16$) similar to that of average MORB in the time duration of 4.56 Ga from a chondritic initial Hf at $^{176}Lu/^{177}Hf_{DM} =$

0.0384 (Røhr et al. 2008). The resulting mantle evolution line is indistinguishable from the $f_{Lu/Hf} = 0.16$ (i.e. $^{176}Lu/^{177}Hf = 0.038$) curve of Vervoort and Blichert-Toft (1999).

Standard zircons mounted on a separate epoxy disk were run as unknowns at frequent intervals. These reference zircons are listed in Table 3. Data obtained from these standards over a two-year period show excellent accuracy and external reproducibility of ±0.000050 (2σ) for Mud Tank zircon, which is low in REEs, and somewhat higher standard deviation ±0.000065 (2σ) for Temora-2 zircon, which has higher and more variable Yb/Hf (Røhr et al. 2008).

3.5.3 Pb-Pb

The Pb-Pb whole-rock analyses were performed on the 9 rocks dated by in situ U-Pb analyses and further examined by Lu-Hf analyses in this study on the same LA-MC-ICPMS instrument.

Following separation of Pb from other elements using an anion exchange column (section 3.4 and Appendix) the solutions were spiked with a thallium (Tl) solution (2% HNO_3 solution containing 10ppb Tl) with $^{205}Tl/^{203}Tl$ ratio, which is used for mass-fractionation corrections (Chernyshev et al. 2007). The sample solutions were then aspirated at approximately 100µL/min through a desolvation nebulizer (DSN100) into the inductively coupled plasma source. To be able to use the SRM 981 Pb standard (25ppb Pb and 10ppb Tl) a long term calibration is required that is obtained by adjusting the values of the $^{205}Tl/^{203}Tl$ to acceptable ratios. The adjusted value is then used to correct for mass discrimination in the analysed unknowns by using an exponential law. The choice of Tl for mass discrimination correction is determined by the fact that Pb does not have stable isotopes that can be applied for correction, and even though Tl does not reproduce Pb fractionation exactly, the ratio is relatively constant. Mass 202 (for ^{202}Hg) has to be measured in order to correct for mass interference between ^{204}Pb and ^{204}Hg.

4 Results

4.1 Samples and sample localities

The samples studied were collected during the summer and fall of 2006. The sample localities are shown in Figure 3. Nine samples were used for U-Pb *in situ* zircon dating, Lu-Hf isotopic analysis and Pb-Pb whole rock isotopic determinations. Below, a brief description of the sample localities and the petrography of the sampled rocks are presented, along with a

description of zircons in the samples. In general, all the samples were quite rich in zircons, which typically had inclusions of mainly apatite and/or sphene and were yellow or brownish to transparent. Zircons in metamorphic rocks and in granites tend to have complex internal structures that reflect inheritance, recrystallisation and zircon growth. Selected zircons from the samples were imaged in BSE, and some representative images are presented below. The images were used to select the precise locations of *in situ* LA-ICP-MS analyses to determine separate ages for cores and overgrowths.

4.1.1 Granitic gneiss: sample 105-23-10

This rock is a medium to fine grained, massive, pink granitic gneiss collected in a road-cut several tens of meters from pegmatites, amphibolites, quartz veins and fault- and shear-zones that locally cross-cut the rock. Small, folded pegmatites cross-cut the 340/70 NE gneissic fabric of the host rock. No neosomes were observed in this road-cut. The main rock-forming minerals are quartz and (perthitic) K-feldspar, along with some (saussuritised) plagioclase, biotite and hornblende. There are a large number of opaque minerals, zircons, apatite, chlorite and secondary carbonate minerals present in the rock. Some myrmekite was observed. The biotite is dark, showing strong pleochroism and some places it is altered to chlorite. Zircons typically occur in the biotite and/or chlorite as inclusions surrounded by pleochroic haloes. Most of the zircon crystals are 60-150 µm in size and contain inclusions of apatites, K-feldspars and micas. Most of the crystals are subhedral or sub-rounded. The majority of the grains show regular zoning in BSE, or faint, broad zoning, but some are homogenous (Figure 6).

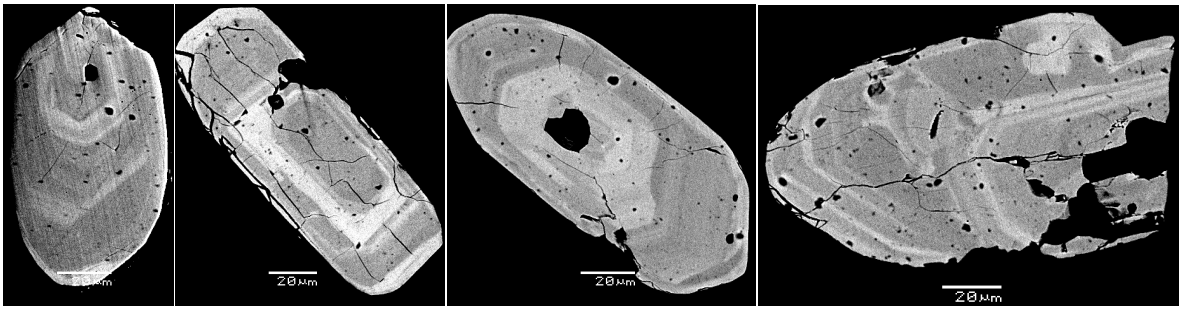

Figure 6. Zircon crystals in BSE from granitic gneiss (105-23-10)

4.1.2 Alkali feldspar granite: sample 106-23-10

This rock is a strongly penetratively deformed, medium to fine grained pink alkali feldspar granite from Spro. It has large K-feldspar phenocrysts surrounded by fine grained mineral assemblies showing mylonite like texture. The main rock-forming minerals are quartz and K-feldspar, with minor plagioclase (<10% of the total feldspar content), biotite and some

hornblende. Other minerals in minor and accessory amounts are chlorite (forming as a result of biotite alteration), muscovite, apatite, opaque minerals and zircons. The relict large feldspar grains are mainly K-feldspars, but a few large plagioclase grains, surrounded by corona-like sericite alterations, are present as well. Minor myrmekite is observed. Quartz is fine grained and forms ribbon texture in the rock. Most zircon grains (Figure 7) are subhedral and vary in size from 50 to 100 µm. In BSE the zircons area typically homogenous or faintly zoned, many of them are altered, and many contain apatite inclusions.

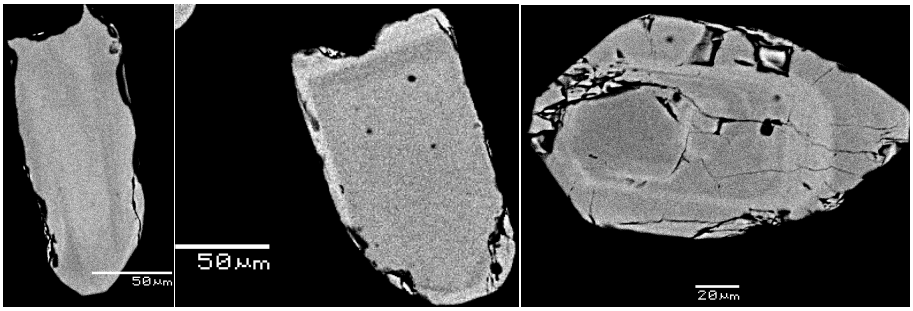

Figure 7. Zircon crystals in BSE from alkali feldspar granite (106-23-10)

4.1.3 Pegmatite: sample 102-23-10

The sample represents a pegmatite in the tonalitic gneiss described below. The pegmatites are both parallel and oblique to the gneissic fabric and do not share the fabric of the host rock, indicating that the pegmatites post-date the gneissic fabric. Attempts were also made to analyse zircons from a large pegmatite from Spro for comparison. However, zircons are rare in this particular pegmatite. One large grain was provided by the Natural History Museum, University of Oslo, wich was hihgly metamict and had large amounts of common lead, making it impossible to analyse.

The sampled pegmatite from the tonalite gneiss is medium to coarse grained and has partly sharp, and partly diffuse boundaries to its host rock. The main rock-forming minerals are microcline, quartz, plagioclase, and minor biotite and hornblende. Accessory minerals are euhedrale sphene, zircons and apatite, but clinozoisite is also present. The quartz grains have undulatory extinction. Some sericitisation of feldspars occur, along with local chlorite alteration of the bitote, and myrmekite is common. Zircon zonation is visible in plane polarized light. Most of the zircons are homogenous in BSE (Figure 8) and are ca. 60-100 µm long. In BSE, only a few grains have faint zoning, many shows extensive alteration and have inclusions of apatite and other dark minerals.

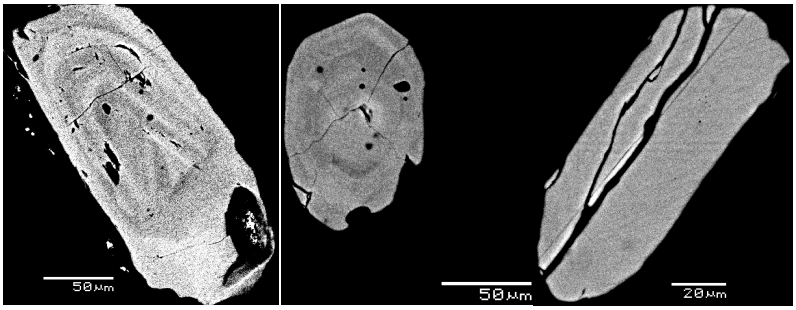

Figure 8. Zircon crystals in BSE from pegmatite (102-23-10)

4.1.4 Coarse grained granite: sample EPB-06-05

This rock is an undeformed coarse-grained granite collected in the Spro area. The main rock-forming minerals are quartz, K-feldspar and plagioclase together with biotite that is somewhat altered to chlorite. Accessory minerals are zircon, apatite, sphene and some opaque minerals. Zircons are typically subhedral or sub-rounded, 50-100 µm in size and contain inclusions of apatites and feldspars. Many of them are homogenous or show only faint, broad zoning in BSE, but grains with oscillatory zoning characteristic of magmatic zircon also occurs along with core and rim relations (Figure 9).

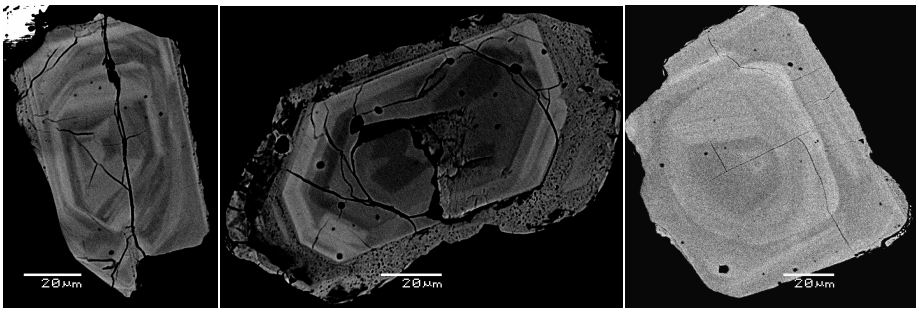

Figure 9. Zircon crystals in BSE from coarse grained granite (EPB-06-05)

4.1.5 Garnet-biotite gneiss: sample 103-23-10

This sample is a medium to coarse grained garnet-biotite gneiss of granitic composition collected from a road-cut. The 190/80 W gneissic fabric is mainly defined by biotite. The gneiss is cross-cut by an amphibolite dyke more or less parallel to the gneissic fabric. The gneiss contains some felsic pockets interpreted as neosomes. Rock-forming minerals are K-feldspar, quartz, plagioclase, biotite and garnet, with the K-feldspars (mainly microcline with micro-perthites in a few grains) and the typically poikiloblastic garnets being noticeably larger than the other minerals. Some plagioclase is altered to sericite, and intergrowth with quartz, myrmekite, also occurs (a common feature of gneisses and granites). Sphene and epidote are also present in the rock. Zircon is abundant in the rock and many of them occur as inclusions in biotite surrounded by pleochroic haloes. Most zircon grains are subhedral, with a few rounded grains. The subhedral grains are mostly long prismatic and ca. 100-150 µm in

size. Some crystals are altered and have inclusions, whereas others are faintly zoned or have chaotic inner patterns suggesting recrystallisation and alteration, but most of them are homogenous (Figure 10).

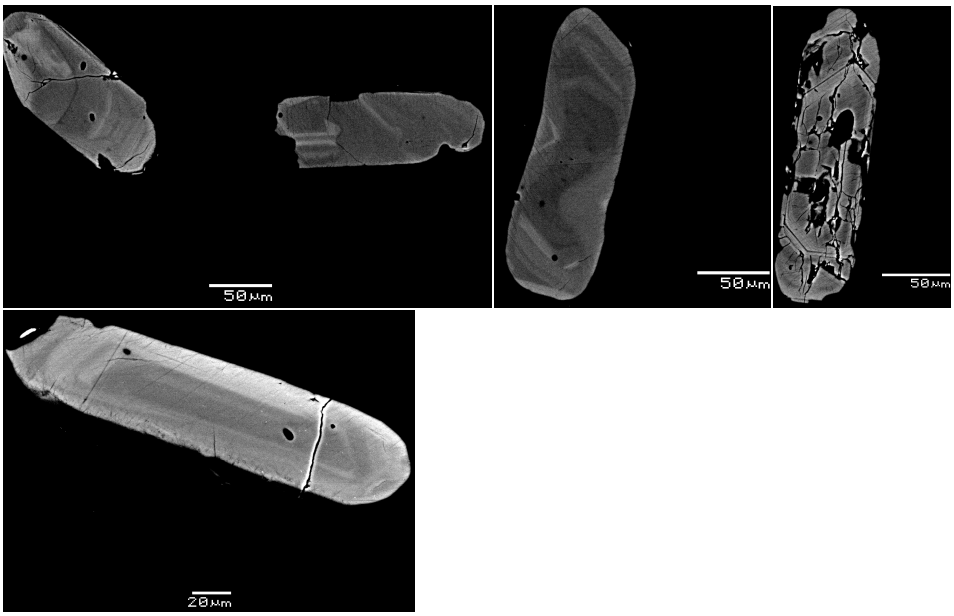

Figure 10. Zircon crystals in BSE from garnet-biotite gneiss (103-23-10)

4.1.6 Augen gneiss: sample 112-23-10

This sample is a red augen gneiss with medium to coarse grained feldspars augens, collected on the eastern part of Nesodden in the Torget area (also known as Torvet), which is outside of the main study area (Figure 3). The main rock-forming minerals are K-feldspar, quartz, plagioclase and biotite. Other accessory minerals are zircons, sphene, apatite, opaque minerals and epidote or clinosoisite along with a secondary carbonate mineral. The K-feldspars is locally microperthitic, and the plagioclase in the rock is altered to saussurite, and myrmekite is also present. The quartz grains have undulatory extinction and the biotites are strongly altered to chlorite. Zircons and sphene are euhedral to subhedral, whereas apatite is subhedral or even anhedral. Zircon grains from the sample are typically ca. 60-100 µm, with long-prismatic habit, and exhibit a faint zoning in BSE (Figure 11). Inclusions are common, and some grains are altered.

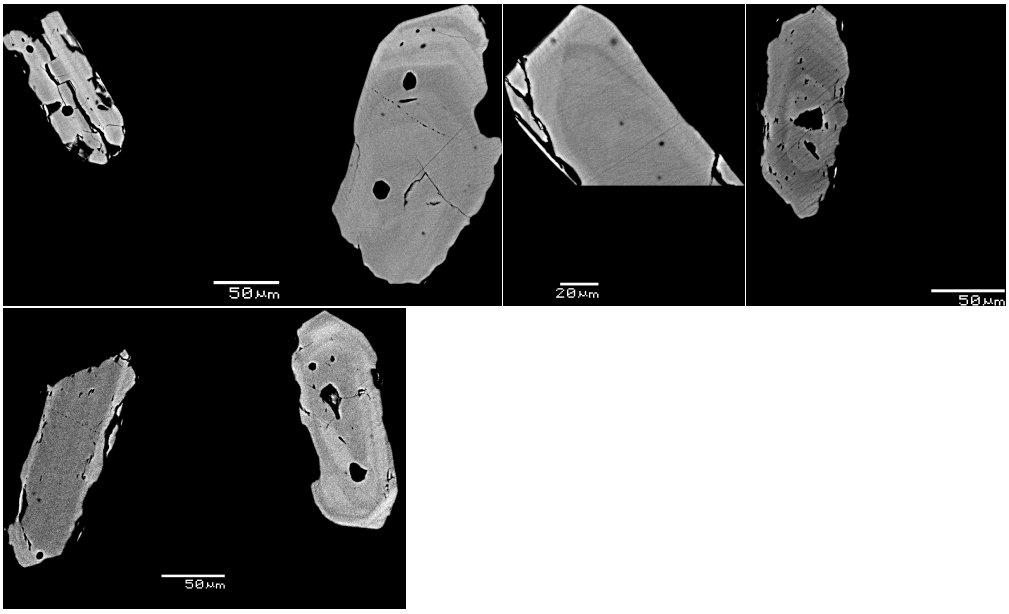

Figure 11. Zircon crystals in BSE from augen gneiss (112-23-10)

4.1.7 Fine grained granite: sample EPB-06-04

This rock is a fine grained granitic rock from the Spro area, adjacent to sample 106-23-10. At this outcrop the rocks are generally deformed and cross-cut by amphibolites that were subsequently deformed as well. It is difficult to make sense of all the deformed dykes, host-rocks and mylonites in the outcrop. The main rock-forming minerals in the sample are quartz, K-feldspar, plagioclase and biotite. Accessory minerals are zircon, apatite and sphene, and a small amount of garnet is also present. The biotite is strongly altered to chlorite. The zircon crystals in this sample are mostly homogenous, only a small number shows faint zoning in BSE (Figure 12). Several of the zircons are altered, and some are sub-rounded. Subhedral grains are typically long-prismatic and are ca. 100 and 200 µm long, i.e., somewhat larger than zircons from the other samples.

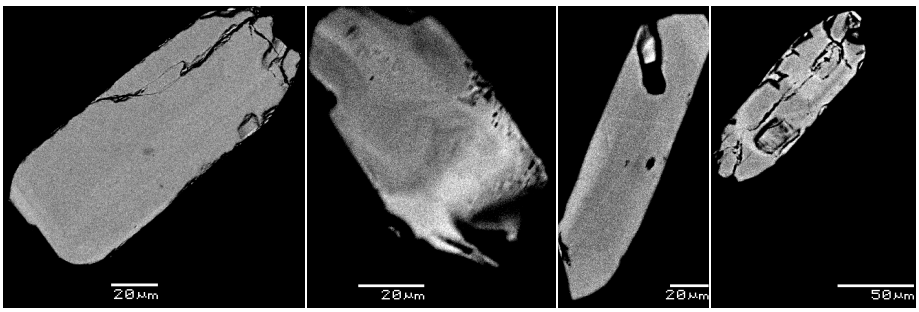

Figure 12. Zircon crystals in BSE from fine-grained granite (EPB-06-04)

4.1.8 Red granite: sample EPB-06-06

This fine grained, red granitic rock was also collected in the Spro area. The main rock-forming minerals are quartz, K-feldspar, plagioclase and biotite. The biotite is commonly

altered to chlorite. There is a fair amount of opaque minerals in the rock and other accessory minerals include zircon and apatite. The zircon crystals are at 40-100 µm in size somewhat smaller than those found in most of the studied samples. The majority of the zircons are sub-rounded and contain inclusions of e.g. apatite. They are either homogenous, or show faint zoning in BSE, however, a few crystals are subhedral to euhedral and show oscillatory zoning (Figure 13).

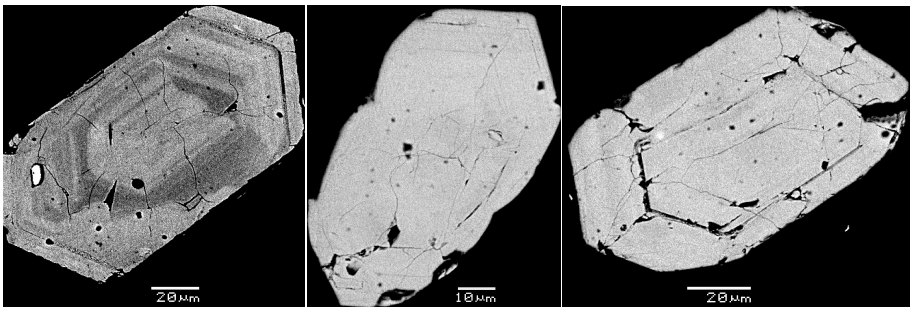

Figure 13. Zircon crystals in BSE from red granite (EPB-06-06)

4.1.9 Tonalitic gneiss: sample 101-23-10

This medium to fine grained greyish tonalitic gneiss was sampled in a road-cut at the southernmost edge of the field area. The 300/63 NE gneissic fabric is defined by biotite. Several small pegmatites intrude the tonalitic gneiss, exhibiting both sharp and diffuse boundaries to the host rock. Felsic neosomes and quartz veins are also observed in the gneiss. The neosomes indicate minor anatexis. The main rock-forming minerals in the heterogranular gneiss are plagioclase, quartz, biotite and hornblende, but some microcline can be found as well. Accessory minerals are zircon, apatite and sphene. The presence of clinozoisite, partially sericitised plagioclase and chloritized biotite indicate retrograde metamorphism. Intergrowth in plagioclase with quartz in a form of myrmekites can be seen in a few places. The quartz grain boundaries are typically embayed and the grains show undulatory extinction. Zircon inclusions in biotites surrounded by pleochroic haloes are common. Many of the zircons show zoning and they occur as inclusions in hornblende as well. Most of the zircon grains from this sample are subhedral, have numerous inclusions of apatites and about half of the studied grains are homogenous in BSE, or show faint and broad zoning, whereas the other half show regular oscillatory growth zoning, typically associated with magmatic zircon (Figure 14). Some crystals are sub-rounded, 50-150 µm in size, with no visible xenocrystic cores.

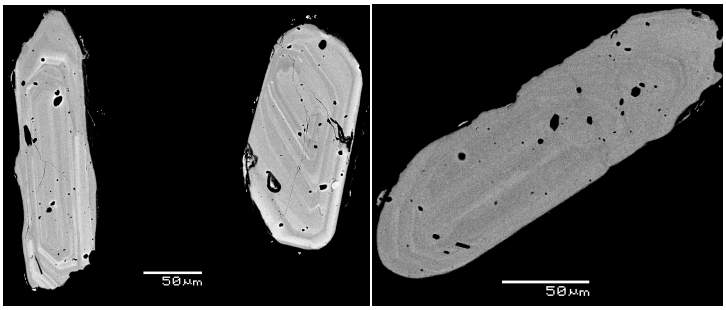

Figure 14. Zircon crystals in BSE from tonalitic gneiss (101-23-10)

4.2 U-Pb

4.2.1 Granitic gneiss: sample 105-23-10

Thirty-six zircons were analysed for U-Pb. Of these, 21 analyses containing high amounts of common lead ($^{204}Pb/^{206}Pb$ < 2000) were excluded (Table 4 in Appendix). Eight of the remaining zircons give a Concordia age of 1536 ± 5 Ma (MSWD = 0.083) (Figure 15a-II). A regression line calculated for all 15 zircons gives an upper intercept at 1515 ± 380 Ma and an unconstrained lower intercept at 1476 ± 510 Ma (MSWD = 0.58) (Figure 15a-I). Anchoring the lower intercept to 1100 ± 10 Ma yields a regression line with an upper intercept at 1518 ± 32 Ma (MSWD = 0.89) that overlaps the 1536 ± 5 Ma Concordia age. The preferred interpretation is that the Concordia age of 1536 ± 5 Ma dates crystallisation of the granite, and that the remaining analyses reflect Sveconorwegian metamorphism at around 1100 Ma.

4.2.2 Alkali feldspar granite: sample 106-23-10

Of 29 zircons 2 were excluded due to low error correlations (ρ = -0.018 and ρ = 0.293) (Table 4 in Appendix). The 27 remaining grains define a regression line with unconstrained intercepts at -270 ± 720 Ma and 1541 ± 7 Ma (MSWD = 0.51) (Figure 15b-I). A Concordia age calculated from 25 analyses yield an age of 1542 ± 5 Ma (MSWD = 1.7) (Figure 15b-II). To calculate the Concordia age, one discordant (-11.2%) analysis was excluded, along with the analysis with the highest $^{207}Pb/^{235}U$ and $^{206}Pb/^{238}U$ ages, which represents a zircon that in BSE images seems to have both a core and several inclusions and cracks. A regression line including all 27 zircons with a forced lower intercept at 0 ± 10 Ma, yield an upper intercept of 1541 ± 7 Ma (MSWD = 0.51) that is in good agreement with the Concordia age. The 1542 ± 5 Ma Concordia age is interpreted as the crystallisation age of the rock.

4.2.3 Pegmatite: sample 102-23-10

Of 35 analysed zircons 2 were discarded due to high common lead content ($^{206}Pb/^{20}Pb$ < 2000) (Table 4 in Appendix). The remaining 33 grains form a regression line (model-2 fit)

with lower and upper intercepts at 1034 ± 40 Ma and 1522 ± 46 Ma (MSWD = 7.9), respectively (Figure xc-I). The zircons form two distinct populations. The younger one contains a total of 17 analyses (white ellipses in Figure 15c-I). A Concordia age calculated from 14 of these analyses yield an age of 1051 ± 5 Ma (MSWD = 0.66) (Figure 15c-II). The 3 zircons excluded from the Concordia age calculation had the lowest $^{207}Pb/^{206}Pb$ ages and two of them were highly discordant, -15.6% and 5.9%. The 1051 ± 5 Ma Concordia age is interpreted as the emplacement age of the pegmatite.

The older group consists of 5 analyses (grey ellipses in Figure 15c-I). These have distinctly higher $^{207}Pb/^{235}U$ and $^{206}Pb/^{238}U$ ages than the other analyses from the sample, and give a Concordia age of 1531 ± 16 Ma (MSWD = 0.63). The remaining 11 analyses (yellow ellipses in Figure 15c-I) plot on a line towards the 1051 ± 5 Ma Concordia age. Anchoring all 16 points to the young Concordia age of 1051 ± 5 gives an upper intercept at 1553 ± 46 Ma (MSWD = 1.8) that overlaps with the Concordia age of the older group.

The 1531 ± 16 Ma Concordia age is interpreted to date the age of inherited zircons in the pegmatite (Figure 15c-III), and likely represents the magmatic age of its protolith. The 11 grains that plot in-between this age and the Sveconorwegian age of the pegmatite are interpreted to represent either mixing of the two age components, or Sveconorwegian lead loss in inherited zircons.

4.2.4 Coarse-grained granite: sample EPB-06-05

Of 41 zircons analysed 9 were discarded because of high contents of common lead ($^{206}Pb/^{204}Pb < 2000$) or too low error correlation ($\rho = 0.248$) (Table 4 in Appendix). The remaining 32 grains form a large cluster of concordant to slightly discordant analyses that appear to belong to two different age groups. The first group consists of 26 zircons that for the most part overlap the Concordia curve, along with a few discordant grains (white and yellow ellipses in Figure 15d-I). Of these, 21 zircons are concordant at 1537 ± 3 Ma (MSWD = 0.103) (Figure 15d-II). Together with 5 discordant zircons they define a lead loss line from an upper intercept of 1533 ± 5 Ma to an unconstrained lower intercept at 273 +200/-210 Ma (MSWD = 1.5). The upper intercept is equal to the Concordia age. Forcing the lower intercept through 290 ± 20 Ma, the estimated age of Permian magmatic and tectonic activity in the Oslo Rift (Sundvoll et al. 1990), produces an upper intercept age of 1532 ± 8.0 Ma with a slightly lower MSWD of 1.3. The 1537 ± 3 Ma Concordia age is interpreted as the emplacement age of the EPB-06-05 granite, and the discordance likely reflects Permian lead loss.

The second, older group consists of 5 analyses with slightly lower internal precision than the other analyses (grey ellipses in Figure 15d-I). Together they define a regression line with an upper intercept at 1595 +45/-30 Ma and a lower intercept at 547 +280/-260 Ma (MSWD = 1.8). Of the 5 analyses 4 yield a regression line with upper and lower intercepts of 1595 +36/-26 and 349 +310/-380 Ma (MSWD = 0.40) respectively; when anchored to 290 +20/-20 Ma the upper intercept age changes to 1591 +20/-19 Ma (MSWD = 0.31) (Figure 15d-I). The excluded point plots between the lead loss trajectories of the 1591 Ma and the 1537 Ma ages, and is interpreted to represent mixing of two different age domains in the zircon. The preferred interpretation is that this older age represents inherited zircons, affected by Permian lead loss. The oldest known event of Gothian calc-alkaline magmatism in the Norwegian part of the Kongsberg-Marstrand block is represented by a metarhyolite from Slemmestad, which has been dated to 1615 ± 31 Ma (Andersen et al. 2004a).

4.2.5 Garnet-biotite gneiss: Sample 103-23-10

Eighteen of 23 analysed zircons from the garnet-biotite gneiss give a Concordia age of 1492 ± 9 Ma (MSWD = 0.17) (Figure 15e-II). The remaining 5 analyses were discarded due to high common lead content ($^{206}Pb/^{204}Pb < 2000$; Table 4 in Appendix). The 1492 ± 9 Ma Concordia age is interpreted as the crystallisation age of the garnet-biotite gneiss, but minor Sveconorwegian lead loss may lead to a slight underestimation of the real age of the gneiss.

4.2.6 Augen gneiss: sample 112-23-10

Of 22 zircon analyses 2 were discarded because of high common lead content ($^{206}Pb/^{204}Pb < 2000$) (Table 4 in Appendix). A Concordia age calculated from the remaining 20 data points give an age of 1504 ± 7 Ma (MSWD = 0.67) (Figure 15f-II). The same analyses define a poorly constrained regression line with an upper intercept at 1496 ± 50 Ma (MSWD = 0.12) that overlaps with the Concordia age (Figure 15f-I), and a lower intercept at 1133 ± 670 Ma. A constrained lower intercept at 1100 ± 10 Ma results in a regression line with an upper intercept at 1497 ± 39 Ma (MSWD = 0.117), which is in good agreement with the calculated Concordia age of 1504 ± 7 Ma. As with the previous sample, the coincidence of the lower intercept with the Sveconorwegian event is suggestive of minor lead loss at this time. The preferred interpretation is that the crystallisation age of the Torget augen gneiss is 1504 ± 7 Ma. If, on the other hand, the data reflect minor Sveconorwegian lead loss, the maximum age of the gneiss is constrained by the 1497 ± 39 Ma age.

4.2.7 Fine grained granite: sample EPB-06-04

A total of 26 zircons were analysed, of which 3 were discarded because of high common lead content ($^{206}Pb/^{204}Pb < 2000$) and 2 due to low error correlations ($\rho = 0.045$ and $\rho = -0.019$) (Table 4 in Appendix). A further 8 zircons, 2 with the highest $^{207}Pb/^{206}Pb$ ages and 6 with the lowest $^{207}Pb/^{206}Pb$ ages were excluded for the Concordia age calculations. A group of 13 zircons give a Concordia age of 1503 ± 7 Ma (MSWD = 1.5) (Figure 15g-II).

A regression line calculated for all zircons, a total of 21 grains that for the most part overlap the Concordia curve, gives an upper intercept at 1468 ± 61 Ma and a unconstrained lower intercept at 1219 ± 440 Ma (MSWD = 0.120) (Figure 15g-I). Forcing the lower intercept through 1100 ±10 Ma yields an upper intercept at 1474 ± 34 Ma (MSWD = 0.13) that overlaps with the Concordia age of 1503 ± 7 Ma. The preferred interpretation is that the Concordia age gives the best estimate for the emplacement age of the rock, whereas the unconstrained and constrained lower intercepts resulting in an overlapping age with the 1503 ± 7 Ma Concordia age reflect Sveconorwegian lead loss.

4.2.8 Red granite: sample EPB-06-06

Of 29 zircons analysed 17 were discarded due to high common lead content ($^{206}Pb/^{204}Pb < 2000$), and 1 because of low error correlations ($\rho = -0.078$) (Table 4 in Appendix). The remaining 11 zircons have $^{206}Pb/^{204}Pb$ in the range 2305 and 8032, and were corrected for common lead using Stacey-Kramers model for common lead composition at 1.5 Ga, i.e., $^{206}Pb/^{204}Pb = 18.7$, $^{207}Pb/^{204}Pb = 15.628$ and $^{208}Pb/^{204}Pb = 38.63$ (Stacey and Kramers 1975). These zircons define a regression line with an upper intercept at 1494 +21/-18 Ma and an unconstrained lower intercept at 494 +110/-110 Ma (MSWD = 0.36) (Figure 15h-I). The upper intercept overlaps with a Concordia age of 1493 ± 11 Ma (MSWD = 0.096) (Figure 15h-II) calculated for the 6 analyses with the highest $^{207}Pb/^{206}Pb$ ages. The 1493 ± 11 Ma Concordia age is interpreted as the best estimate for the emplacement of the fine grained N-Spro granite. The imprecise, unconstrained lower intercept overlaps with the age of the Caledonian orogeny.

4.2.9 Tonalitic gneiss: sample 101-23-10

Of 19 zircons 10 give a Concordia age at 1495 ± 5 Ma (MSWD = 1.11) (Figure 15i-II). Reference lines drawn between 1495 and 0 and between 1495 and 1100 (Figure 15i-I) show possible lead loss lines for the sample. The preferred interpretation is that the 1495 ± 5 Ma Concordia age is the crystallisation age of the tonalitic gneiss. The remaining analyses are

interpreted to reflect a combination of Sveconorwegian influence and resent lead loss. Inherited zircons from a Sveconorwegian pegmatite hosted by the tonalitic gneiss (102-23-10; Figure 15c-II) gave an age of 1531 ± 36 Ma, overlapping with the 1495 ± 5 Ma age of the tonalitic gneiss. The data is thus compatible with a local origin of the pegmatite. The slightly younger age of the tonalitic gneiss may reflect the effect of unresolved Sveconorwegian lead loss and/or zircon growth.

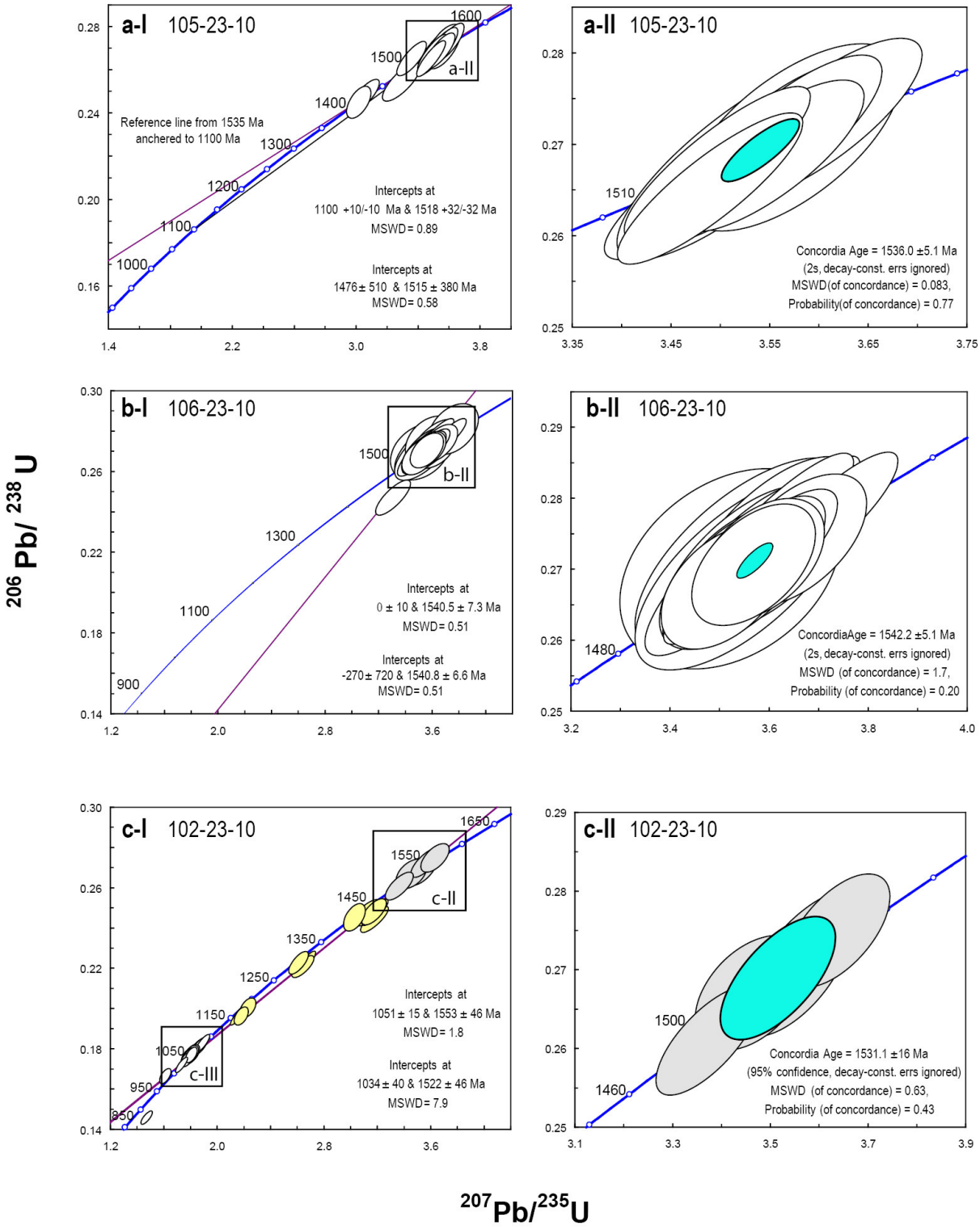
a-I 105-23-10
Reference line from 1535 Ma
anchered to 1100 Ma
Intercepts at
1100 +10/-10 Ma & 1518 +32/-32 Ma
MSWD= 0.89
Intercepts at
1476± 510 & 1515 ± 380 Ma
MSWD= 0.58
a-II 105-23-10
Concordia Age = 1536.0 ±5.1 Ma
(2s, decay-const. errs ignored)
MSWD(of concordance) = 0.083,
Probability(of concordance) = 0.77
b-I 106-23-10
Intercepts at
0 ± 10 & 1540.5 ± 7.3 Ma
MSWD= 0.51
Intercepts at
-270± 720 & 1540.8 ± 6.6 Ma
MSWD= 0.51
b-II 106-23-10
ConcordiaAge = 1542.2 ±5.1 Ma
(2s, decay-const. errs ignored)
MSWD (of concordance) = 1.7,
Probability (of concordance) = 0.20
c-I 102-23-10
Intercepts at
1051± 15 & 1553 ± 46 Ma
MSWD= 1.8
Intercepts at
1034± 40 & 1522 ± 46 Ma
MSWD= 7.9
c-II 102-23-10
Concordia Age = 1531.1 ±16 Ma
(95% confidence, decay-const. errs ignored)
MSWD (of concordance) = 0.63,
Probability (of concordance) = 0.43
206Pb/238U
207Pb/235U

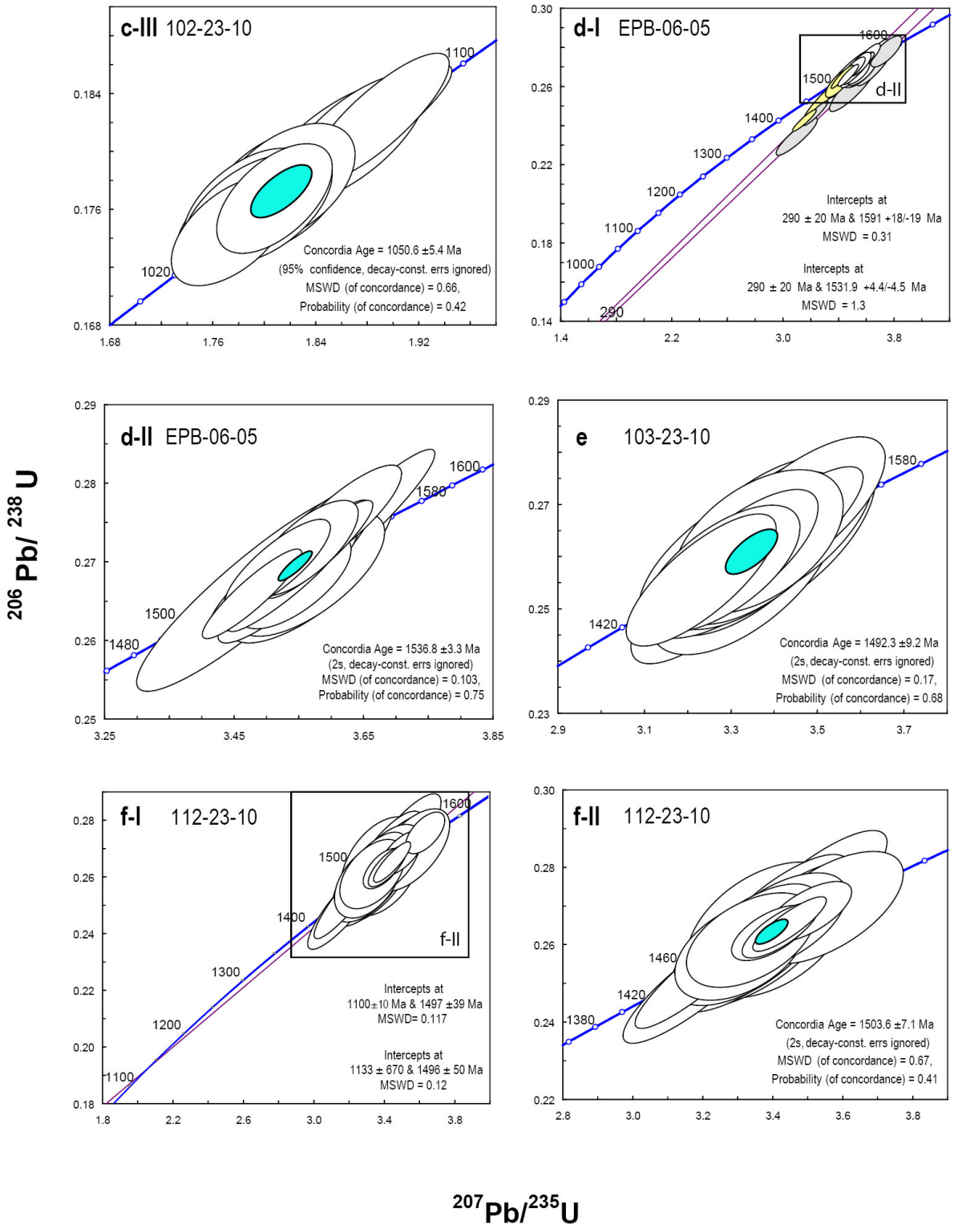
c-III 102-23-10
1100
1020
Concordia Age = 1050.6 ±5.4 Ma
(95% confidence, decay-const. errs ignored)
MSWD (of concordance) = 0.66,
Probability (of concordance) = 0.42
d-I EPB-06-05
1600
1500
d-II
1400
1300
1200
1100
1000
290
Intercepts at
290 ± 20 Ma & 1591 +18/-19 Ma
MSWD = 0.31
Intercepts at
290 ± 20 Ma & 1531.9 +4.4/-4.5 Ma
MSWD = 1.3
d-II EPB-06-05
1600
1580
1500
1480
Concordia Age = 1536.8 ±3.3 Ma
(2s, decay-const. errs ignored)
MSWD (of concordance) = 0.103,
Probability (of concordance) = 0.75
e 103-23-10
1580
1420
Concordia Age = 1492.3 ±9.2 Ma
(2s, decay-const. errs ignored)
MSWD (of concordance) = 0.17,
Probability (of concordance) = 0.68
f-I 112-23-10
1600
1500
1400
f-II
1300
1200
1100
Intercepts at
1100±10 Ma & 1497 ±39 Ma
MSWD= 0.117
Intercepts at
1133 ± 670 & 1496 ± 50 Ma
MSWD = 0.12
f-II 112-23-10
1460
1420
1380
Concordia Age = 1503.6 ±7.1 Ma
(2s, decay-const. errs ignored)
MSWD (of concordance) = 0.67,
Probability (of concordance) = 0.41
$^{206}Pb/^{238}U$
$^{207}Pb/^{235}U$

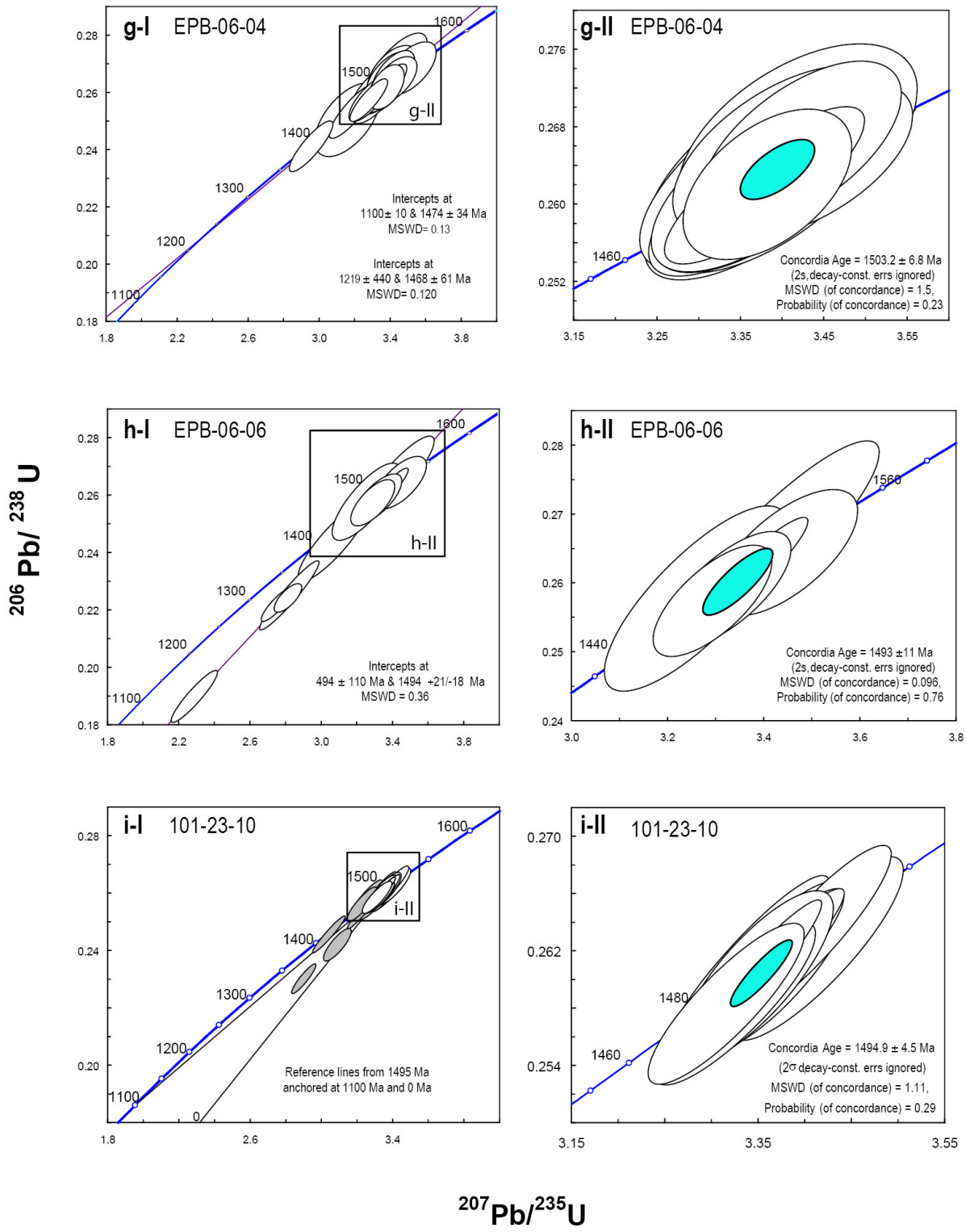

Figure 15a-i. Concordia diagrams for the 9 samples. Error ellipses are shown at ±2σ. For detailed discussion see text.

4.3 Lu-Hf

The LA-MC-ICPMS Lu-Hf isotope data were collected from 220 zircons that were previously dated by in situ U-Pb analyses, and 2 grains not analysed for U-Pb (sample 105-23-10,

number 11 and 17). The analytical data are listed in Table 5 (Appendix), including $^{176}Hf/^{177}Hf$, $^{176}Lu/^{177}Hf$ and $^{176}Yb/^{177}Hf$ for individual analyses, and time-corrected $^{176}Hf/^{177}Hf$ ratios (i.e., the ratio recalculated from the measured Lu in the zircon and its U-Pb age).

Zircons typically have Lu/Hf ratios between 0.0016 and 0.034 (Faure and Mensing 2005), as do the studied samples where the ratios range from 0.00038 to 0.00582 (Table 5 in Appendix). Within this span, 5 zircons from samples EPB-06-05 and EPB-06-06 exhibit the highest Lu/Hf ratios, followed by a small group of zircons with Lu/Hf ratios from 0.002 to 0.0027. The zircons from the Sveconorwegian pegmatite (102-23-10) have the lowest Lu/Hf ratios, ranging from 0.00038 to 0.00109, which points to a highly evolved (crustal) source.

The data are illustrated in $^{176}Lu/^{177}Hf$ vs. $^{176}Hf/^{177}Hf$ diagrams where each analysis is represented by an error box showing the internal analytical uncertainty (±1σ) (Figure 16a-i). Reference isochrons plotted in the diagrams show the expected trend of $^{176}Hf/^{177}Hf$ from *in situ* radiogenic accumulation since the crystallization age. To create the reference lines the U-Pb age of the samples and a convenient $^{176}Hf/^{177}Hf$ initial ratio were used together with the decay constant of Lu (i.e. λ=0.0186). Analyses plotting above or below the main trend of the data as visualized by the reference lines suggest more juvenile and evolved (crust) components, respectively. The main group of zircons, representing the 1500-1540 Ma rocks, including inherited zircons from the Sveconorwegian pegmatite, have $^{176}Hf/^{177}Hf$ from 0.28191 to 0.28207. The Sveconorwegian zircons from the pegmatite, and a few older zircons (that likely have Sveconorwegian overgrowths), have higher $^{176}Hf/^{177}Hf$ ratios, ranging from 0.28208 to 0.2822, compatible with two different zircon populations in the studied rocks.

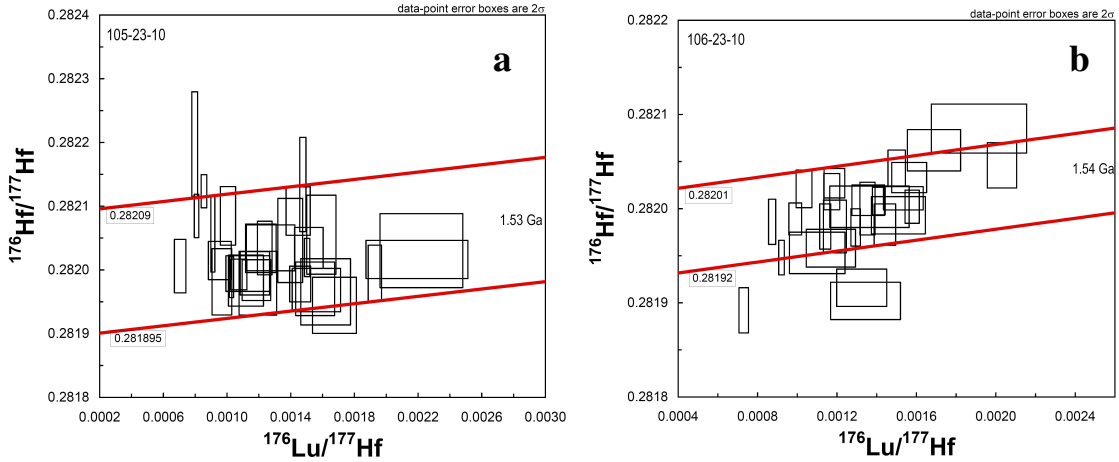

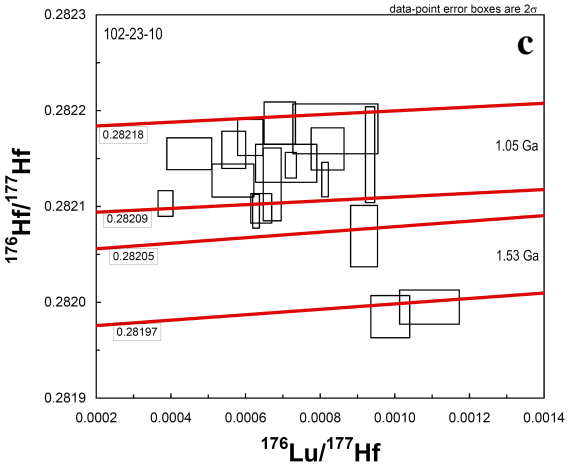
data-point error boxes are 2σ
102-23-10
c
1.05 Ga
1.53 Ga
0.28218
0.28209
0.28205
0.28197
$^{176}Hf/^{177}Hf$
$^{176}Lu/^{177}Hf$

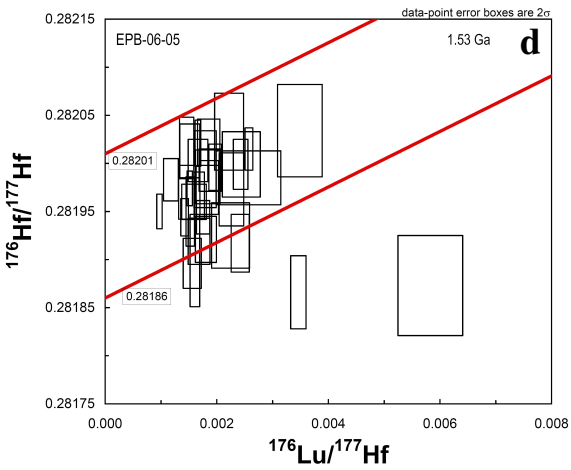
data-point error boxes are 2σ
EPB-06-05
1.53 Ga
d
0.28201
0.28186
$^{176}Hf/^{177}Hf$
$^{176}Lu/^{177}Hf$

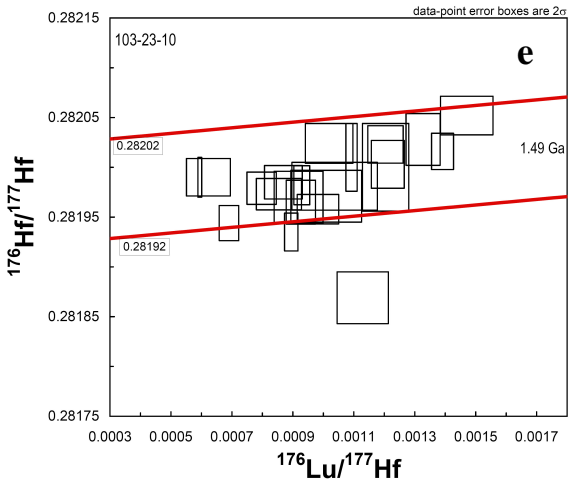
data-point error boxes are 2σ
103-23-10
e
1.49 Ga
0.28202
0.28192
$^{176}Hf/^{177}Hf$
$^{176}Lu/^{177}Hf$

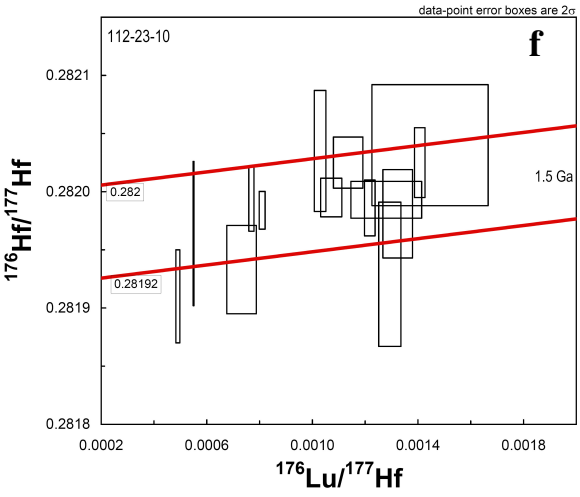
data-point error boxes are 2σ
112-23-10
f
1.5 Ga
0.282
0.28192
$^{176}Hf/^{177}Hf$
$^{176}Lu/^{177}Hf$

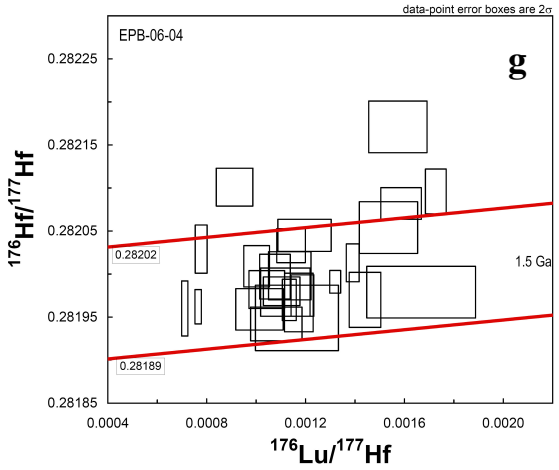
data-point error boxes are 2σ
EPB-06-04
g
1.5 Ga
0.28202
0.28189
$^{176}Hf/^{177}Hf$
$^{176}Lu/^{177}Hf$

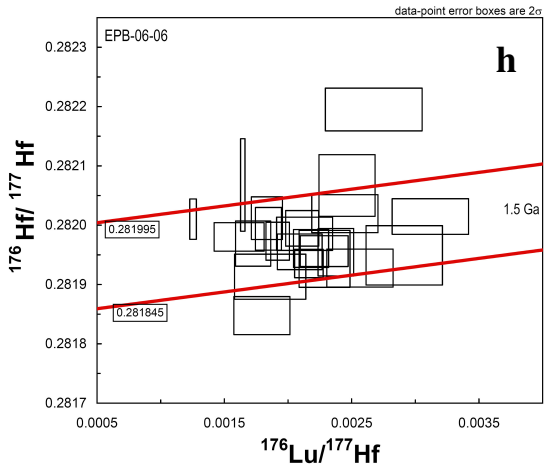
data-point error boxes are 2σ
EPB-06-06
h
1.5 Ga
0.281995
0.281845
$^{176}Hf/^{177}Hf$
$^{176}Lu/^{177}Hf$

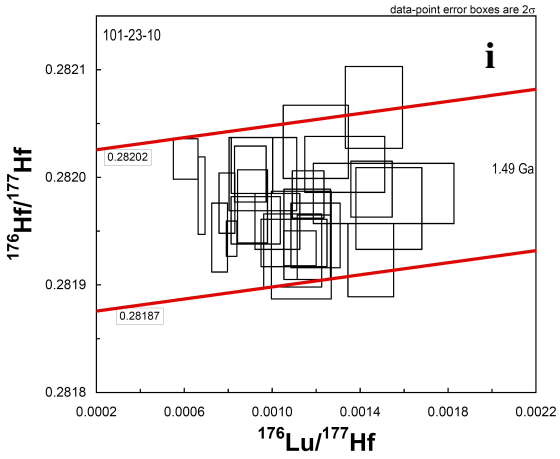

Figure 16a-i. Lutetium-hafnium correlation diagrams showing the present-day variations in $^{176}Hf/^{177}Hf$ vs. $^{176}Lu/^{177}Hf$. The error boxes show the analytical uncertainties. a) 105-23-10, granitic gneiss b) 106-23-10, alkali feldspar granite c) 102-23-10, pegmatite d) EPB-06-05, coarse-grained granite e) 103-23-10, garnet-biotite gneiss f) 112-23-10, augen gneiss g) EPB-06-04, fine-grained granite h) EPB-06-06, red granite i) 101-23-10, tonalitic gneiss.

It is useful to illustrate the total variation of the time-corrected initial $^{176}Hf/^{177}Hf$ ratios (Hf_i) in an accumulated probability plot with histogram plot (Figure 17). The main peak in the plot, with Hf_i ranging from 0.28185 to 0.28205, mainly represents zircons from the ca. 1500-1540 Ma rocks. The second, smaller peak from 0.28205 to 0.28218 mainly contains zircons from the Sveconorwegian pegmatite. A few analyses from the pegmatite plot within the larger peak, and correspond to older, inherited zircons. Also, a few analyses from the older rocks plot within the smaller peak, likely representing secondary Sveconorwegian zircon growth on Mesoproterozoic zircons.

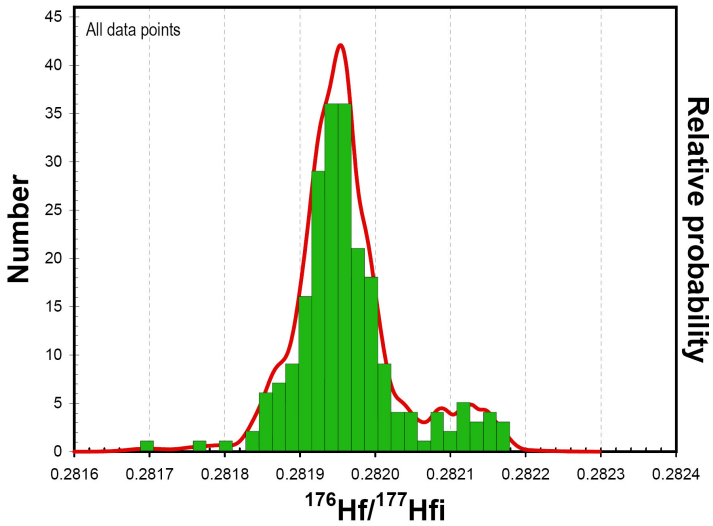

Figure 17: Accumulated probability plot with histogram plot for all analysed zircons. In the diagram, the histogram for time-corrected initial $^{176}Hf/^{177}Hf$ ratios (Hf_i) is enclosed within a Gaussian curve that includes the errors for each measurement.

Another useful way to evaluate the data is to plot it in a linear probability diagram with a regression line. In Figure 18, most of the data (plotted with 1σ error bars) conform to a normal distribution along a linear trend, illustrating the similarities in initial Hf between the ca. 1500-1540 Ma zircons from the different rock types. These roughly coeval rocks are from a relatively small geographical area and may thus be related, and/or reflect similar settings of formation. The outliers towards higher initial Hf ratios correspond to Sveconorwegian zircons and overgrowths (105-23-10:07, 10, 31, 72 (11 and 17), EPB-06-04:24, 26, 62, 75 and EPB-06-06:51). In the plot, three grains plot towards significantly lower initial Hf ratios (EPB-06-05:01, 36, and EPB-06-06:41). These zircons have $^{206}Pb/^{204}Pb$ ratios <2100 (Table 4 in Appendix), but do not have older U-Pb ages than the Concordia ages of their respective host rocks. The data can reflect inherited older zircons, and/or a more evolved (crustal) source. Probability plots created for each sample separately show similar patterns (Appendix).

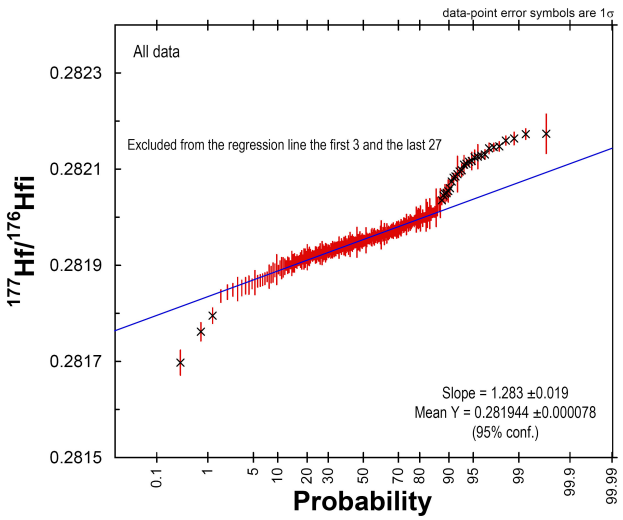

Figure 18: Linear probability plot showing all zircon analyses with 1σ error bars. If the data represent a suite that conforms to a normal distribution, the data points will define a (regression) line. Three zircons at the lower end and 27 at the upper end of the probability limit deviate from the normal trend. These outliers are crossed over, illustrating that they are not included when calculating the regression line. Analyses in the upper end of the probability limit represent samples EPB-06-04 and 105-23-10 with 4 and 6 zircons, respectively, whereas sample EPB-06-06 has one zircon at each end of the probability limit. The two other analyses at the lower end of the probability limit are from sample EPB-06-05. However, most of the zircons (16 st) deviating from the normal trend are from the pegmatite (102-23-10), and represent Sveconorwegian zircon growth, as opposed to the Mesoproterozoic zircons that form the normal trend. The remaining zircons above the trend line are similarly interpreted to represent Sveconorwegian zircon and variable contributions of the older component, compatible with rim and core relations.

The Hf isotope data for 222 zircons, arranged by age and rock type, are plotted in Hf_i vs. age ($^{207}Pb/^{206}Pb$) diagrams in Figure 19a-b, along with published data from the Southwest Scandinavian Domain (Andersen et al. 2002a, Andersen et al. 2004a, Andersen et al. 2006). The green reference lines show the evolution of the Hf isotopic ratio in the depleted mantle

with time (Griffin et al. 2000), and the blue reference lines represent the evolution of the ratio in CHUR (Bouvier et al. 2007). The red reference lines illustrate the path the Hf isotopic ratio would have evolved in the rock from which the analysed zircons formed, at a specific $^{176}Lu/^{177}Hf$ ratio. Since zircons have very low Lu/Hf ratios, extrapolating a reference line from a zircon to the DM growth curve using the zircons Lu/Hf ratio yields a nearly horizontal line, giving a minimum age for the crustal residence time of the Hf in the zircon, i.e., the zircon model-age (t_{DMz}) (Andersen et al. 2002a). However, since the crystallization ages of the zircons are known it is possible to get a more realistic model age for the host rock of the zircons, by forcing a growth curve through the zircon initial ratio with Lu/Hf ratio corresponding to the whole rock. When whole-rock concentration data are not available, as is the case for this study, a $^{176}Lu/^{177}Hf = 0.01$ for granites and $^{176}Lu/^{177}Hf = 0.015$ for an average crustal reservoir (Griffin et al. 2002, Andersen et al. 2002a) may be used. The obtained model-age (whole-rock model age, t_{DMw}) represents the time when the Hf in the zircon last was in isotopic equilibrium with the global depleted mantle reservoir (Andersen et al. 2002a).

The zircons in most samples have a range of Hf_i ratios well outside the analytical uncertainties (±1.5-2 ε-units). Such ranges in ε_{Hf} values are quite common in granites (Griffin et al. 2002, Andersen et al. 2002a) and suggest that the magma was heterogeneous with contributions from isotopically distinct sources. If magma homogenization is slower than crystallization of the zircons, different parts of the crystals may sample different domains of the heterogeneous magma. Samples 101-23-10, 103-23-10, 106-23-10, 112-23-10 and EPB-06-04 all have a moderate range of 5-6 ε_{Hf} units, and all plot above CHUR. Samples 105-23-10, EPB-06-05 and EPB-06-06 have much larger ranges in ε_{Hf}, from 9 to 11 units, suggesting mixing of different magma sources. Some of the analyses plot on the DM reference line, indicating a juvenile component. The EPB-06-06 sample, along with samples 102-23-10, 103-23-10 and EPB-06-05 contain zircons that plot on the CHUR line, suggesting a less depleted average source, or mixing of DM and crustally derived components.

Sveconorwegian zircons from the pegmatite show a moderate ε_{Hf} range from -2 to 4, compatible with a crustal source (e.g., anatexis of the host rock). The inherited zircons in the pegmatite plot above CHUR, and in one case on the DM line, suggesting juvenile crust formation from a depleted mantle source, and also show a moderate ε_{Hf} range of 6.

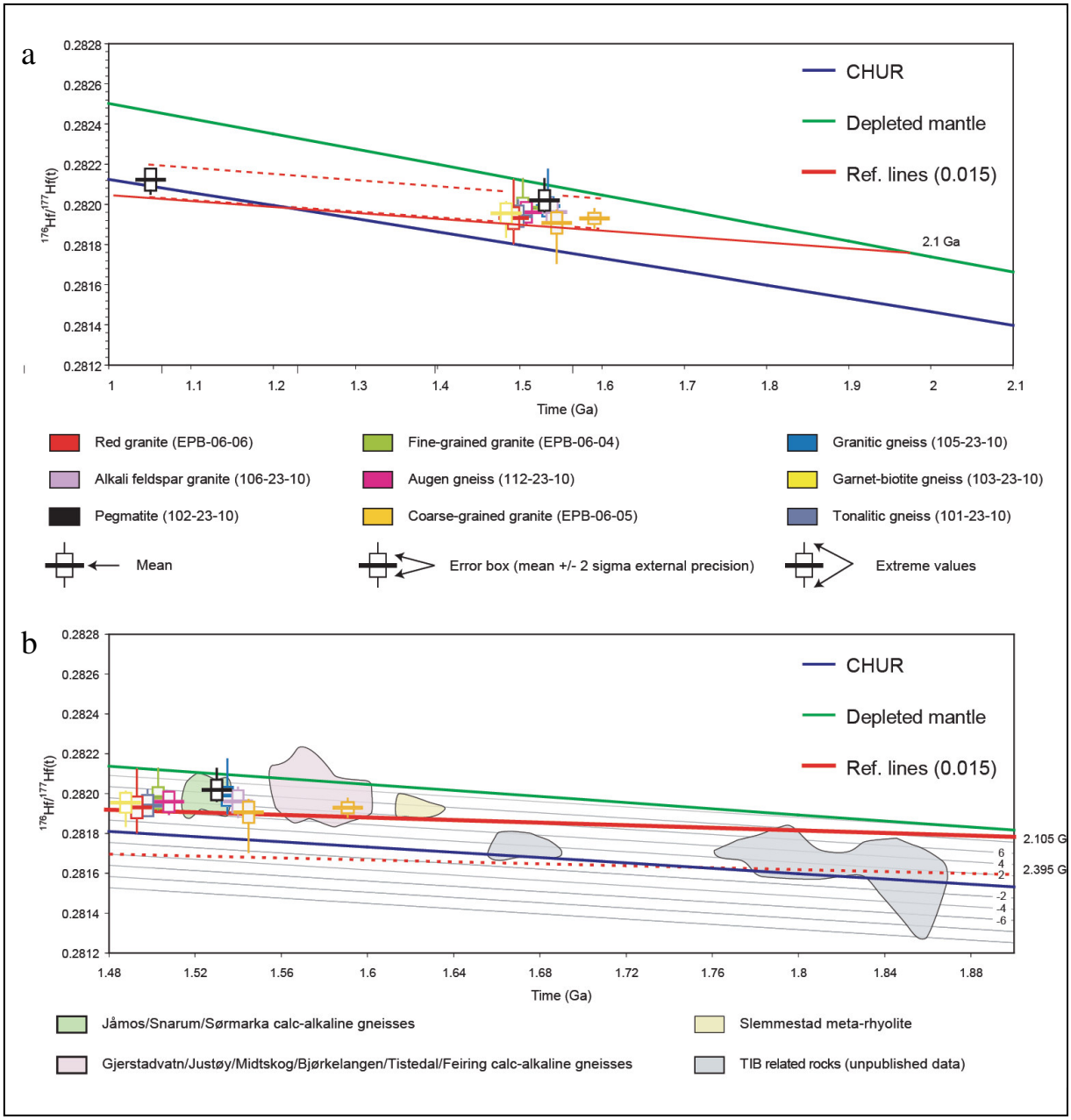

Figure 19a, b. Time-corrected initial $^{176}Hf/^{177}Hf$ ratio vs. time (Ga) diagrams illustrating the initial Hf isotopic composition of zircons at the time of crystallization. The Hf isotope data from Table 5 were recalculated to crystallization ages using data from Table 4 (Appendix). Reference data: DM from Griffin et al. (2000); CHUR from Bouvier et al. (2007); ranges of Hf isotopic composition for 1.5-1.6 Ga calc-alkaline gneisses and related rocks and of TIB and TIB equivalent rocks from Andersen et al. 2002a, 2004a, 2006 and unpublished data from T. Andersen.

4.4 Pb-Pb and multi-stage U-Th-modelling

Isotopic Pb compositions from 9 whole-rock samples are listed in Table 6 (Appendix). The present day $^{206}Pb/^{204}Pb$, $^{207}Pb/^{204}Pb$ and $^{208}Pb/^{204}Pb$ ratios vary widely, from 17.282 to 29.586, from 15.487 to 16.414 and from 36.901 to 45.912, respectively. The Pb data do not yield isochrons, but form a rough linear array when plotted in a $^{206}Pb/^{204}Pb$ vs. $^{207}Pb/^{204}Pb$ diagram,

except for one sample (112-23-10) that plots under the array. In a $^{206}Pb/^{204}Pb$ vs. $^{208}Pb/^{204}Pb$ diagram the data scatter somewhat, yielding two linear arrays near each other, again with the exception of 112-23-10. This indicates that the lead was isotopically heterogeneous at the time of crystallization. The considerably larger scatter in the data in the $^{206}Pb/^{204}Pb$ vs. $^{208}Pb/^{204}Pb$ diagram implies widely variable Th/U ratios. Sample 112-23-10 plots well below the two arrays in the diagram, indicating a significant disturbance of the system (possible U mobility) that occurred after emplacement of the rock. The Pb isotope composition of 112-23-10 is compatible with that of the Sveconorwegian pegmatite (102-23-10) and its host rock (101-23-10).

A three-stage model of the Pb isotopic evolution (Andersen 1998 and references therein) was applied using the PBI-Excel program (Andersen 1998) to better understand the geological environments where the Pb has evolved in the past and to get an indication of possible magma sources (Figure 20, 21). In the three-stage model, the first-stage is constrained by the age of the earth (t_0 = 4.57 Ga, Faure and Mensing 2005 and references therein) and by the time of separation (t_1 = 2.1 Ga) from the first reservoir, i.e. the protolith age, which is estimated from the Lu-Hf protolith ages (section 4.3). During the first-stage, the Pb evolved in a depleted mantle environment characterized by a μ_1-value of 7.9 and by a $\kappa_1 = 4$ from initial meteoric Pb composition (Tatsumoto et al. 1973). The second-stage is constrained by t_1 and t_2, where the latter is the emplacement age of the rocks (t_2 = 1.53 Ga). The Pb in the samples evolved in different reservoirs during the second-stage, with μ_2-values ranging from 10 to 16 and a κ_2-value of 4. A different t_2 age was used to constrain the second-stage for sample 112-23-10, since it can only be made to fit the model isochron using a Sveconorwegian age. Thus, t_2 was set to 1050 Ma, the best estimate for the age of metamorphism of the rock (see section 4.2), and which is also the age of the pegmatite (102-23-10) and metamorphism of its host rock (101-23-10). All these three samples plot on a line (Figure 20, 21). This indicates a reservoir with a μ_2-value of 13 and $\kappa_2 = 4$. The final stage represents the time from the last homogenization of Pb until present. The Pb in the different samples evolved in different reservoirs with μ_3-values ranging from 33 to 70 and κ_3-values ranging from 2.5 to 4. For sample 112-23-10 the third-stage represents a reservoir characterized by a μ_3-value of 70 and a κ_3-value of 0.5.

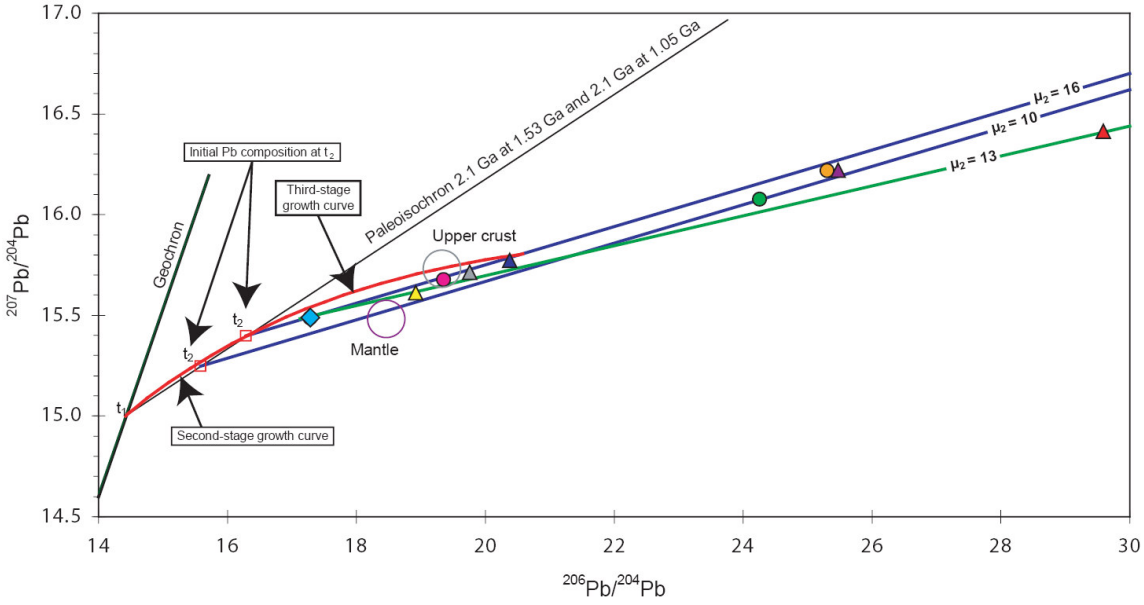

Figure 20. $^{206}Pb/^{204}Pb$ vs. $^{207}Pb/^{204}Pb$ diagram illustrating the three-stage model evolution applied to all samples. The black and blue lines illustrate the three-stage evolution of 8 of the 9 analysed samples (μ_1=7.9, t_1=2.1 Ga, μ_2 varying between 10 and 16 and t_2=1.53 Ga). The black and green lines illustrate the three-stage evolution of the ninth sample (112-23-10: augen gneiss; μ_1=7.9, t_1=2.1 Ga, μ_2=13 and t_2=1.05 Ga).

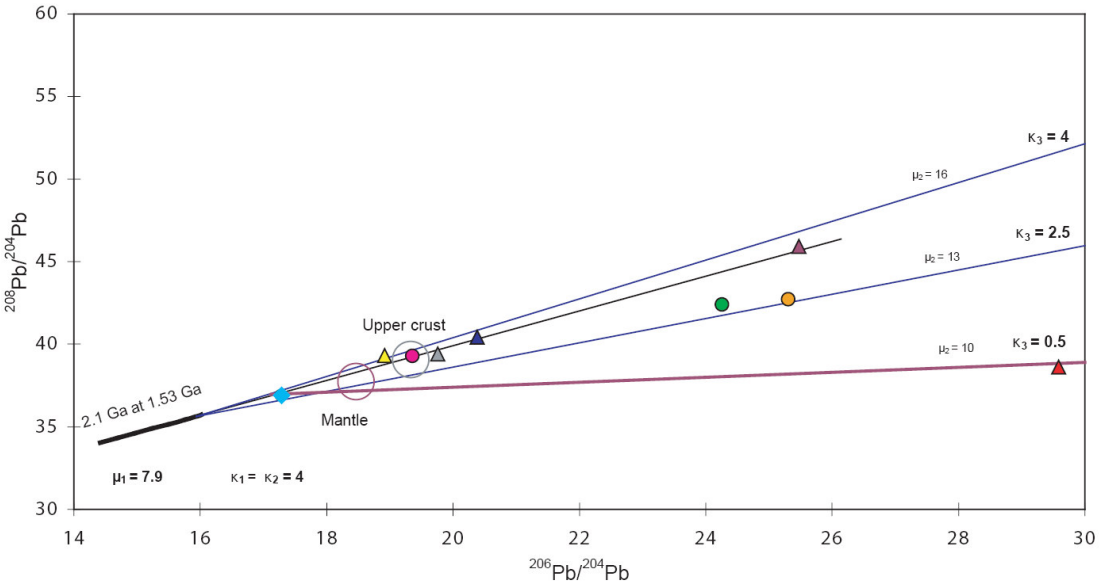

Figure 21. $^{206}Pb/^{204}Pb$ vs. $^{208}Pb/^{204}Pb$ diagram illustrating the three-stage model for thorogenic Pb. Symbols as in Figure 20, see text in section 4.4 for detailed description.

5 Discussion

5.1 The age of magmatism and metamorphism on the Nesodden Peninsula

The Nesodden Peninsula consists of various ortho- and paragneisses along with granites, amphibolites and diabase dykes. The rocks testify to a complex geological evolution, which until now has been poorly constrained. The U-Pb ages obtained in this study confirm

Mesoproterozoic magmatism in the area, yielding emplacement ages at 1.54-1.53 Ga for foliated granites and granitic gneisses (Figure 15a-d), and slightly younger emplacement ages at 1.50-1.49 Ga for a second group of granitic and tonalitic rocks (Figure 15e-i). Sparse inherited zircons in the coarse grained 1.54 Ga granite (EPB-06-05) yield an age of 1591 +20/-19 Ma. The remaining Mesoproterozoic rocks do not contain inherited zircons, suggesting either predominantly juvenile magma sources, or a paucity of zircon in the hypothetical crustal component, or zircon dissolution in the magmas. The youngest age was obtained for a 1050 Ma granitic pegmatite. Inherited zircons in the pegmatite yield a Concordia age of 1531 ± 16 Ma. This age is slightly older than that of the 1.49 Ga host rock, but is similar to that of older gneisses and granites in the area, and is consistent with anatexis of these rocks as the magma source. This interpretation is further supported by Hf data from the inherited zircons in the pegmatite (see below), which show a time-corrected range that match that of several of the sampled rocks in the area, but seems less compatible with the more evolved Hf_i ratio of the host rock. It is interesting to note that the granitic gneiss (105-23-10) adjacent to the host rock tonalite gneiss not only provides the closest match in terms of geography, age and Hf isotope ratios, but also shows the most pronounced Sveconorwegian zircon growth (as determined from the Hf signature, see section 5.3). Neosomes suggestive of anatexis are locally present in most gneisses in the area, including the tonalitic host rock, but are absent from the exposed granitic gneiss suggested as the source of the pegmatite. All the same, anatexis of the granitic gneiss is suggested as a likely source of the pegmatite. The dated pegmatite is one of several in the exposed host rock; the pegmatites are either parallel to the gneissic fabric of the host rock, or cross cut it at a high angle. Though the pegmatites locally are folded, they do not share the gneissic fabric themselves, hence they constrain the age of the gneissic fabric and the folding to pre- and post 1050 Ma, respectively.

The partly discordant U-Pb data from the Mesoproterozoic rocks have lower intercepts in the Sveconorwegian, Permian and recent sectors of the Concordia curve, suggesting Pb-loss and/or zircon growth at these times. The ca. 1100 Ma intercepts correlate to the regionally important Sveconorwegian orogeny, and local anatexis and pegmatite emplacement in the area (this study). The Permian intercept correlates to magmatic activity in the Oslo Rift area at ca. 290 Ma (Sundvoll et al. 1990). In contrast, zircons from the garnet-biotite gneiss do not seem to be affected by the geological events in the area following emplacement at 1492 Ma.

5.2 Magma sources

The creation of the Earth's crust is an ongoing process that started with the formation of the planet (Condie 2005). Over time, the felsic components that make up the crust have been extracted from the mantle, and today melting of the mantle and re-melting of the crust represents the two end-member sources of magmas. Studies of Lu/Hf and $^{176}Hf/^{177}Hf$ ratios allow the identification of juvenile (mantle) and/or evolved (crust) components in a rock, the constraining of possible crustal sources, and gauging of the model age, i.e., the time when the initial extraction from the DM of the evolved component took place.

The Hf_i of zircons from the 1.54-1.53 Ga and 1.50-1.49 Ga rocks in this study reflect heterogeneous magmas at the time of zircon crystallisation. Generation of this wide range of Hf_i ratios from a single source is unlikely: the high Hf_i ratios (0.2819 to 0.2821 at 1.54-1.49 Ga) points to a source with a DM composition, the lower end of the Hf_i ratios, on the other hand, suggest an older crustal component with a higher Lu/Hf ratio. Hence, contributions from two or more sources with different Hf isotopic composition are inferred, compatible with a mix of mantle derived material extracted at 1.55-1.5 Ga (particularly EPB-06-06, EPB-06-04 and 105-23-10), and re-melting of older crust (all samples). Possible sources for the crustal component (-s) can be evaluated by comparing to published and unpublished data from south-eastern Norway and south-western Sweden (Figure 19b). The lower end of the Hf_i range (+6 to -2 ε_{Hf} assuming average crustal Lu/Hf) crosses into the field of 1.85-1.65 Ga TIB rocks at 1.54-1.49 Ga (Andersen et al. 2006); thus, rocks of TIB ages and compositions are a pssible source of the crustal component. The Hf_i ranges in the analysed samples also overlap with the 1.60-1.54 Ga calc-alkaline gneiss complexes in the Østfold-Akershus sector east of the Nesodden Peninsula, including the Feiring, Sørmarka, Midtskog, Bjørkelangen and Tistedal gneiss complexes (Andersen et al. 2004a). Inherited zircons in the coarse grained granite (EPB-06-05) are ca. 1.59 Ga old and have intermediate Hf_i (< 0.2821, ε_{Hf} = +5 to +8). This suggests that part of the crustal component of the rocks in the study area derives from recycling of these or similar gneiss complexes. Rocks of similar ages and Hf_i characteristics are also present across the Oslo fjord in the Kongsberg sector, i.e., the Slemmestad metarhyolite and the Snarum calc-alkaline gneisses, and slightly further away to the south west, the Justøy tonalities, the Jomås granodiorite and the Gjerstadvatn tonalite in the Bamble sector (Andersen et al. 2002a, Andersen et al. 2004a).

The Sveconorwegian zircons in the pegmatite exhibits a moderate ε_{Hf} range (-2 to +4) and plot on the CHUR line, partly overlapping with the Hf_i of the Mesoproterozoic rocks in

the study, including the tonalitic host rock (Figure 19a). However, the inherited zircons in the Sveconorwegian pegmatite are 1.53 Ga and testify to a juvenile component that is absent from the Hf_i range of the tonalite, but match that of the neighbouring 1.54 granitic gneiss (105-23-10). Thus, the most likely candidate for the inherited zircons is the granitic gneiss and/or rocks of similar age and composition in the vicinity.

The model ages (t_{DMw}) for the evolved component of the studied 1.54-1.49 Ga rocks are estimated for Lu/Hf ratios of 0.015 and 0.010, corresponding to average crust and average granite compositions, respectively. The projected Hf isotopic evolution for both Lu/Hf ratios overlap the field of the TIB Hf_i, as noted above, and intersect with the DM yielding crustal residence ages of Hf in the zircons at up to 2.4 Ga (Lu/Hf = 0.015) and 2.2 Ga (Lu/Hf = 0.010), respectively. A conservative estimate of the minimum crustal residence time, excluding three points with negative ε_{Hf} from two rocks and gracing the most evolved components of the bulk of the data in the diagram (Figure 19), yields an age of ca. 2.1 Ga (Lu/Hf = 0.015), matching models of crustal formation in central Sweden at 2.1-2.0 Ga (e.g., Anderson et al., 2006 and references therein).

The evolution of the crustal component can be further constrained by examining the isotopic composition of Pb, and in addition, the application of a second isotopic system makes the constraints more robust (e.g., Andersen et al. 1994). A three-stage growth model applied to the studied rocks (see section 4.4.) with the protolith age (t_1) set to 2.1 Ga fits well with the obtained Pb data. Following separation from the DM reservoir the Pb evolved in different environments until 1.54-1.49 Ga (t_2), and in the case of the pegmatite and the augen gneiss (112-23-10), until ca. 1.05 Ga. These reservoirs were characterized by intermediate $^{238}U/^{204}Pb$ ratios (μ_2-values) ranging from 10 to 16 and $^{232}Th/^{204}Pb$ ratios (κ_2-value) of ca. 4, supporting the presence of both a mantle derived and crust derived components. The U-Pb data dates emplacement of the augen gneiss (112-23-10) at 1.50 Ga, and minor Pb-loss (or less likely, zircon growth) indicates metamorphism at ca. 1.1 Ga. In the $^{206}Pb/^{204}Pb$ vs. $^{207}Pb/^{204}Pb$ diagram t_2 has to be constrained to the Sveconorwegian (here 1.05 Ga, i.e., the age of local pegmatites and anatexis) in order to obtain a meaningful μ_2-value for the rock. The Pb data thus supports the metamorphic age, and also indicates that the Pb composition of the rock was considerably reset at this time. Resetting probably took place through homogenization of Pb between feldspars and other minerals, whereas zircons, which are typically very resistant to metamorphism, were only slightly disturbed, and still provide mostly concordant U-Pb data from the time of emplacement of the gneiss.

For the remaining samples the whole rock Pb isotope data are consistent with the U-Pb and Lu-Hf data. Thus, the Pb data confirm the crustal residence and emplacement ages derived from the U-Pb and Hf data, and the mixing of DM and crustal components as the magma sources.

5.3 Regional implications

Evidence of calc-alkaline magmatism in the SSD from ca. 1.66 to 1.50 Ga suggest an active continental margin with a long lived subduction zone, representing the westwards growth of the Baltic Shield (Brewer et al. 1998, Nordgulen 1999, Andersen et al. 2001b). Previous studies of the calc-alkaline rocks that formed throughout this period indicate an immature to moderately mature volcanic arc setting at a continental margin (Brewer et al. 1998, Andersen et al. 2001b). Isotopic studies further indicate that 1.9-1.7 Ga rocks of a more evolved character (possibly TIB related) are present at depth on both sides of the Permian Oslo Rift (Andersen and Knudsen 2000, Andersen et al. 2001a, Andersen et al. 2002a). However, southern Norway and south-western Sweden are divided into different sectors by Sveconorwegian crustal scale shear zones (Andersen et al. 2005 and references therein), suggested to juxtapose different parts of the Baltic Shield due to predominantly sinistral movements along the faults (Park et al. 1991).

The Nesodden Peninsula is part of the Østfold-Akershus sector (western-most parts of the Western Segment), where convergent-margin magmatism has been dated to 1.55-152 Ga (Hisingen; Åhäll and Connelly 2008). It was also suggested by Åhäll and Connelly (2008), and Andersen et al. (2004), that post-1.52 Ga subduction-related magmatism could be expected, since rocks with appropriate tectonic affinity and ages (i.e., 1.52-1.49 Ga) occur in the Rogaland-Vest Agder, Suldal, Hardangervidda and Telemark sectors ("Telemarkia terrane" of Bingen et al. 2005) to the west of the Østfold-Akershus sector, suggesting the continuation of the subduction (although these parts of southern Norway might have been situated further north at the time). Geochemistry from similar gneisses east and west of the Nesodden Peninsula (Andersen et al. 2002a, Andersen et al. 2004a, Åhäll and Connelly 2008) suggests that the studied rocks are calc-alkaline, which fits well with a subduction zone setting.

The 1.54-1.49 Ga emplacement ages of the rocks in this study fall within the last stages of 1.75 – 1.5 Ga Gothian magmatism-metamorphism in the SSD (Gaál and Gorbatschev 1987), and the 1.53-1.54 Ga rocks are coeval with the last stage of the 1.55-152 Ga Hisingen

magmatism (Åhäll and Connelly 2008). The younger group of rocks in this study, dated to 1.5-1.49 Ga, confirms the conjecture of Åhäll and Connelly (2008) and Andersen et al. (2004), by documenting magmatism of this age in the Østfold-Akershus sector.

During the 1.2 - 0.9 Ga Sveconorwegian (Starmer 1990) the SSD was extensively deformed, metamorphosed and intruded by several generations of magmatic rocks. A number of different tectonic settings have been documented during the Sveconorwegian, including ca. 1.13 Ga terrane accretion in the south (the Bamble sector; Kullerud and Dahlgren 1993; Knudsen and Andersen 1999), extension and bimodal magmatism at 1.16-1.12 Ga (Telemark; Andersen et al. 2007b), subduction and emplacement of the 1.05 Ga Feda suite (Rogaland-Vest Agder; Bingen and van Breemen 1998), continent-continent (?) collision and crustal thickening illustrated by 0.97 Ga eclogite formation (south-western Sweden; Möller 1998), and ca. 0.96-0.93 Ga orogenic collapse (Rogaland – Vest Agder; Bingen et al. 2006). During this time, Andersen et al. (2007b) recognises 5 different generations of Sveconorwegian granites in south-western Norway.

Sveconorwegian metamorphism, anatexis and pegmatite emplacement at ca. 1.05 Ga in the gneisses on the Nesodden Peninsula documented in this study thus forms part of the complex tectonometamorphic evolution of the Sveconorwegian in south Norway. The anatexis may be the result of a rise in temperature related to the introduction of an external heat source, e.g., underplating and mafic magmatism (Andersen et al. 2007a), or reflect decompression due to extension related tectonics, e.g., back-arc basin extension or, perhaps less likely at this time, orogenic collapse. The complex regional geological evolution is perhaps mirrored in the complex local geology of the Spro area where four of the samples in this study were collected. Here, amphibolite dykes in the Spro granite (106) are deformed along with the host rock by steep mylonitic shear zones. It is tempting to speculate that the shearing is related to the crustal scale shear zones that transect south-western Norway (Swensson 1986). Furthermore, these shear zones are locally dated to 1.05-1.035 Ga (Mandal-Ustaoset shear zone; Bingen and van Breemen, 1998), and are thus coeval with anatexis in the Spro area. Alternatively, the amphibolites that occur throughout the field area may be Sveconorwegian, and related to a heat influx that triggered anatexis in the local gneisses at 1.05 Ga. These questions were not part of the scope of this thesis, but present a few of many possible follow up studies in this intriguing geological area at the door step of Oslo.

6 Conclusions

Nine felsic lithologies on the Nesodden Peninsula were dated by U-Pb in situ zircon dating, yielding emplacement ages at 1.54-1.53 Ga for foliated granites and granitic gneisses, and at 1.50-1.49 Ga for a second group of granitic and tonalitic rocks. Time-corrected Hf isotopic ratios obtained for dated zircons in the rocks indicate contributions from both a ca. 1.5 Ga juvenile component and from an older, crustal component. Model-ages at ca. 2.1 Ga from magmatic zircons point to TIB rocks as a likely source of the crustal component, supporting previous suggestions that TIB related rocks are present at a lower crustal level in the region. Three-stage Pb-Pb modelling confirms the crustal residence time obtained by the Hf analyses, and contributions from different sources to the isotopic make-up of the protoliths. Inherited zircons in coarse grained granite further indicate that part of the crustal component detected in the rocks in the study area derives from recycling of marginally older, calc-alkaline gneiss complexes in the region. The data presented in this study confirm previously inferred Mesoproterozoic younging to the west in the Østfold-Akershus sector, and are proposed to support westwards growth of the Baltic Shield along a long lived active continental margin.

A folded granitic pegmatite in a tonalitic gneiss yielded an age of 1.05 Ga, constraining folding and the age of the gneissic fabric to post- and pre-1.05 Ga, respectively. Inherited zircons in the pegmatite, its association with neosomes in the field, and Hf data indicate that the pegmatite reflects anatexis of the felsic gneisses on the western side of the Nesodden Peninsula at ca. 1.05 Ga. The effect of Sveconorwegian metamorphism is also reflected in discordant U-Pb data from the gneisses, and confirmed by Pb-Pb modelling. Permian lower intercepts correlates to magmatic activity in the Oslo Rift area at ca. 290 Ma, and are proposed to reflect heating associated with emplacement of numerous diabase dykes in the Nesodden rocks.

7 References

Åhäll, K.-I. and Gower, C.F. 1997. The Gothian and the Labradorian Orogens: Variations in Accretionary Tectonism Along a Late Paleoproterozoic Laurentia-Baltica Margin. *Geologiska Föreningens Stockholm Forhandlinger* 119, 181-191.

Åhäll, K.-I. and Connelly, J.N. 2008. Long-Term Convergence Along Sw Fennoscandia: 330 M.Y. Of Proterozoic Crustal Growth. *Precambrian Research* 161 (3-4), 452-474.

Andersen, T. 1997. Radiogenic Isotope Systematics of the Herefoss Granite, South Norway: An Indicator of Sveconorwegian (Grenvillian) Crustal Evolution in the Baltic Shield. *Chemical Geology* 135, 139-158.

Andersen, T. 1998. Pbi-an Excel Workbook for Interactive Graphical Modelling of Lead Isotope Data on Minerals and Rocks. *Computers & Geosciences* 24 (2), 197-199.

Andersen, T. 2005. Terrane Analysis, Regional Nomenclature and Crustal Evolution in the Southwest Scandinavian Domain of the Fennoscandian Shield. *GFF* 127, 159-168.

Andersen, T., Andersson, U.B. and Graham, S. 2006. Hf Isotope Variations in Transscandinavian Igneous Belt Zircons. Paper read at The 27th Nordic Geological Winter Meeting, 9-12/01/06, at Oulu, Finland.

Andersen, T., Andresen, A. and Sylvester, A.G. 2001a. Nature and Distribution of Deep Crustal Reservoirs in the Southwestern Part of the Baltic Shield: Evidence from Nd, Sr and Pb Isotope Data on Late Sveconorwegian Granites. *Journal of the Geological Society, London* 158, 253-267.

Andersen, T., Andresen, A. and Sylvester, A.G. 2002b. Timing of Late- to Post-Tectonic Sveconorwegian Granitic Magmatism in South Norway. *NGU Bulletin* 440, 5-18.

Andersen, T., Graham, S. and Sylvester, A.G. 2007b. Timing and Tectonic Significance of Sveconorwegian a-Type Granitic Magmatism in Telemark, Southern Norway: New Results from Laser-Ablation Icpms U-Pb Dating of Zircon. *NGU Bulletin* 447, 17-31.

Andersen, T., Griffin, W.L., Jackson, S.E. and Knudsen, T.-L. 2001b. Timing of Mid-Proterozoic Calc-Alkaline Magmatism across the Oslo Rift: Implications for the Evolution of the South-Western Margin of the Baltic Shield *Geonytt* 1, 25-26.

Andersen, T., Griffin, W.L., Jackson, S.E., Knudsen, T.L. and Pearson, N.J. 2004a. Mid-Proterozoic Magmatic Arc Evolution at the Southwest Margin of the Baltic Shield. *Lithos* 73, 289-318.

Andersen, T., Griffin, W.L. and Pearson, N.J. 2002a. Crustal Evolution in the Sw Part of the Baltic Shield: The Hf Isotope Evidence. *Journal of Petrology* 43 (9), 1725-1747.

Andersen, T., Griffin, W.L. and Sylvester, A.G. 2007a. Sveconorwegian Crustal Underplating in Southwestern Fennoscandia: Lam-Icpms U-Pb and Lu-Hf Isotope Evidence from Granites and Gneisses in Telemark, Southern Norway. *Lithos* 93, 273-287.

Andersen, T., Hagelia, P. and Whitehouse, M.J. 1994. Precamnrian Multi-Stage Crustal Evolution in the Bamble Secor of South Norway: Pb Isotopic Evidence from a Sveconorwegian Deep-Seated Granitic Intrusion. *Chemical Geology (Isotope Geoscience Section)* 116, 327-343.

Andersen, T. and Knudsen, T.-L. 2000. Crustal Contaminants in the Permian Oslo Rift, South Norway: Constraints from Precambrian Geochemistry. *Lithos* 53, 247-264.

Andersen, T., Laajoki, K. and Saeed, A. 2004b. Age, Provenance and Tectonostratigraphic Status O the Mesoproterozoic Blefjell Quartzite, Telemark Sector, Southern Norway. *Precambrian Research* 135, 217-244.

Andersson, U.B., Sjöström, H., Höghdal, K. and Eklund, O., eds 2004. *The Transscandinavian Igneous Belt, Evolutionary Models*. Ed. Huhma, H., Andersson, U.B. and Eklund, O., *The Transscandinavian Igneous Belt (Tib) in Sweden: A Review of Its Character and Evolution*: Geological Survey of Finland: Special Paper 37.

Andersson, U.B. and Wikström, A., eds 2004. *The Småland-Värmland Belt -Overview*. Ed. Höghdal, K., Andersson, U.B. and Eklund, O., *The Transscandinavian Igneous Belt (Tib) in Sweden: A Review of Its Character and Evolution*: Geological Survey of Finland: Specila Paper 37.

Berthelsen, A. 1980. Towards a Palinspastictectonic Analysisof the Baltic Shield. *In* Cogne, J. and Slansky, M. (eds). *Geology of Europe, from Precambrian to the Post-Hercynian Sedimentary Basins*: Memoires du B.R.G.M., 5-21.

Berthelsen, A., Olerud, S. and Sigmond, E.M.O. 1996. Geologisk Kart over Norge, Berggrunnskart Oslo, M 1:250 000. *Norges Geologisk Undersøkelse*.

Bibikova, E.V., Skiöld, T., Bogdanova, S.V., Gorbatschev, R. and Slabunov, A.I. 2001. Titanite-Rutile Thermochronometry across the Boundary between the Archaean Craton in Karelia and the Belomorian Mobile Belt, Eastern Baltic Shield. *Precambrian Research* 105, 315-330.

Bingen, B. and Bremen, O.v. 1998. Tectonic Regimes and Terrane Boundaries in the High-Grade Sveconorwegian Belt of Sw Norway, Inferred from U–Pb Zircon Geochronology and Geochemical Signature of Augen Gneiss Suites. *Journal of Geological Society, London* 155, 143-154.

Bingen, B., Nordgulen, Ø. and Sigmond, E.M.O. 2001. Correlation of Supracrustal Sequences and Origin of Terranes in the Sveconorwegian Orogen of Sw Scandinavia: Sims Data on Zircon in Clastic Metasediments. *Precambrian Research* 108, 293-318.

Bingen, B., Skår, Ø., Marker, M., Sigmond, E.M.O., Nordgulen, Ø., Ragnhildstveit, J., Mansfeld, J., Tucker, R.D. and Liégeois, J.-P. 2005. Timing of Continental Building in

the Sveconorwegian Orogen, Sw Scandinavia *Norwegian Journal of Geology* 85, 87-116.

Bouvier, A., Vervoort, J.D. and Patchett, P.J. 2007. The Lu–Hf Chur Value. *Goldschmidt Conference Abstracts* A116.

Brewer, T.S., Daly, J.S. and Åhäll, K.-I. 1998. Contrasting Magmatic Arcs in the Palaeoproterozoic of the South-Western Baltic Shield. *Precambrian Research* 92, 297-315.

Broch, H. 1927. *Untersuchungen Über Die Marine Bodenfauna Bei Lindesness Im Juni 1926*, Oslo. 32 pp.

Chernyshev, I.V.A.V., Chugaev, A.V. and Shatagin, K.N. 2007. High-Precision Mc-Icp-Ms Lead Isotope Analysis Using Tl-Normalization: Calibration and Applications to Lead Isotope Study of Ore Deposits. *Goldschmidt Conference Abstracts*, A170.

Condie, K.C. 2005. *Earth as an Evolving Planetary System*, San Diego: Elsevier Academic Press. 447 pp.

Dahlgren, S.H., Heaman, L. and Krogh, T.E. 1990. Geological Evolution and U-Pb Geochronology of the Proterozoic Central Telemark Area, Norway. *Geonytt* 17 (1), 38 (Abstract).

DePaolo, D.J. and Wasserburg, G.J. 1976. Nd Isotopic Variations and Petrogenetic Models *Geophysical Research Letters* 3 (5), 249-252.

Eliasson, T. and Schöberg, H. 1991. U-Pb Dating of the Post-Kinematic Sveconorwegian (Grenvillian) Bohus Granite, Sw Sweden: Evidence of Restitic Zircon. *Precambrian Research* 51, 337-350.

Faure, G. and Mensing, T.M. 2005. *Isotopes: Pribciples and Applications*. 3rd ed, Hoboken, New Jersey: John Wiley & Sons Inc.

Gaál, G. and Gorbatschev, R. 1987. An Outline of the Precambrian Evolution of the Baltic Shield. *Precambrian Research* 35, 15-52.

Geoversum. *Major Tectono-Stratigraphic Units of the Baltic Shield*, 29/04/2007 Accsessed. Available at http://geoguide.geoversum.info/?page=geology.

Gleditsch, C.C. 1952. Oslofjordens Prekambriske Områder. I. Innledende Oversikt. Hurum. Les Formations Precambriennes Du Fjord D'Oslo. 181, 1-118.

Gorbatschev, R., ed. 2004. *The Transscandinavian Igneous Belt -Introduction and Backgroung*. Ed. Höghdal, K., Andersson, U.B. and Eklund, O., *The Transscandinavian Igneous Belt (Tib) in Sweden: A Review of Its Character and Evolution*: Geological Survey of Finland: Specila Paper 37.

Graversen, O. 1984. Geology and Structural Evolution of the Precambrian Rocks of the Oslofjord-Øyeren Area, Southeast Norway. *Norges Geologisk Undersøkelse Bulletin* 398.

Griffin, W.L., Pearson, N.J., Belousova, E., Jackson, S.E., Van Achterbergh, E., O'Reilly, S.Y. and Shee, S.R. 2000. The Hf Isotope Composition of Cratonic Mantle: Lam-Mc-Icpms Analysis of Zircon Megacrysts in Kimberlites. *Geochimica et Cosmochimica Acta* 64, 133-147.

Griffin, W.L., Wang, X., Jackson, S.E., Pearson, N.J., O'Reilly, S.Y., Xu, X. and Zhou, X. 2002. Zircon Chemistry and Magma Mixing, Se China: In-Situ Analysis of Hf Isotopes, Tonglu and Pingtan Igneous Complexes. *Lithos* 61, 237-269.

Haas, G.J.L.M.d., Andersen, T. and Vestin, J. 1999. Application of Detrital Zircon Geochronology to Assembly of a Proterozoic Terrain - an Example from the Baltic Shield. *Journal of Geology* 107, 569-586.

Huhma, H. 1986. Sm-Nd, U-Pb and Pb-Pb Isotopic Evidence for the Origin of the Early Proterozoic Svecokarelian Crust in Finland. *Geological Survey of Finland* Bulletin 337

Ireland, T.R. and Williams, I.S., eds 2003. *Considerations in Zircon Geochronology by Sims*. Ed. Ribbe, P.H., Rosso, J.J., Hanchar, J.M. and Hoskin, P.W.O., *Reviews in Mineralogy & Geochemistry: Zircon*. Washington, D.C.: Mineralogical Society of America.

Jackson, S.E., Pearson, N.J., Griffin, W.L. and Belousova, E.A. 2004. The Aplication of Laser Ablation-Inductively Coupled Plasma-Mass Spectrometry to in Situ U-Pb Zircon Geochronology. *Chemical Geology (Isotope Geoscience Section)* 211, 47-69.

Jahn, B.M., Vidal, P. and Kröner, A. 1984. Multi-Chronometric Ages and Origin of Archaean Tonalitic Gneisses in Finnish Lapland: A Case for Long Crustal Residence Time *Contributions to Mineralogy and Petrology* 86 (4), 398-408.

Käpyaho, A., Mänttäri, I. and Huhma, H. 2006. Growth of Archean Crust in the Kuhmo District, Eastern Finland: U-Pb and Sm-Nd Isotope Constraints on Plutonic Rocks. *Precambrian Research* 146, 95-119.

Kinny, P.D., Compston, W. and Williams, I.S. 1991. A Reconnaissance Ion-Probe Study of Hafnium Isotopes in Zircons. *Geochimica et Cosmochimica Acta* 55, 849-859.

Knudsen, T.L. and Andersen, T. 1999. Petrology and Geochemistry of the Tromøy Gneiss Complex, South Norway, an Alleged Example of Proterozoic Depleted Lower Continental Crust. *Journal of Petrology* 40 (6), 909-933.

Košler, J. and Sylvester, P.J. 2003. Present Trends and the Future of Zircon in Geochronology: Laser Ablation Icpms. *Reviews in mineralogy & geochemistry: Zirkon* 53, 243-275.

Kullerud, L. and Dahlgren, S.H. 1993. Sm-Nd Geochronology of Sveconorwegian Granulite-Facies Mineral Assemblages in the Bamble Shear Belt, South Norway. *Precambrian Research* 64, 389-402.

Kullerud, L. and Machado, N. 1991. End of a Controversy: U-Pb Geochronological Evidence for Significant Grenvillian Activity in the Bamble Area, Norway. *Terra Abstracts* 3, 504.

Isoplot 3.00, a Geochronological Toolkit for Microsoft Excel. Berkeley Geochronology Center Special Publication No. 4, Berkeley CA.

Lundquist, T. 1979. The Precambrian of Sweden. *Sveriges Geologisca Undersökning* 73 (9).

Mulch, A. 2003. *Integrated High-Spatial Resolution 40ar/39ar Geochronology, Stable Isotope Geochemistry, and Structural Analysis of Extensional Detachment Systems: Case Studies from the Porsgrunn-Kristiansand Shear Zone (S-Norway) and the Shuswap Metamorphic Core Complex (Candada)*, Faculté des Sciences, Université de Lausanne, Lausanne, Switzerland. 333.

Mutanen, T. and Huhma, H. 2003. The 3.5 Ga Siurua Trondhjemite Gneiss in the Archean Pudasjärvi Granulite Belt, Northern Finland. *Bulletin of the Geological Society Finland* 75, 51-68.

Naterstad, J., Bockelie, J.F., Bockelie, T., Graversen, O., Hjelmeland, H., Larsen, B.T. and Nilsen, O. 1990 *Berggrunnskart Asker 1814 I, M 1:50 000.* Norges geologisk undersøkelse.

Nironen, M. 1997. The Svecofennian Orogen: A Tectonic Model. *Precambrian Research* 86, 21-44.

Nordgulen, Ø. 1999. *Geologisk Kart over Norge, Berggrunnskart Hamar, M 1:250 000*. Norges geologisk undersøkelse.

Park, R.G., Åhäll, K.-I. and Boland, M.P. 1991. The Sveconorwegian Shear-Zone Network of Sw Sweden in Relation to Mid-Proterozoic Plate Movements. *Precambrian Research* 49, 245-260.

Patchett, J. and Kouvo, O. 1986. Origin of Continental Crust of 1.9-1.7 Ga Age: Nd Isotopes and U-Pb Zircon Ages in the Svecokarelian Terrain of South Finland. *Contributions to Mineralogy and Petrology* 92, 1-12.

Røhr, T.S., Andersen, T. and Dypvik, H. 2008. Provenance of Lower Cretaceous Sediments in the Wandel Sea Basin, North Greenland. *Journal of Geological Society, London* 165, 1-13.

Samsonov, A.V., Bogina, M.M., Bibikova, E.V., Petrova, A.Y. and Shchipansky, A.A. 2005 and references therein. The Relationship between Adakitik, Calc-Alkaline Volcanic Rocks and Ttgs: Implicationsfor the Tectonic Setting of the Karelian Greenstone Belts, Baltic Shield. *Lithos* 79, 83-106.

Scherer, E., Münker, C. and Mezger, K. 2001. Calibration of the Lutetium-Hafnium Clock. *Science* 293, 683-687.

Sigmond, E.M.O. 1985. The Mandal-Ustaoset Line, a Newly Discovered Major Fault Zone in South Norway. *In* Tobi, A.C. and Touret, J.L.R. (eds). *The Deep Proterozoic Crust in the North Atlantic Provinces*. Nato Asi Series Advanced Science Institute Series - Mathematical and Physical Sciences. 158. Dordrecht/Boston/Lancaster: D. Reidel Publishing Company, 323-331.

Sigmond, E.M.O. 1998. *Geologisk Kart over Norge, Bergrunnskart Odda, M 1:250 000*. Norges geologisk undersøkelse.

Sigmond, E.M.O., Gjelle, S. and Solli, A. 1997a. Telemarkgruppens Oppbygningfra Det Sentrale Telemark Nordover Til De Kaledonske Dekkene-Rjukangruppens Underlag Og Bergartene I Uvdalsplutonbeltet. *Geonytt* 24 (1), 82 (Abstract).

Sigmond, E.M.O., Gjelle, S. and Solli, A. 1997b. The Rjukan Proterozoic Rift Basin, Its Basement and Cover, Volcanic and Sedimentary Infill, and Associated Intrusions *Norges Geologisk Undersøkelse Bulletin* 433, 6-7.

Simonsen, S.L. 1997. *Radiogenic Isotope Systematics of Charnockite and Retrograded Augen Gneiss in the Gjeving Complex, South Norway*, Mineralogical-Geological Museum, University of Oslo, Oslo.

Slabunov, A.I., Lobach-Zhuchenko, S.B., Bibikova, E.V., Balagansky, V.V., Sorjonen-Ward, P., Volodichev, O.I., Shchipansky, A.A., Svetov, S.A., Chekulaev, V.P., Arestova, N.A. and Stepanov, S.A. 2006. The Archean of the Baltic Shield: Geology, Geochronology, and Geodynamic Settings. *Geotectonics* 40 (6), 409-433.

Söderlund, U., Jarl, L.-G., Persson, P.-O., Stephens, M.B. and Wahlgren, C.-H. 1999 and references therein. Protolith Ages and Timing of Deformation in the Eastern , Marginal Part of the Sveconorwegian Orogen, Southwestern Sweden. *Precambrian Research* 94, 29-48.

Söderlund, U., Möller, C., Andersson, J., Johansson, L. and Whitehouse, M.J. 2002. Zircon Geochronology in Polymetamorphic Gneisses in the Sveconorwegian Orogen, Sw Sweden: Ion Microprobe Evidence for 1.46-1.42 and 0.98-0.96 Ga Reworking. *Precambrian Research* 113, 193-225.

Söderlund, U., Patchett, P.J., Vervoort, J.D. and Isachsen, C.E. 2004. The ^{176}lu Decay Constant Determined by Lu-Hf and U-Pb Isotope Systematics of Precambrian Mafic Intrusions. *Earth and Planetary Sctence Letters* 219, 311-324.

Stacey, J.C. and Kramers, J.D. 1975. Approximation of Terrestrial Lead Isotope Evolution by a Two-Stage Model. *Earth and Planetary Sctence Letters* 26, 207-221.

Starmer, I. C. 1990. Mid-Proterozoic evolution of the Kongsberg-Bamble Belt and adjacent areas, southern Norway, in *Mid-Proterozoic Laurentia-Baltica*, edited by C. F. Gower, T. Rivers and B. Ryan, pp. 279-305, Geol. Assoc. Can., Toronto.

Steiger, R.H. and Jäger, E. 1977. Subcommission on Geochronology: Convention on the Use of Decay Constants in Geo- and Cosmochronology. *Earth and Planetary Sctence Letters* 36, 359-362.

Stephens, M.B., Wahlgren, C.-H., Weijermans, R. and Cruden, A.R. 1996. Left-Lateral Transpressive Deformation and Its Tectonic Implications, Sveconorwegian Orogen, Baltic Shield, Southewestern Sweden *Precambrian Research* 79, 261-279.

Sundvoll, B., Neumann, E.-R., Larsen, B.T. and Tuen, E. 1990. Age Relations among Oslo Rift Magmatic Rocks: Implications for Tectonic and Magmatic Modelling. *Tectonophysics* 178, 67-87.

Swensson, E. 1986. *Nesoddforkastningen, En Strukturell Detaljstudie Av Oslo Grabens Østlige Hovedforkastning, En Reaktivert Sidelengs- Eller Normalforkastning*. Hovedoppgave, Institute for Geology, University of Oslo, Oslo. 220.

Tatsumoto, M., Knight, R.J. and Allègre, C.J. 1973. Time Differences in Formation of Meteorites as Determined from the Ratio of Lead-207 to Lead-206. *Science* 180, 1279-1283.

Taylor, P.N., Moorbath, S., Goodwin, R. and Petrykowski, A.C. 1980. Crustal Contamination as an Indicator of the Extent of Early Archaean Continental Crust: Pb Isotopic Evidence from the Late Archaean Gneisses of West Greenland. *Geochimica et Cosmochimica Acta* 44, 1437-1453.

VERVOORT, J.D. & BLICHERT-TOFT, J. 1999. Evolution of the depleted mantle: Hf isotope evidence from juvenile rocks through time. *Geochimica et Cosmochimica Acta,* **63,** 533-556.

Wolf, R.E. *What Is Icp-Ms?...And More Importantly, What Can It Do?* , 26-Jul-2005 2005 Accsessed. Available at http://minerals.cr.usgs.gov/icpms/intro.html.

8 Appendix

8.1 Weighing in for Pb-Pb analyses

Table 2. Weights of samples for Pb-Pb analyses, target mass is 0.0500g

Sample	101-23-10	102-23-10	103-23-10	105-23-10	106-23-10	112-23-10
Mass (g)	0.0500	0.0493	0.0498	0.0505	0.0476	0.0509

Sample	EPB-06-04	EPB-06-05	EPB-06-06	BLANK-Pb*	BCR1-Pb
Mass (g)	0.0495	0.0521	0.0499	0.01999	0.0494

*For the blank 20µl ^{204}Pb spike dilute 0.005198µmol/g (^{204}Pb (1.06ppm)) = 0.0199g has been used.

8.2 Lead separation procedure

The lead separation procedure for whole-rock lead isotope analysis was done using an anion exchange column to separate Pb from other elements:

- Solution preparation
  1. Dissolve sample in 2ml concentrated HF + 1ml concentrated HNO_3 in Teflon bombs in oven at 80 ˚C in a time duration of 48 hours.
  2. Dry down the samples to hard evaporation cakes on a hot plate (bombs placed minimum 4 cm from each other to prevent cross contamination).
  3. Add enough 6N HCl to each sample to dissolve the solid and then repeat step 2.
  4. Re-dissolve in 0.8N HBr and repeat step 2.
  5. Finally re-dissolve the samples in less than 1ml 0.8N HBr.

- Preparation of disposable columns
  1. Wash each column with full reservoir MQ water followed by a full reservoir 6N HCl: repeat procedure once.
  2. Fill up each column with MQ water.
  3. Add <0.2 ml pre-cleaned AG1-X8 resin drop-wise to each column.
  4. Let the resin settle.
  5. Wash the resin through with 2 ml MQ water.
  6. Wash again with 2 ml 6N HCl and repeat step 5.
  7. Finally add 1 ml 0.8N HBr to each column.

- Chemistry
  1. Load samples (one in each column).
  2. Add 15 drops of 0.8N HBr to each.
  3. Repeat step 2.
  4. Collect Pb fraction in bomb! Add 2ml 0.5N HNO_3.
  5. Collect Pb fraction! Add 1ml 0.5N HNO_3.
  6. Evaporate each sample in bomb on hot plate.
  7. Add 2-3 drops of 0.8N HBr to every sample and repeat step 6.
  8. Re-dissolve the evaporation cakes in <1ml 0.8N HBr.
  9. Regeneration of the columns. Add 2ml MQ water to each column.
  10. Wash with 1ml 6N HCl.

11. Wash with 1ml MQ water.
12. Repeat step 11.
13. Add 1ml 0.8N HBr to each column.
14. Load the samples.
15. Add 15 drops of 0.8N HBr to each sample.
16. Repeat step 15.
17. Collect Pb fraction in bomb! Add 2ml 0.5N HNO_3.
18. Collect Pb fraction! Add 1ml 0.5N HNO_3.

8.3 Single sample linear probability plots

Data that form a linear array in a Hf_i probability plot likely belong to a suite of zircons formed from a source (or mix of sources) with a distinct Hf_i ratio. Data that plot under the lower probability limit indicate the presence a more evolved component (crust), whereas data that plot above the upper probability limit suggest a more juvenile component. These may for example represent inheritance or secondary zircon growth.

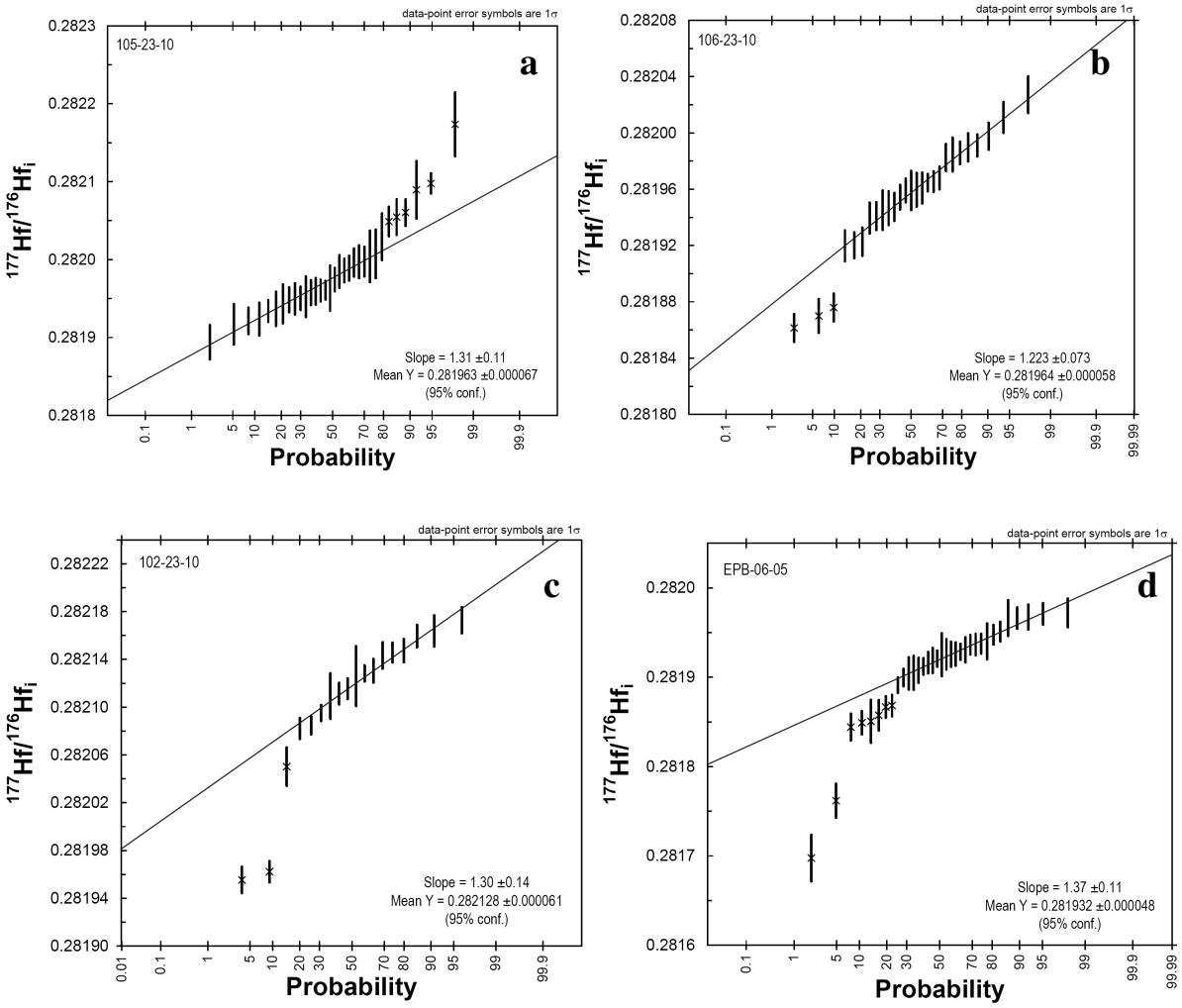

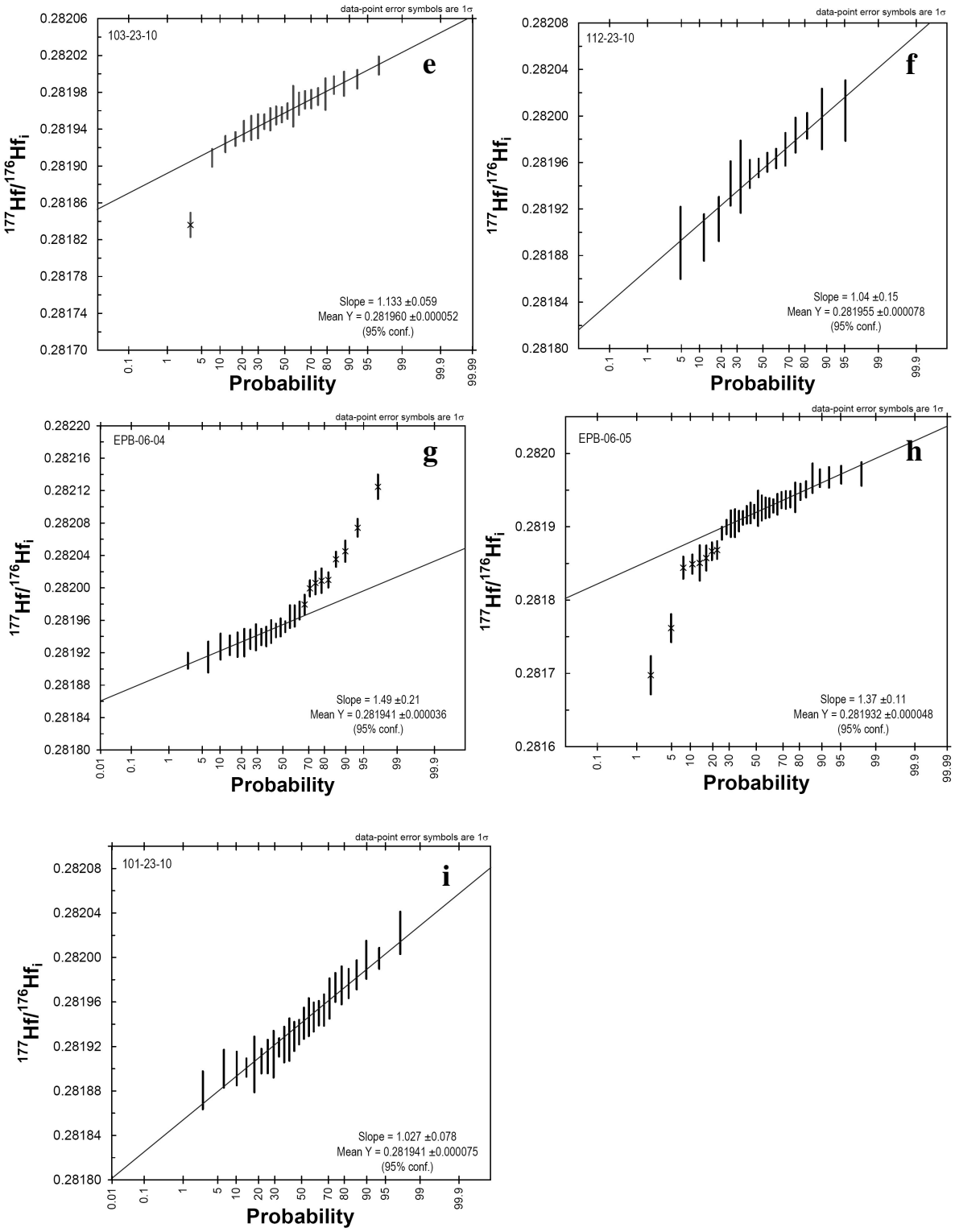

Figure 22a-i. Linear probability plots showing zircon analyses for each sample with 1σ error bars. a) Granitic gneiss, 105-23-10. Outliers in this plot are also outliers in Figure 17. b) Alkali feldspar granite, 106-23-10. Three analyses plot below the lower probability limit and were thus excluded from the regression. These are not outliers in Figure 17. c) Pegmatite, 102-23-10. Three analyses plot below the lower probability limit and are excluded from the regression. Two of these analyses are also outliers in Figure 17. The third poinjt to an older component, however, the U-Pb analysis of the zircon grain was poor due to high common Pb. d) Coarse-grained granite, EPB-06-05. Nine grains plot below the lower probability limit and are excluded from the regression. Two of these are outliers in Figure 17. e) Garnet-biotite gneiss, 103-23-10. One analysis plot below the lower probability limit, but is not an outlier in

Figure 17. f) Augen gneiss, 112-23-10. The data define a regression line, no outliers. g) Fine-grained granite, EPB-06-04. Nine analyses plot above the upper probability limit and were excluded from the regression. Four of these are outliers in Figure 17. h) Red granite, EPB-06-06. One analysis plot above the upper probability limit and one plot below the lower limit, both are thus excluded from the regression. However, the zircon at the lower end plots almost on the regression line. The two grains are outliers in Figure 17. i) Tonalitic gneiss, 101-23-10. All data plot on a regression line, no outliers.

8.4 LA-MC-ICPMS U-Pb data

Table 4. LA-MC-ICPMS U-Pb zircon data

Sample	ppm				Ratios						Discordance	Ages					
Analysis	U	^{206}Pb	^{206}Pb$_c$(%)	^{206}Pb/^{204}Pb	^{207}Pb/^{206}Pb	1s	^{207}Pb/^{235}U	1s	^{206}Pb/^{238}U	1s	Rho	Central (%)	^{207}Pb/^{206}Pb	1s	^{207}Pb/^{235}U	1s	^{207}Pb/^{238}U	1s
Granitic gneiss																		
105-57	324	50.5	4.90E-01	2507	0.08951	0.00039	3.02005	0.03221	0.24475	0.00307	0.57	-0.3	1415	8	1413	8	1411	16
105-01	350	60.4	4.80E-01	2344	0.09238	0.00052	3.36423	0.03894	0.26513	0.00326	0.80	2.7	1475	10	1496	9	1516	17
105-10	258	44.1		2081	0.09564	0.00034	3.48984	0.03865	0.26515	0.0034	0.87	-2	1541	7	1525	9	1516	17
105-09	324	56.4		2980	0.09493	0.00033	3.4974	0.0387	0.26792	0.00344	0.86	.	1527	6	1527	9	1530	17
105-48	310	53.6		3072	0.09536	0.00042	3.53883	0.04006	0.26941	0.00383	0.84	0.1	1535	8	1536	9	1538	19
105-38	203	34.8		2069	0.09586	0.00043	3.54991	0.0395	0.26872	0.00341	0.78	-0.8	1545	8	1538	9	1534	17
105-33	168	29.2		2354	0.09557	0.00037	3.56893	0.03915	0.27116	0.00353	0.79	0.4	1539	7	1543	9	1547	18
105-47	402	70.2		4198	0.09585	0.0004	3.60272	0.04194	0.27274	0.00364	0.79	0.7	1545	8	1550	9	1555	18
105-02	543	87	4.60E-01	3506	0.08986	0.00053	3.05692	0.03974	0.24767	0.0032	0.80	-0.1	1422	11	1422	10	1426	17
105-58	214	37.5		4470	0.09577	0.00057	3.57275	0.04532	0.27076	0.00421	0.64	.	1543	11	1543	10	1545	21
105-62	525	91		4292	0.09516	0.00055	3.51648	0.04963	0.26819	0.00443	0.82	.	1531	10	1531	11	1532	23
105-51	301	52.9		2292	0.09558	0.0005	3.55707	0.04855	0.27009	0.00442	0.89	.	1540	9	1540	11	1541	22
105-63	431	68.4		3616	0.09397	0.00073	3.29755	0.04966	0.25422	0.00365	0.78	-3.4	1508	14	1480	12	1460	19
105-76	262	44.2		2265	0.09515	0.00066	3.54354	0.05428	0.26963	0.00396	0.86	0.8	1531	13	1537	12	1539	20
105-59	238	40		2064	0.09529	0.00073	3.53049	0.06037	0.26836	0.0045	0.89	.	1534	14	1534	14	1532	23
Excluded samples																		
High common lead																		
105-86	374	52.2	7.90E-01	1390	0.08566	0.0006	2.55772	0.04924	0.21685	0.0044	0.94	-5.5	1331	13	1289	14	1265	23
105-83	181	26.1		971	0.08749	0.00035	2.74798	0.03287	0.22786	0.00307	0.94	-3.9	1371	7	1342	9	1323	16
105-56	196	31.1		1512	0.09117	0.00033	3.12643	0.03414	0.24886	0.00323	0.82	-1.4	1450	7	1439	8	1433	17
105-08	497	54.9		1001	0.09307	0.00039	2.17391	0.02689	0.17001	0.00236	0.95	-34.8	1489	8	1173	9	1012	13
105-69	202	34.5		1710	0.09476	0.00035	3.50987	0.04021	0.26855	0.00367	0.89	0.8	1523	7	1529	9	1533	19
105-07	218	37.5		1284	0.09484	0.00035	3.44825	0.04109	0.26445	0.00352	0.94	-1.2	1525	7	1515	9	1513	18
105-54	224	37.3		1408	0.09517	0.00035	3.42138	0.0391	0.26082	0.00347	0.90	-2.8	1531	7	1509	9	1494	18
105-03	196	34.3		1727	0.09513	0.00035	3.51869	0.03968	0.26908	0.00349	0.85	0.1	1531	7	1531	9	1536	18
105-31	193	33.5		1510	0.09522	0.00036	3.54527	0.04173	0.27039	0.00362	0.92	0.6	1532	7	1537	9	1543	18
105-72	234	40.2		1832	0.09539	0.00036	3.55201	0.04023	0.26997	0.00369	0.79	0.4	1536	7	1539	9	1541	19
105-06	615	85.9		1205	0.09545	0.00036	2.81285	0.0338	0.21445	0.00275	0.96	-20.6	1537	7	1359	9	1252	15
105-35	90	16.1		1232	0.09549	0.00035	3.66365	0.04186	0.27855	0.00372	0.86	3.3	1538	7	1563	9	1584	19
105-42	119	19.7		1035	0.0955	0.00036	3.40375	0.03923	0.25868	0.00342	0.91	-4.1	1538	7	1505	9	1483	18
105-28	108	18.9		1039	0.09561	0.00038	3.58198	0.0403	0.27212	0.00357	0.69	0.7	1540	7	1546	9	1552	18
105-44	152	25.7		1583	0.09561	0.00036	3.47925	0.03894	0.26407	0.00347	0.80	-2.2	1540	7	1523	9	1511	18
105-20	124	21.8		995	0.09567	0.00036	3.57498	0.03996	0.27147	0.00355	0.76	0.3	1541	7	1544	9	1548	18
105-32	169	29.8		1476	0.09565	0.00036	3.59173	0.04126	0.27268	0.00366	0.89	0.9	1541	7	1548	9	1554	19
105-23	248	43.6		1744	0.09577	0.00034	3.59944	0.04018	0.273	0.00357	0.87	0.8	1543	6	1549	9	1556	18
105-40	170	29.5		1609	0.09596	0.00034	3.59358	0.04085	0.27179	0.00362	0.91	0.1	1547	6	1548	9	1550	18
105-18	92	16.1		565	0.09601	0.00036	3.58773	0.04042	0.27151	0.00354	0.79	-0.1	1548	7	1547	9	1548	18
105-41	242	40.5		1963	0.09718	0.00038	3.49704	0.04544	0.26115	0.00383	0.96	-5.4	1571	7	1527	10	1496	20

Sample	ppm				Ratios							Discordance	Ages					
Analysis	U	^{206}Pb	$^{206}Pb_c$(%)	$^{206}Pb/^{204}Pb$	$^{207}Pb/^{206}Pb$	1s	$^{207}Pb/^{235}U$	1s	$^{206}Pb/^{238}U$	1s	Rho	Central (%)	$^{207}Pb/^{206}Pb$	1s	$^{207}Pb/^{235}U$	1s	$^{207}Pb/^{238}U$	1s
Alkali fedspar granite																		
106-76	268	50.2		5794	0.0948	0.0007	3.52106	0.09158	0.26996	0.0058	0.33	1	1524	13	1532	21	1541	29
106-68	131	23.9		4708	0.09506	0.00067	3.52727	0.07309	0.27001	0.00504	0.84	0.5	1529	13	1533	16	1541	26
106-78	236	43.9		4361	0.09506	0.00057	3.54956	0.09071	0.27141	0.00581	0.66	1.2	1529	11	1538	20	1548	29
106-59	172	31.1		11485	0.09516	0.00061	3.564	0.06581	0.27225	0.0044	0.90	1.3	1531	12	1542	15	1552	22
106-30	391	74.1		9975	0.09532	0.00064	3.50825	0.05195	0.26733	0.00358	0.47	-0.7	1534	12	1529	12	1527	18
106-42	130	25.6		10299	0.09534	0.00061	3.53057	0.05909	0.26905	0.00401	0.88	-0.1	1535	11	1534	13	1536	20
106-32	251	47.5		5065	0.09543	0.00064	3.53845	0.05453	0.26935	0.00375	0.52	-0.1	1536	12	1536	12	1537	19
106-63	262	46.5		8333	0.09538	0.00064	3.53543	0.06169	0.26943	0.00401	0.85	-0.1	1536	12	1535	14	1538	20
106-62	153	29		4236	0.09538	0.00068	3.57687	0.07458	0.27288	0.00513	0.85	1.1	1536	13	1544	17	1555	26
106-55	235	41.7		8814	0.09541	0.00059	3.60691	0.06752	0.27489	0.00467	0.88	1.9	1536	11	1551	15	1566	24
106-60	262	48.3		6276	0.09546	0.00069	3.53953	0.05548	0.26939	0.00392	0.91	-0.1	1537	13	1536	12	1538	20
106-28	273	51.8		9180	0.09547	0.00066	3.54403	0.05356	0.26958	0.00359	0.51	.	1537	13	1537	12	1539	18
106-66	188	35.9		7108	0.09552	0.00058	3.54773	0.06971	0.27013	0.00474	0.65	.	1538	11	1538	16	1541	24
106-71	227	40.3		8354	0.09551	0.00074	3.60323	0.07967	0.27456	0.00531	0.29	1.5	1538	14	1550	18	1564	27
106-80	207	39.9		13104	0.09561	0.00071	3.542	0.08764	0.26936	0.00562	0.67	-0.4	1540	14	1537	20	1538	29
106-37	235	44.4		9035	0.09559	0.00052	3.56487	0.06796	0.27104	0.00466	0.73	0.3	1540	10	1542	15	1546	24
106-47	220	39.5		9300	0.09567	0.00075	3.56204	0.05459	0.27027	0.00402	0.94	.	1541	14	1541	12	1542	20
106-75	220	40.8		8044	0.09578	0.00069	3.56855	0.05144	0.27053	0.00352	0.50	-0.1	1543	13	1543	11	1544	18
106-49	243	39.3		5977	0.09588	0.00078	3.5798	0.08375	0.27142	0.00593	0.92	.	1545	15	1545	19	1548	30
106-10	212	37.2		33984	0.09592	0.00066	3.58401	0.05342	0.27139	0.00363	0.67	.	1546	13	1546	12	1548	18
106-08	147	27.3		9239	0.09595	0.00067	3.58541	0.05194	0.27135	0.00351	0.45	-0.1	1547	13	1546	12	1548	18
106-04	120	21.7		10403	0.09594	0.00061	3.60804	0.07228	0.27351	0.00503	0.64	0.6	1547	11	1551	16	1559	25
106-81	137	25		6026	0.09609	0.00075	3.6012	0.05648	0.2722	0.00371	0.76	.	1550	15	1550	12	1552	19
106-52	243	43.6		6707	0.09626	0.00064	3.61317	0.07088	0.27284	0.0048	0.90	.	1553	11	1552	16	1555	24
106-77r	257	44.8		16485	0.09701	0.00066	3.65896	0.05682	0.27408	0.00382	0.55	-0.6	1567	12	1562	12	1562	19
106-77	346	64.3		23020	0.09739	0.00064	3.76568	0.07698	0.28126	0.00518	0.39	1.3	1575	12	1585	16	1598	26
106-45	132	23.6		7944	0.09751	0.00069	3.72248	0.05728	0.27722	0.00379	0.86	-0.1	1577	13	1576	12	1577	19
106-51	269	48.3		21343	0.09756	0.00086	3.31466	0.05388	0.24703	0.00356	0.79	-11.2	1578	16	1485	13	1423	18
Excluded sample																		
Low Rho																		
106-22	479	91.4		13000	0.09579	0.00074	3.5343	0.05097	0.26781	0.00333	-0.02	-1.1	1544	14	1535	11	1530	17

Sample	ppm				Ratios							Discordance	Ages					
Analysis	U	^{206}Pb	$^{206}Pb_c$(%)	$^{206}Pb/^{204}Pb$	$^{207}Pb/^{206}Pb$	1s	$^{207}Pb/^{235}U$	1s	$^{206}Pb/^{238}U$	1s	Rho	Central (%)	$^{207}Pb/^{206}Pb$	1s	$^{207}Pb/^{235}U$	1s	$^{207}Pb/^{238}U$	1s
Pegmatite																		
Young zircons																		
102-19	639	92.1	3.90E-01	3294	0.07035	0.0003	1.60959	0.01839	0.16617	0.00154	0.60	5.9	938	9	974	7	991	8
102-14	672	97.1		10900	0.07325	0.00025	1.73302	0.01822	0.17172	0.00153	0.84	.	1021	7	1021	7	1022	8
102-42	637	77.9		6988	0.07337	0.00035	1.4697	0.01729	0.14553	0.00138	0.78	-15.6	1024	9	918	7	876	8
102-10	500	76.3		5071	0.07358	0.0003	1.78406	0.02161	0.17605	0.0017	0.68	1.5	1030	8	1040	8	1045	9
102-04	527	73.3		4965	0.07361	0.00054	1.79294	0.02405	0.17725	0.00207	0.25	1.9	1031	14	1043	9	1052	11
102-09	491	74.9		3916	0.07367	0.00028	1.78755	0.02089	0.17617	0.00165	0.52	1.3	1032	7	1041	8	1046	9
102-12	746	112.4		13620	0.0737	0.0003	1.78609	0.02028	0.17596	0.00154	0.58	1.1	1033	8	1040	7	1045	8
102-18	386	56.7		3705	0.0738	0.00027	1.77388	0.01898	0.17444	0.00154	0.55	.	1036	7	1036	7	1037	8
102-06	652	96.1		22094	0.07387	0.00024	1.78535	0.01972	0.17549	0.00161	0.73	0.3	1038	6	1040	7	1042	9
102-55	415	63.4		4214	0.07412	0.00032	1.80901	0.02209	0.17716	0.00174	0.44	0.6	1045	8	1049	8	1051	10
102-58	560	85.1		5473	0.07419	0.00027	1.80188	0.02104	0.1763	0.00167	0.53	-0.1	1047	7	1046	8	1047	9
102-01	415	63.1		8271	0.07422	0.00032	1.81672	0.02206	0.17774	0.00172	0.48	0.6	1047	8	1052	8	1055	9
102-20	532	76.8		2780	0.07425	0.00037	1.80827	0.01849	0.17672	0.00156	0.56	.	1048	10	1048	7	1049	9
102-29	294	45.1		71249	0.07438	0.00033	1.84491	0.02386	0.17997	0.00188	0.79	1.5	1052	8	1062	9	1067	10
102-41	598	92.9		5893	0.07502	0.00031	1.86999	0.02296	0.18094	0.0018	0.70	0.2	1069	8	1071	8	1072	10
102-36b	245	37.4		6780	0.07517	0.00028	1.88942	0.02245	0.18233	0.00184	0.83	0.6	1073	7	1077	8	1080	10
102-53	338	52.1		4771	0.07526	0.00042	1.88313	0.0259	0.18153	0.00182	0.91	.	1075	11	1075	9	1075	10
102-48	384	60		5833	0.07976	0.00039	2.16309	0.02551	0.19676	0.00212	0.89	-3.1	1191	10	1169	8	1158	11
102-56	277	43.9		4593	0.08073	0.0004	2.18267	0.02175	0.19615	0.00183	0.49	-5.4	1215	9	1176	7	1155	10
102-38	438	70.2		25449	0.0809	0.00035	2.23352	0.02416	0.20026	0.00197	0.48	-3.8	1219	8	1192	8	1177	11
102-31	298	54.9		12582	0.08512	0.00032	2.61322	0.03037	0.22253	0.00231	0.72	-1.9	1318	7	1304	9	1295	12
102-27	311	55.1		9595	0.08684	0.00044	2.66546	0.0303	0.22246	0.00251	0.87	-5	1357	10	1319	8	1295	13
102-50	384	73.6	3.30E-01	3053	0.08702	0.0004	2.64778	0.03394	0.22086	0.00225	0.75	-6.1	1361	9	1314	9	1286	12
Older zircons																		
102-28	264	51.7		13707	0.08954	0.00044	3.03338	0.03344	0.24536	0.00282	0.50	.	1416	9	1416	8	1415	15
102-02	208	44.5		6144	0.09195	0.00046	3.13932	0.04296	0.24758	0.00266	0.65	-3	1466	9	1442	11	1426	14
102-37	219	44.5		2686	0.09287	0.00042	3.18063	0.03857	0.2482	0.00268	0.67	-4.1	1485	8	1452	9	1429	14
102-35	422	87.8		12956	0.09335	0.00035	3.18991	0.04046	0.24774	0.00262	0.86	-5	1495	7	1455	10	1427	14
102-30	275	59.7		13966	0.09366	0.00035	3.37158	0.04324	0.26085	0.00284	0.73	-0.4	1501	7	1498	10	1494	14
102-34	287	65.7		13022	0.09401	0.0004	3.46224	0.04702	0.26697	0.00299	0.45	1.3	1508	8	1519	11	1525	15
102-36a	344	72.3		12562	0.0946	0.00046	3.18506	0.04319	0.24425	0.00267	0.82	-8.2	1520	9	1454	10	1409	14
102-69	284	64.7		3770	0.09479	0.00041	3.56704	0.04414	0.27262	0.00296	0.74	2.3	1524	8	1542	10	1554	15
102-26	190	42.3		13246	0.09549	0.00044	3.54714	0.04614	0.26907	0.00313	0.64	.	1538	8	1538	10	1536	16
102-59	153	34.8		3366	0.09591	0.0005	3.63943	0.04407	0.27494	0.00296	0.60	1.6	1546	9	1558	10	1566	15
Excluded samples																		
High common lead																		
102-21	271	56.1	7.80E-01	1484	0.08849	0.00033	2.98509	0.0336	0.24456	0.0024	0.70	1.4	1393	7	1404	9	1410	12
102-64	136	32.2		1510	0.09581	0.00049	3.61491	0.0506	0.27354	0.00305	0.72	1.1	1544	9	1553	11	1559	15

Sample	ppm				Ratios						Discordance		Ages					
Analysis	U	^{206}Pb	$^{206}Pb_c$(%)	$^{206}Pb/^{204}Pb$	$^{207}Pb/^{206}Pb$	1s	$^{207}Pb/^{235}U$	1s	$^{206}Pb/^{238}U$	1s	Rho	Central (%)	$^{207}Pb/^{206}Pb$	1s	$^{207}Pb/^{235}U$	1s	$^{207}Pb/^{238}U$	1s
Coarse-grained granite																		
EPB-05-76	410	74.1		19459	0.09372	0.00107	3.43344	0.03293	0.26517	0.00244	0.94	1.2	1503	20	1512	8	1516	12
EPB-05-64	372	62.2		5717	0.09417	0.00112	3.27159	0.04976	0.25189	0.00397	0.95	-4.6	1512	22	1474	12	1448	20
EPB-05-06	243	36.6		5548	0.09424	0.00059	3.40542	0.03861	0.2617	0.00293	0.78	-0.9	1513	11	1506	9	1499	15
EPB-05-81	221	36.6		2634	0.09439	0.00113	3.16133	0.03529	0.24264	0.0023	0.94	-8.4	1516	22	1448	9	1400	12
EPB-05-73	457	84.1		47188	0.09445	0.00109	3.51709	0.03353	0.2695	0.00239	0.82	1.8	1517	21	1531	8	1538	12
EPB-05-74	456	79.9		15722	0.09455	0.00109	3.42721	0.03908	0.26268	0.00341	0.92	-1.1	1519	21	1511	9	1504	17
EPB-05-12	210	30.7		6348	0.09456	0.00079	3.48043	0.07439	0.26627	0.00526	0.91	0.4	1519	15	1523	17	1522	27
EPB-05-71	322	57.9		6345	0.09471	0.00106	3.47727	0.03144	0.26583	0.00234	0.91	.	1522	20	1522	7	1520	12
EPB-05-72	153	28.3		10019	0.09487	0.00111	3.56045	0.03351	0.27167	0.00249	0.73	2	1525	21	1541	7	1549	13
EPB-05-01	465	73.6		10965	0.09492	0.00055	3.54255	0.03899	0.27026	0.00281	0.96	1.3	1526	10	1537	9	1542	14
EPB-05-08	352	55.5		11427	0.09508	0.00056	3.5251	0.03857	0.26858	0.00269	0.75	0.4	1530	11	1533	9	1534	14
EPB-05-28	318	51.6		17862	0.09511	0.00056	3.61536	0.03847	0.27535	0.00281	0.84	2.9	1530	11	1553	8	1568	14
EPB-05-02	436	69.4		53326	0.09518	0.00056	3.56354	0.03825	0.27115	0.00273	0.93	1.2	1532	11	1541	9	1547	14
EPB-05-50	169	28		9465	0.09525	0.00066	3.55246	0.05777	0.27084	0.00395	0.93	0.8	1533	13	1539	13	1545	20
EPB-05-33	496	72		83838	0.09538	0.00057	3.24036	0.03646	0.24647	0.00258	0.93	-8.4	1536	11	1467	9	1420	13
EPB-05-17	329	51.8		14449	0.09542	0.00056	3.52679	0.03927	0.26785	0.00275	0.89	-0.4	1536	11	1533	9	1530	14
EPB-05-40	175	27.7		9738	0.09539	0.00063	3.56013	0.04273	0.27048	0.00317	0.84	0.6	1536	12	1541	10	1543	16
EPB-05-62	284	52.6		7854	0.09545	0.00101	3.58076	0.03425	0.27152	0.00255	0.90	1.1	1537	19	1545	8	1549	13
EPB-05-32	127	20		6496	0.09554	0.0006	3.53755	0.04122	0.26839	0.00297	0.86	-0.4	1539	11	1536	9	1533	15
EPB-05-52	156	24.8		18190	0.09567	0.00062	3.54759	0.03916	0.26892	0.00285	0.80	-0.4	1541	11	1538	9	1535	14
EPB-05-34	193	29.5		11375	0.09566	0.00058	3.57381	0.05083	0.27027	0.00403	0.76	0.3	1541	11	1544	11	1542	20
EPB-05-68	427	76.7		5507	0.09572	0.00123	3.52773	0.03573	0.26691	0.00242	0.93	-1.1	1542	24	1533	8	1525	12
EPB-05-35	179	28.2		24039	0.0958	0.00059	3.52068	0.03955	0.26646	0.00283	0.87	-1.5	1544	11	1532	9	1523	14
EPB-05-26	307	47.8		26992	0.0958	0.00058	3.63597	0.05071	0.27465	0.00395	0.94	1.7	1544	11	1557	11	1564	20
EPB-05-58	394	70.5		12833	0.096	0.00124	3.54386	0.03564	0.26737	0.00244	0.68	-1.3	1548	24	1537	8	1527	12
EPB-05-14	423	61.4		2813	0.09608	0.00073	3.10396	0.06088	0.23433	0.00389	0.90	-13.8	1549	13	1434	15	1357	20
EPB-05-15	183	29.5		4912	0.09643	0.00068	3.56024	0.049	0.26765	0.00333	0.73	-1.9	1556	13	1541	11	1529	17
EPB-05-51	370	60.1		4161	0.09653	0.00064	3.56717	0.04732	0.26833	0.00322	0.68	-2	1558	13	1542	11	1532	16
EPB-05-53	384	63.1		15514	0.0978	0.0007	3.75173	0.04593	0.27816	0.00323	0.76	.	1583	13	1582	10	1582	16
EPB-05-42	610	89.7		3379	0.09788	0.00069	3.5089	0.06912	0.25949	0.00497	0.88	-6.7	1584	13	1529	16	1487	25
EPB-05-44	384	58.9		26148	0.09806	0.00058	3.66176	0.05166	0.27025	0.004	0.86	-3	1587	11	1563	11	1542	20
EPB-05-20	195	29		2375	0.09928	0.00063	3.60127	0.0461	0.26287	0.00342	0.25	-7.3	1611	11	1550	10	1505	17
Excluded samples																		
High common lead																		
EPB-05-43	303	44.6	1.00E+01	174	0.08283	0.00356	2.57282	0.15908	0.2252	0.00282	0.92	3.9	1265	77	1293	45	1309	15
EPB-05-09	463	63.5	9.30E+00	177	0.08481	0.0041	2.49451	0.17189	0.21326	0.00286	0.86	-5.4	1311	91	1270	50	1246	15
EPB-05-36	351	53	2.30E+00	608	0.09207	0.0006	3.17133	0.03468	0.2498	0.00261	0.41	-2.4	1469	12	1450	8	1437	13
EPB-05-54	184	21.5	1.70E+00	724	0.09219	0.00067	2.53901	0.0326	0.20011	0.00265	0.82	-22.1	1471	13	1283	9	1176	14
EPB-05-37	388	55.5	2.60E+00	549	0.09282	0.00064	3.02504	0.03406	0.23649	0.00259	0.76	-8.7	1484	12	1414	9	1368	14
EPB-05-55	213	28.8		1645	0.10088	0.00063	3.69411	0.07685	0.2653	0.00493	0.58	-8.3	1640	11	1570	17	1517	25
EPB-05-05	871	88		823	0.10122	0.00071	2.41416	0.02569	0.17348	0.00175	0.69	-40.6	1647	13	1247	8	1031	10
EPB-05-07	362	49.1		684	0.10971	0.00078	3.49777	0.03777	0.2317	0.0023	0.15	-28	1795	13	1527	9	1343	12
EPB-05-79	493	57.5		504	0.11427	0.00092	3.61303	0.07946	0.22969	0.00437	-0.12	-31.8	1868	14	1552	17	1333	23

Sample	ppm				Ratios							Discordance	Ages					
Analysis	U	^{206}Pb	$^{206}Pb_c$(%)	$^{206}Pb/^{204}Pb$	$^{207}Pb/^{206}Pb$	1s	$^{207}Pb/^{235}U$	1s	$^{206}Pb/^{238}U$	1s	Rho	Central (%)	$^{207}Pb/^{206}Pb$	1s	$^{207}Pb/^{235}U$	1s	$^{207}Pb/^{238}U$	1s
Garnet-biotite gneiss																		
103-37	244	40.4		4853	0.09188	0.00107	3.23208	0.07116	0.25551	0.00517	0.77	.	1465	21	1465	17	1467	27
103-47	133	22.2		2455	0.09227	0.00113	3.29663	0.08611	0.25893	0.00598	0.62	0.9	1473	23	1480	20	1484	31
103-42	325	54.6		4335	0.09246	0.00113	3.28155	0.07359	0.25767	0.00498	0.64	.	1477	23	1477	17	1478	26
103-46	195	33.3		4362	0.0928	0.00105	3.36483	0.08073	0.26288	0.00566	0.49	1.6	1484	21	1496	19	1505	29
103-31	339	57		8464	0.09288	0.00111	3.32062	0.07483	0.25979	0.00536	0.73	.	1486	22	1486	18	1489	27
103-19	138	22.6		55127	0.09312	0.00112	3.33829	0.08547	0.26047	0.00641	0.63	.	1490	22	1490	20	1492	33
103-14	280	44.7		9691	0.09324	0.00122	3.2885	0.08963	0.25622	0.00689	0.80	-1.8	1493	24	1478	21	1470	35
103-09	165	27.7		6649	0.09337	0.00118	3.36071	0.08386	0.26169	0.00602	0.60	.	1495	24	1495	20	1499	31
103-29	216	36.2		683331	0.09341	0.00108	3.3493	0.08534	0.26055	0.00598	0.63	-0.4	1496	22	1493	20	1493	31
103-34	214	36.9		3164	0.09342	0.00117	3.44791	0.08622	0.26799	0.00615	0.73	2.4	1496	23	1515	20	1531	31
103-06	391	63.4		18889	0.09351	0.0012	3.36985	0.09324	0.2618	0.00711	0.61	-0.1	1498	24	1497	22	1499	36
103-16	75	12.4		2245	0.09355	0.00124	3.3775	0.09595	0.26222	0.00706	0.78	.	1499	25	1499	22	1501	36
103-07	213	34.9		20264	0.09357	0.00123	3.37826	0.0934	0.26233	0.00711	0.78	.	1499	24	1499	22	1502	36
103-28	130	21.1		9771	0.09361	0.00125	3.39059	0.09344	0.26297	0.00714	0.75	0.2	1500	24	1502	22	1505	36
103-45	96	15.5		2455	0.09369	0.00126	3.33033	0.08949	0.25775	0.00681	0.60	-1.7	1502	25	1488	21	1478	35
103-01	82	13.9		3348	0.0938	0.00122	3.41857	0.08681	0.26506	0.00617	0.63	0.6	1504	23	1509	20	1516	31
103-44	162	27.6		2853	0.09392	0.00117	3.40873	0.08149	0.26349	0.00564	0.84	.	1507	22	1506	19	1508	29
103-33	185	30.8		3683	0.09395	0.0012	3.41311	0.09116	0.26373	0.00681	0.65	.	1507	23	1507	21	1509	35
Excluded samples																		
High common lead																		
103-43	86	13.6		1135	0.09266	0.00128	3.31054	0.09023	0.25931	0.00697	0.62	0.3	1481	26	1484	21	1486	36
103-50	194	33.5		1852	0.09283	0.00115	3.37763	0.07641	0.26381	0.00518	0.45	1.9	1484	22	1499	18	1509	26
103-30	94	16.2		1564	0.09341	0.00116	3.45809	0.08337	0.26888	0.00623	0.51	2.8	1496	22	1518	19	1535	32
103-49	106	16.7		808	0.09401	0.00127	3.26198	0.08913	0.25164	0.00672	0.68	-4.5	1508	24	1472	21	1447	35
103-36	69	11.7		1140	0.09402	0.00116	3.4114	0.0827	0.26359	0.00565	0.64	-0.2	1508	23	1507	19	1508	29

Sample	ppm				Ratios							Discordance	Ages					
Analysis	U	^{206}Pb	$^{206}Pb_c$(%)	$^{206}Pb/^{204}Pb$	$^{207}Pb/^{206}Pb$	1s	$^{207}Pb/^{235}U$	1s	$^{206}Pb/^{238}U$	1s	Rho	Central (%)	$^{207}Pb/^{206}Pb$	1s	$^{207}Pb/^{235}U$	1s	$^{207}Pb/^{238}U$	1s
Augen gneiss																		
112-11	658	106	4.10E-01	2800	0.09161	0.00112	3.21019	0.08394	0.25382	0.00636	0.91	.	1459	22	1460	20	1458	33
112-50	899	140.7		7243	0.09208	0.00122	3.18806	0.08877	0.25025	0.0065	0.88	-1.9	1469	25	1454	22	1440	34
112-20	190	32.7		5111	0.09245	0.00105	3.35648	0.07421	0.26312	0.00519	0.60	2.3	1477	21	1494	17	1506	27
112-27	282	48.4		7654	0.09259	0.0011	3.33759	0.07523	0.26112	0.00501	0.48	1.3	1479	23	1490	18	1496	26
112-56	111	18.3		3073	0.09266	0.00123	3.40513	0.09022	0.26585	0.00717	0.78	3.2	1481	24	1506	21	1520	36
112-25	101	17.1		3790	0.09271	0.00117	3.3095	0.07708	0.25858	0.00532	0.46	0.2	1482	23	1483	18	1483	27
112-02	103	17.3		5066	0.0929	0.00112	3.32727	0.08821	0.25931	0.00619	0.61	0.2	1486	22	1487	21	1486	32
112-51	131	21.2		3614	0.09291	0.00127	3.38738	0.09536	0.2638	0.00719	0.42	2	1486	25	1501	22	1509	37
112-54	123	20.2		3123	0.09298	0.00119	3.3257	0.0899	0.25869	0.00662	0.70	-0.1	1487	23	1487	21	1483	34
112-41	174	29.4		6960	0.09311	0.00118	3.49443	0.09622	0.27139	0.00742	0.83	4.7	1490	24	1526	22	1548	38
112-21	51	8.6		2404	0.09315	0.00119	3.34123	0.09491	0.25955	0.00654	0.63	.	1491	24	1491	22	1488	33
112-32	187	32.8		8106	0.09328	0.00116	3.42383	0.07783	0.26586	0.00521	0.57	2.1	1494	24	1510	18	1520	27
112-65	116	25.7		22343	0.09357	0.0004	3.39589	0.04571	0.26304	0.00293	0.63	0.5	1499	8	1503	11	1505	15
112-33	144	24.9		3150	0.09366	0.00138	3.38017	0.07851	0.2614	0.00539	0.86	-0.2	1501	28	1500	18	1497	28
112-44	162	28		2864	0.09368	0.00117	3.45644	0.09118	0.2669	0.00617	0.75	2	1502	23	1517	21	1525	31
112-61	191	42.2		3729	0.09408	0.00039	3.42384	0.04487	0.26373	0.00293	0.77	.	1510	7	1510	10	1509	15
112-73	476	104.9		4625	0.09421	0.00034	3.44977	0.04308	0.26534	0.00291	0.86	0.4	1512	6	1516	10	1517	15
112-67	102	23.3		2361	0.09457	0.00047	3.50388	0.051	0.26853	0.00322	0.66	1.1	1519	9	1528	11	1533	16
112-68	203	46.6		2432	0.09562	0.00037	3.63787	0.04532	0.27564	0.00301	0.60	2.2	1540	7	1558	10	1569	15
112-34	232	40.7		2391	0.09564	0.00115	3.56174	0.08791	0.26957	0.00597	0.60	.	1541	23	1541	20	1539	30
Excluded samples																		
High common lead																		
112-79	178	40		2066	0.09347	0.00039	3.45726	0.04612	0.26797	0.00301	0.65	2.6	1497	8	1518	11	1530	15
112-75	119	27.2		1886	0.0941	0.0005	3.48686	0.04944	0.26858	0.00311	0.45	1.8	1510	9	1524	11	1534	16

Sample	ppm				Ratios							Discordance	Ages					
Analysis	U	^{206}Pb	$^{206}Pb_c$(%)	$^{206}Pb/^{204}Pb$	$^{207}Pb/^{206}Pb$	1s	$^{207}Pb/^{235}U$	1s	$^{206}Pb/^{238}U$	1s	Rho	Central (%)	$^{207}Pb/^{206}Pb$	1s	$^{207}Pb/^{235}U$	1s	$^{207}Pb/^{238}U$	1s
Fine-grained granite																		
EPB-04-49	222	35.9		7969	0.08915	0.00061	2.95904	0.05066	0.24117	0.00364	0.87	-1.3	1407	13	1397	13	1393	19
EPB-04-26	856	142.7	4.00E-01	4630	0.09144	0.00072	3.19072	0.05344	0.25329	0.00382	0.86	-0.1	1456	14	1455	13	1455	20
EPB-04-82	413	71.5		9958	0.09177	0.00069	3.16406	0.07517	0.25043	0.00527	0.57	-1.8	1463	14	1448	18	1441	27
EPB-04-54	138	23		6880	0.09252	0.00078	3.28914	0.04832	0.25787	0.00328	0.77	0.1	1478	15	1478	11	1479	17
EPB-04-62	139	22.7		6471	0.09255	0.00082	3.28523	0.04402	0.25736	0.00309	0.85	-0.1	1479	17	1478	10	1476	16
EPB-04-61	185	32.5		6566	0.09281	0.00062	3.31321	0.05789	0.25947	0.00418	0.67	.	1484	12	1484	14	1487	21
EPB-04-08	90	15.9		4920	0.09303	0.00062	3.39879	0.05323	0.26537	0.00364	0.58	2	1488	13	1504	12	1517	19
EPB-04-83	53	9.2		14524	0.09302	0.00091	3.41924	0.05876	0.26664	0.00406	0.52	2.7	1488	17	1509	14	1524	21
EPB-04-31	102	18.8		8807	0.0931	0.00062	3.43314	0.0737	0.26811	0.00522	0.73	2.9	1490	13	1512	17	1531	27
EPB-04-36	81	14.5		591576	0.09318	0.00074	3.37246	0.05862	0.26325	0.00416	0.69	0.8	1492	15	1498	14	1506	21
EPB-04-33	103	17.8		3881	0.09331	0.00074	3.42369	0.0493	0.26616	0.00352	0.60	2	1494	15	1510	11	1521	18
EPB-04-63	96	17		15494	0.09336	0.00061	3.38177	0.06007	0.26322	0.00426	0.60	0.6	1495	12	1500	14	1506	22
EPB-04-03	75	13.1		2109	0.09352	0.00067	3.37387	0.05362	0.26206	0.00373	0.66	.	1498	13	1498	12	1500	19
EPB-04-75	221	37.4		6427	0.09356	0.00073	3.37912	0.04919	0.26189	0.00334	0.82	.	1499	14	1500	11	1500	17
EPB-04-27	176	31.1		10503	0.09355	0.00058	3.40126	0.05554	0.26408	0.0039	0.62	0.7	1499	11	1505	13	1511	20
EPB-04-56	62	10.6		3282	0.09358	0.00073	3.38115	0.05513	0.26215	0.00379	0.69	0.1	1500	14	1500	13	1501	19
EPB-04-71	367	60.7		30234	0.09359	0.00078	3.38299	0.04162	0.26199	0.00319	0.49	0.1	1500	16	1500	10	1500	16
EPB-04-43	118	21.1		26180	0.09366	0.00061	3.38574	0.06164	0.26274	0.00433	0.72	.	1501	12	1501	14	1504	22
EPB-04-53	111	19.6		3025	0.09364	0.00064	3.38438	0.05907	0.26254	0.00411	0.75	.	1501	12	1501	14	1503	21
EPB-04-13	121	20.8		2216	0.09418	0.0008	3.43185	0.0514	0.26453	0.0033	0.57	.	1512	16	1512	12	1513	17
EPB-04-18	178	31.9		25514	0.0952	0.00076	3.51938	0.05995	0.26851	0.00382	0.60	.	1532	15	1532	13	1533	19
Excluded samples																		
High common lead, row Rho																		
EPB-04-39	60	10.5		1799	0.0934	0.00063	3.36433	0.06038	0.26166	0.00415	0.64	.	1496	12	1496	14	1498	21
EPB-04-42	60	10.8		1594	0.09362	0.00067	3.38311	0.06048	0.26265	0.00441	0.53	.	1501	13	1500	14	1503	23
EPB-04-38	115	20.8		6352	0.09386	0.00081	3.45673	0.05896	0.26787	0.0041	-0.02	1.6	1505	16	1517	13	1530	21
EPB-04-24	153	26		7460	0.09402	0.00074	3.41984	0.04457	0.26388	0.00294	0.05	0.1	1508	14	1509	10	1510	15
EPB-04-67	108	20.2		1718	0.09407	0.00072	3.50072	0.08812	0.27025	0.00592	0.37	2.3	1510	14	1527	20	1542	30

Sample	ppm				Ratios							Discordance	Ages					
Analysis	U	^{206}Pb	$^{206}Pb_c$(%)	$^{206}Pb/^{204}Pb$	$^{207}Pb/^{206}Pb$	1s	$^{207}Pb/^{235}U$	1s	$^{206}Pb/^{238}U$	1s	Rho	Central (%)	$^{207}Pb/^{206}Pb$	1s	$^{207}Pb/^{235}U$	1s	$^{207}Pb/^{238}U$	1s
Red granite																		
EPB-06-18	1005	96.4	6.20E-01	2305	0.0874	0.00064	2.2889	0.05335	0.18968	0.00374	0.92	-19.7	1369	13	1209	16	1120	20
EPB-06-41	654	67.4	4.10E-01	3588	0.0901	0.00064	2.75229	0.03539	0.22165	0.00238	0.87	-10.6	1428	13	1343	10	1291	13
EPB-06-51	825	94.2	5.80E-01	2329	0.09087	0.00057	2.82384	0.06817	0.22496	0.00492	0.95	-10.2	1444	12	1362	18	1308	26
EPB-06-43	905	94.7	4.50E-01	2495	0.09121	0.0007	2.81566	0.03185	0.22409	0.00205	0.73	-11.3	1451	14	1360	8	1303	11
EPB-06-20	797	106.1	5.10E-01	2922	0.0912	0.00073	3.07191	0.08107	0.24359	0.00563	0.88	-3.2	1451	15	1426	20	1405	29
EPB-06-16	483	66	5.00E-01	2493	0.09148	0.00057	3.25851	0.07798	0.25768	0.00551	0.79	1.9	1457	11	1471	19	1478	28
EPB-06-12	820	99	3.10E-01	4486	0.09262	0.00059	3.29428	0.05077	0.25736	0.0033	0.69	.	1480	12	1480	12	1476	17
EPB-06-39	828	99.8	3.40E-01	3949	0.09295	0.00076	3.32627	0.05375	0.25904	0.00344	0.70	.	1487	15	1487	13	1485	18
EPB-06-35	599	84.2	2.70E-01	3974	0.09327	0.00058	3.4329	0.08537	0.26625	0.0059	0.88	2.4	1493	12	1512	20	1522	30
EPB-06-31	856	105.6	1.40E-01	8032	0.09331	0.0006	3.35477	0.05665	0.26026	0.00379	0.94	.	1494	11	1494	13	1491	19
EPB-06-11	717	88.4	2.50E-01	3699	0.0944	0.00067	3.44973	0.06034	0.26436	0.00376	0.66	.	1516	13	1516	14	1512	19
Excluded samples																		
High common lead, low Rho																		
EPB-06-28	960	76.8		1420	0.09416	0.00061	2.13368	0.04545	0.16465	0.00326	0.97	-37.8	1511	12	1160	15	983	18
EPB-06-80	577	64.9		1625	0.09585	0.00058	3.05809	0.06128	0.23141	0.00418	0.96	-14.6	1545	11	1422	15	1342	22
EPB-06-71	789	92.1		1575	0.09661	0.00058	3.19213	0.0645	0.2396	0.00441	0.97	-12.4	1560	11	1455	16	1385	23
EPB-06-79	645	74		1361	0.09799	0.00062	3.18721	0.06205	0.23595	0.00417	0.81	-15.4	1586	11	1454	15	1366	22
EPB-06-21	948	88.5		1349	0.0981	0.00068	2.56133	0.04632	0.18959	0.00317	0.89	-32.2	1588	13	1290	13	1119	17
EPB-06-17	951	91.1		1017	0.09912	0.00064	2.66505	0.0484	0.19522	0.00296	0.77	-31.1	1608	11	1319	13	1150	16
EPB-06-50	241	33		1286	0.09926	0.0006	3.84814	0.07906	0.28077	0.00516	0.93	-0.9	1610	11	1603	17	1595	26
EPB-06-73	840	101.4		1347	0.0997	0.0006	3.40192	0.06734	0.24746	0.00441	0.93	-13.3	1618	10	1505	16	1425	23
EPB-06-22	798	97.8		1690	0.0997	0.00071	3.41769	0.06469	0.24845	0.00403	-0.08	-12.9	1618	13	1508	15	1430	21
EPB-06-48	864	91.9		1054	0.10004	0.00068	2.99874	0.06158	0.21754	0.00369	0.96	-24.2	1625	13	1407	16	1269	20
EPB-06-55	867	109.8		1374	0.10091	0.0006	3.60626	0.0726	0.2591	0.00466	0.96	-10.6	1641	11	1551	16	1485	24
EPB-06-49	725	88.4		1111	0.1012	0.0007	3.48068	0.07134	0.24938	0.00428	0.92	-14.3	1646	12	1523	16	1435	22
EPB-06-68	899	111.3		1599	0.10135	0.00103	3.54872	0.0784	0.25392	0.00453	0.66	-12.9	1649	18	1538	18	1459	23
EPB-06-44	980	109.4		900	0.10369	0.00064	3.25389	0.0621	0.22776	0.00372	0.89	-24.1	1691	11	1470	15	1323	20
EPB-06-67	862	92.9		924	0.10476	0.00151	3.19103	0.08925	0.22125	0.00412	0.94	-27.3	1710	26	1455	22	1288	22
EPB-06-26	1003	92.1		623	0.10716	0.0007	2.7673	0.04935	0.18773	0.00279	0.25	-40	1752	12	1347	13	1109	15
EPB-06-33	730	70.2		330	0.124	0.001	3.33497	0.07512	0.19584	0.00401	0.93	-46.8	2015	14	1489	18	1153	22
EPB-06-24	958	108.3		297	0.13724	0.00248	4.32687	0.11423	0.22981	0.00361	0.28	-43.6	2193	30	1698	22	1334	19
Tonalitic gneiss																		
101-12	275	46.3		18236	0.08978	0.00105	3.04247	0.0376	0.24537	0.00262	0.96	-0.3	1421	22	1418	9	1415	14
101-20	257	45.4		6127	0.09135	0.00112	3.22871	0.03517	0.25585	0.00248	0.87	1.3	1454	23	1464	8	1469	13
101-10	430	68.3	2.40E-01	6601	0.09141	0.001	2.90047	0.02824	0.22988	0.00211	0.92	-9.1	1455	20	1382	7	1334	11
101-35	233	42		10993	0.09143	0.00113	3.25762	0.03633	0.25791	0.00262	0.89	2	1456	22	1471	9	1479	13
101-29	536	94.5		33977	0.09243	0.00111	3.23952	0.03792	0.25375	0.00268	0.96	-1.2	1476	22	1467	9	1458	14
101-34	268	45.3		4529	0.09263	0.00102	3.09061	0.03241	0.24169	0.00232	0.82	-6.3	1480	20	1430	8	1395	12
101-30	345	62.5		19464	0.09263	0.00114	3.33798	0.03601	0.26085	0.00259	0.92	1.2	1480	22	1490	8	1494	13
101-32	312	55.5		25211	0.09298	0.00116	3.31563	0.03438	0.2582	0.0023	0.86	-0.3	1487	22	1485	8	1481	12
101-14	333	59.3		25092	0.09308	0.0011	3.33712	0.03328	0.25955	0.00242	0.95	.	1489	22	1490	8	1488	12
101-05	365	63.6		14458	0.09308	0.00112	3.28538	0.03	0.25557	0.00209	0.85	-1.5	1490	22	1478	7	1467	11
101-24	410	73.8		20801	0.09318	0.00113	3.34756	0.03408	0.26008	0.00246	0.79	0.1	1491	21	1492	8	1490	13
101-28	156	27.7		10324	0.09325	0.00123	3.32494	0.03542	0.25821	0.00232	0.86	-0.8	1493	24	1487	8	1481	12
101-17	399	71.2		10379	0.09329	0.00117	3.3553	0.03603	0.26042	0.00238	0.94	.	1494	24	1494	8	1492	12
101-33	335	60.5		20705	0.0933	0.00118	3.35523	0.03565	0.26034	0.00241	0.91	.	1494	24	1494	8	1492	12
101-22	447	80.7		17029	0.09343	0.00111	3.36577	0.03487	0.26078	0.00247	0.81	.	1497	21	1496	8	1494	13
101-15	361	65.5		25350	0.09373	0.00111	3.4087	0.03465	0.26322	0.00248	0.90	0.5	1503	22	1506	8	1506	13
101-08	329	58.5		13574	0.09417	0.00108	3.37315	0.03433	0.25934	0.00248	0.94	-1.7	1511	20	1498	8	1486	13
101-37	206	37.6		9309	0.09428	0.00118	3.41283	0.03799	0.26206	0.00263	0.85	-0.8	1514	23	1507	9	1500	13
101-38	370	66.7		32806	0.09452	0.0012	3.39512	0.0384	0.26012	0.00251	0.95	-1.9	1519	23	1503	9	1490	13

8.5 LA-MC-ICPMS Hf zircon data

Table 5. LA-MC-ICPMS Lu-Hf data on zircons

Sample																	$^{176}Lu/^{177}Hf$ (0.015)
Analysis	Age(Ma)	$^{176}Hf/^{177}Hf$	1σ	$^{176}Lu/^{177}Hf$	1σ	$^{176}Yb/^{177}Hf$	1σ	t(Ga)	$^{176}Hf/^{177}Hf(t)$	2σ	$\varepsilon_{Hf}(t)$	2σ	t_{DM}	2σ	Protolith age	
Granitic gneiss																
105-01	1536	0.281992946	0.000012	0.00107327	0.000026	0.0359427	0.00045	1.54	0.281960674	2.4E-05	6.634924828	0.796256926	1.72	0.014924883	1.83	
105-07	1536	0.282134043	0.000037	0.00147625	9.7E-06	0.0616463	0.00056	1.54	0.282089654	7.4E-05	11.21235771	2.605518621	1.54	0.049959083	1.55	
105-10	1536	0.282084711	0.000017	0.000808607	7.1E-06	0.0291514	0.0007	1.54	0.282060397	3.4E-05	10.17404346	1.19148885	1.58	0.022442994	1.61	
105-11	1536	0.282197544	0.000041	0.000797047	9.2E-06	0.0306207	0.00057	1.54	0.282173577	8.2E-05	14.19075665	2.890501504	1.43	0.054567159	1.37	
105-16	1536	0.28201954	0.000015	0.00150303	8.3E-06	0.066129	0.0008	1.54	0.281974346	3E-05	7.120133425	1.046969876	1.70	0.019998989	1.80	
105-17	1536	0.282084859	0.000023	0.00100591	0.000024	0.0455625	0.00063	1.54	0.282054613	4.6E-05	9.968757066	1.581293759	1.59	0.029871677	1.62	
105-18	1536	0.282056668	0.00003	0.000911032	6.2E-06	0.0384001	0.00091	1.54	0.282029274	6E-05	9.069506424	2.116135894	1.62	0.039896291	1.68	
105-20	1536	0.282034452	0.000021	0.00123729	0.000023	0.0491775	0.0016	1.54	0.281997248	4.2E-05	7.932931482	1.441470123	1.67	0.027310228	1.75	
105-23	1536	0.282055261	0.000031	0.00159233	0.000046	0.059727	0.001	1.54	0.282007382	6.2E-05	8.292572205	2.102171902	1.66	0.040161914	1.73	
105-26	1536	0.281994275	0.000014	0.00113102	0.000069	0.0418888	0.0022	1.54	0.281960267	2.8E-05	6.620473021	0.846442292	1.72	0.015668105	1.83	
105-27	1536	0.281979152	0.000025	0.00119372	0.000059	0.0429774	0.00081	1.54	0.281943259	5E-05	6.016873672	1.648553081	1.74	0.030890216	1.86	
105-28	1536	0.281983983	0.000016	0.00118468	0.000045	0.0356165	0.00073	1.54	0.281948361	3.2E-05	6.197941889	1.039622041	1.73	0.019452788	1.85	
105-30	1536	0.281983225	0.00002	0.00111882	0.000055	0.0423297	0.001	1.54	0.281949584	4E-05	6.24134934	1.302195358	1.73	0.024326416	1.85	
105-31	1536	0.282092344	0.000019	0.00144687	0.000038	0.0501226	0.00053	1.54	0.282048839	3.8E-05	9.763848026	1.267498574	1.60	0.024180401	1.64	
105-33	1536	0.281988532	0.000016	0.00102791	6.5E-06	0.0396073	0.00044	1.54	0.281957624	3.2E-05	6.526703846	1.121790456	1.72	0.021155398	1.83	
105-35	1536	0.281994646	0.000017	0.00117518	0.000046	0.0386011	0.0003	1.54	0.28195931	3.4E-05	6.586510216	1.108466737	1.72	0.020769623	1.83	
105-38	1536	0.28198134	0.000026	0.000967898	0.000031	0.0413179	0.00067	1.54	0.281952236	5.2E-05	6.335474078	1.779290868	1.73	0.033862395	1.84	
105-40	1536	0.282016433	0.000015	0.00219307	0.00016	0.0759433	0.0051	1.54	0.28195049	3E-05	6.273507104	0.72320498	1.74	0.013148245	1.85	
105-41	1536	0.281977866	0.000014	0.00145943	0.000033	0.0543815	0.00094	1.54	0.281933983	2.8E-05	5.687678172	0.923275095	1.76	0.017421841	1.88	
105-42	1536	0.281970363	0.000021	0.00155349	0.000061	0.0499739	0.00074	1.54	0.281923652	4.2E-05	5.321038123	1.360368831	1.77	0.025608375	1.90	
105-44	1536	0.282005932	0.000021	0.00070552	0.000018	0.0272005	0.00019	1.54	0.281984718	4.2E-05	7.488224559	1.452141346	1.68	0.027131695	1.77	
105-47	1536	0.281994943	0.000022	0.00192868	0.000021	0.0802891	0.0011	1.54	0.28193695	4.4E-05	5.79298992	1.516717552	1.75	0.029195734	1.88	
105-48	1536	0.2820147	0.000015	0.000955004	0.000036	0.0381184	0.002	1.54	0.281985984	3E-05	7.533175852	0.987851302	1.68	0.018479272	1.77	
105-51	1536	0.281944481	0.000022	0.00167472	0.000069	0.0577996	0.0007	1.54	0.281894125	4.4E-05	4.273129377	1.414273815	1.81	0.026571218	1.97	
105-54	1536	0.281965634	0.000026	0.00161936	0.000078	0.0564448	0.0014	1.54	0.281916942	5.2E-05	5.082889922	1.678981375	1.78	0.031602882	1.92	
105-58	1536	0.282034614	0.000018	0.00127379	0.000076	0.0388799	0.001	1.54	0.281996313	3.6E-05	7.899721927	1.115418342	1.67	0.020912039	1.75	
105-63	1536	0.282030247	0.000029	0.00222097	0.00013	0.0687244	0.0026	1.54	0.281963465	5.8E-05	6.733986173	1.780937481	1.72	0.033966248	1.82	
105-69	1536	0.282046239	0.000033	0.00139741	0.000039	0.0421988	0.0006	1.54	0.282004221	6.6E-05	8.180382627	2.259069495	1.66	0.042966608	1.73	
105-72	1536	0.282123498	0.000013	0.00085511	8.7E-06	0.0310332	0.001	1.54	0.282097786	2.6E-05	11.50095563	0.904158297	1.53	0.017060656	1.53	
105-76	1536	0.282033845	0.000019	0.00121218	0.000048	0.0368334	0.00067	1.54	0.281997396	3.8E-05	7.938172089	1.246156129	1.67	0.02347838	1.75	
105-83	1536	0.282034586	0.000016	0.00151376	0.000045	0.0568546	0.00093	1.54	0.281989069	3.2E-05	7.642655432	1.039622041	1.68	0.01971164	1.77	
105-86	1536	0.281968322	0.000017	0.00156139	0.000076	0.0503453	0.0007	1.54	0.281921373	3.4E-05	5.24014368	1.044439401	1.77	0.019465446	1.91	

Sample															$^{176}Lu/^{177}Hf$ (0.015)
Analysis	Age(Ma)	$^{176}Hf/^{177}Hf$	1σ	$^{176}Lu/^{177}Hf$	1σ	$^{176}Yb/^{177}Hf$	1σ	t(Ga)	$^{176}Hf/^{177}Hf(t)$	2σ	$\varepsilon_{Hf}(t)$	2σ	t_{DM}	2σ	Protolith age
Red granite															
EPB-06-09	1493	0.282066943	0.000026	0.00246352	0.00011	0.0714081	0.0029	1.49	0.281994924	5.2E-05	6.866370334	1.617043097	1.68	0.031127653	1.78
EPB-06-11	1493	0.28201021	0.000017	0.0012544	0.000013	0.042459	0.00037	1.49	0.281973539	3.4E-05	6.107496942	1.179550949	1.70	0.022347608	1.83
EPB-06-12	1493	0.282011928	0.000018	0.00183416	0.000061	0.0538243	0.00087	1.49	0.281958308	3.6E-05	5.567014215	1.150932559	1.73	0.021795932	1.86
EPB-06-16	1493	0.281980292	0.000012	0.00161608	0.000098	0.050605	0.0025	1.49	0.281933047	2.4E-05	4.670609001	0.648333232	1.76	0.011696725	1.91
EPB-06-17	1493	0.282014657	0.000015	0.00311818	0.00015	0.100552	0.0051	1.49	0.2819235	3E-05	4.331794513	0.753359569	1.78	0.01376442	1.93
EPB-06-20	1493	0.281956301	0.000013	0.00228386	0.000094	0.0682648	0.0019	1.49	0.281889534	2.6E-05	3.126498657	0.727604389	1.82	0.013301449	2.00
EPB-06-22	1493	0.28195515	0.000015	0.0020922	0.000088	0.0607321	0.0016	1.49	0.281893987	3E-05	3.284504587	0.881997105	1.82	0.016298559	1.99
EPB-06-24	1493	0.281994733	0.000015	0.00211142	0.000065	0.0644199	0.0027	1.49	0.281933008	3E-05	4.669208806	0.929717481	1.76	0.017560796	1.91
EPB-06-28	1493	0.281935412	0.000012	0.00216399	0.000056	0.0672825	0.0013	1.49	0.28187215	2.4E-05	2.509597666	0.735474789	1.85	0.013729173	2.04
EPB-06-31	1493	0.281993925	0.000018	0.00184631	0.000051	0.0538527	0.00054	1.49	0.28193995	3.6E-05	4.915562235	1.171680549	1.75	0.022226865	1.90
EPB-06-35	1493	0.281960773	0.000016	0.00218085	0.000069	0.0640773	0.0014	1.49	0.281897018	3.2E-05	3.392061125	0.992390246	1.81	0.018667309	1.99
EPB-06-39	1493	0.281968955	0.000019	0.00172592	0.000069	0.0535994	0.0012	1.49	0.281918499	3.8E-05	4.154338182	1.205306129	1.78	0.022596516	1.94
EPB-06-41	1493	0.281847629	0.000016	0.00179488	0.00011	0.0565121	0.0019	1.49	0.281795157	3.2E-05	-0.222565436	0.907323488	1.95	0.016011817	2.21
EPB-06-42	1493	0.281949221	0.000025	0.00291292	0.00015	0.095574	0.0022	1.49	0.281864064	5E-05	2.222673826	1.463079178	1.87	0.027337536	2.06
EPB-06-44	1493	0.281985554	0.000014	0.00213042	0.00011	0.0660095	0.0017	1.49	0.281923273	2.8E-05	4.323769899	0.765379567	1.78	0.013983493	1.93
EPB-06-48	1493	0.282019502	0.000016	0.00244636	0.00013	0.0930555	0.0022	1.49	0.281947985	3.2E-05	5.200688767	0.865827509	1.75	0.016029315	1.88
EPB-06-50	1493	0.281913199	0.000019	0.00186012	0.00014	0.0603079	0.0031	1.49	0.28185882	3.8E-05	2.036586801	1.057995402	1.86	0.018902998	2.07
EPB-06-51	1493	0.282195079	0.000018	0.00267339	0.00019	0.0878909	0.0042	1.49	0.282116925	3.6E-05	11.19567137	0.883283493	1.51	0.017350064	1.52
EPB-06-55	1493	0.282067797	0.000039	0.00164481	8.6E-06	0.0727033	0.0004	1.49	0.282019712	7.8E-05	7.745998782	2.750063204	1.64	0.05284591	1.73
EPB-06-67	1493	0.281943249	0.000024	0.00228726	0.0001	0.0687305	0.0017	1.49	0.281876383	4.8E-05	2.659802561	1.495847165	1.84	0.028131364	2.03
EPB-06-68	1493	0.281954384	0.00002	0.00237594	0.00007	0.0675304	0.0012	1.49	0.281884925	4E-05	2.962944164	1.274203291	1.83	0.024215983	2.01
EPB-06-73	1493	0.281973042	0.000016	0.00191876	0.000046	0.0616922	0.0016	1.49	0.281916948	3.2E-05	4.099320451	1.040110622	1.78	0.019715527	1.95
EPB-06-79	1493	0.281927712	0.000016	0.00256511	0.00013	0.0823546	0.0023	1.49	0.281852724	3.2E-05	1.82024843	0.865827509	1.88	0.015557754	2.08
Pegmatite															
102-01	1051	0.282098	7.7E-06	0.000641963	0.000014	0.0252158	0.00032	1.05	0.282084845	1.54E-05	-0.242454609	0.525582317	1.56	0.009679465	1.87
102-02	1530	0.281985	0.000011	0.000987833	0.000026	0.041496	0.0012	1.53	0.281955395	2.2E-05	6.33040376	0.725452922	1.72	0.013545858	1.84
102-04	1051	0.282127	8.6E-06	0.000566218	0.000028	0.0216554	0.0014	1.05	0.282115397	1.72E-05	0.84060188	0.569051876	1.52	0.010322896	1.80
102-06	1051	0.28216	0.000011	0.000819793	0.000022	0.0328953	0.001	1.05	0.282143201	2.2E-05	1.826234869	0.747926241	1.48	0.013872586	1.74
102-09	1051	0.282145	9.9E-06	0.00070886	0.000041	0.0267718	0.0012	1.05	0.282130474	1.98E-05	1.375075707	0.642333829	1.50	0.011600774	1.77
102-10	1051	0.282187	0.000011	0.000691731	0.000021	0.0244224	0.00069	1.05	0.282172825	2.2E-05	2.876396019	0.749379061	1.44	0.013898432	1.68
102-12	1051	0.282159	9.7E-06	0.000568345	0.000016	0.019454	0.00074	1.05	0.282147354	1.94E-05	1.973439765	0.664474546	1.47	0.012290785	1.73
102-14	1051	0.282128	0.000009	0.000813073	4.4E-06	0.0283877	0.00047	1.05	0.282111339	1.8E-05	0.696733385	0.631698006	1.53	0.011867845	1.81
102-18	1051	0.282103	6.7E-06	0.000385582	0.00001	0.0130808	0.00035	1.05	0.282095099	1.34E-05	0.121030473	0.460494662	1.54	0.008461909	1.85
102-19	1051	0.282095	8.8E-06	0.000628065	4.5E-06	0.0197215	0.00033	1.05	0.28208213	1.76E-05	-0.338707364	0.617372937	1.56	0.011526924	1.87
102-20	1051	0.282143	6.7E-06	0.000721299	7.4E-06	0.0246289	0.00059	1.05	0.28212822	1.34E-05	1.295140957	0.464271995	1.50	0.008657122	1.77
102-21	1051	0.282069	0.000016	0.000917514	0.000018	0.0369106	0.00077	1.05	0.282050199	3.2E-05	-1.470652191	1.108232196	1.61	0.020666555	1.94
102-28	1530	0.282154	0.000025	0.0009337	6.2E-06	0.0390187	0.00054	1.53	0.282126018	5E-05	12.38562888	1.761264307	1.50	0.033329737	1.47
102-53	1051	0.282155	8.3E-06	0.0004491	0.00003	0.0149686	0.00045	1.05	0.282145797	1.66E-05	1.918262665	0.544876555	1.48	0.009855346	1.74
102-55	1051	0.282181	0.000013	0.00084071	0.000057	0.0262039	0.00047	1.05	0.282163773	2.6E-05	2.555479366	0.838875404	1.46	0.015233493	1.70
102-56	1051	0.282123	0.000019	0.000671523	0.000012	0.027815	0.00091	1.05	0.28210924	3.8E-05	0.622309396	1.329645922	1.53	0.024843427	1.82
102-58	1051	0.282172	9.4E-06	0.000612676	0.000017	0.0219948	0.00052	1.05	0.282159445	1.88E-05	2.402080356	0.641752045	1.46	0.011877489	1.71
102-59	1530	0.281995	8.9E-06	0.0010929	0.00004	0.0460404	0.0015	1.53	0.281962247	1.78E-05	6.573546907	0.546618589	1.72	0.010136823	1.83

Sample															$^{176}Lu/^{177}Hf$ (0.015)
Analysis	Age(Ma)	$^{176}Hf/^{177}Hf$	1σ	$^{176}Lu/^{177}Hf$	1σ	$^{176}Yb/^{177}Hf$	1σ	t(Ga)	$^{176}Hf/^{177}Hf(t)$	2σ	$\varepsilon_{Hf}(t)$	2σ	t_{DM}	2σ	Protolith age
Augen gneiss															
112-02	1504	0.281995	8.3E-06	0.00107149	0.00002	0.0510993	0.00094	1.51	0.281963357	1.66E-05	6.097467437	0.547167505	1.71	0.010235548	1.84
112-20	1504	0.28191	0.00002	0.000490355	3.8E-06	0.0277357	0.00043	1.51	0.281895519	4E-05	3.690089256	1.411524169	1.80	0.026214631	1.98
112-21	1504	0.281964	0.000031	0.000549938	9.1E-07	0.031374	0.00021	1.51	0.281947759	6.2E-05	5.543955822	2.198300655	1.73	0.04098267	1.87
112-25	1504	0.28204	0.000026	0.00144584	0.00011	0.0771915	0.0072	1.51	0.281997301	5.2E-05	7.302069584	1.61477328	1.67	0.030304976	1.76
112-33	1504	0.282025	0.000011	0.00113555	0.000028	0.059357	0.0019	1.51	0.281991465	2.2E-05	7.094948623	0.722030346	1.68	0.0135555	1.78
112-44	1504	0.281933	0.000019	0.000731902	0.000028	0.0372467	0.00056	1.51	0.281911385	3.8E-05	4.253151471	1.289825968	1.78	0.023926082	1.95
112-47	1504	0.281986	0.000012	0.00121757	0.00001	0.0663502	0.001	1.51	0.281950043	2.4E-05	5.624988905	0.830733206	1.73	0.015706641	1.87
112-50	1504	0.281984	8.1E-06	0.000809818	5.6E-06	0.0409694	0.00054	1.51	0.281960084	1.62E-05	5.981343166	0.56315534	1.72	0.01054648	1.84
112-51	1504	0.282035	0.000026	0.00102926	0.000011	0.05723	0.00014	1.51	0.282004604	5.2E-05	7.56121401	1.822279522	1.66	0.034410081	1.75
112-54	1504	0.281981	0.000019	0.00132322	0.000028	0.0683508	0.0022	1.51	0.281941923	3.8E-05	5.336830377	1.289825968	1.75	0.024352429	1.88
112-61	1504	0.281994	0.000014	0.000769034	4.9E-06	0.0396789	0.0004	1.51	0.281971289	2.8E-05	6.378957524	0.983371827	1.70	0.018429535	1.82
112-65	1504	0.282025	0.000015	0.00140679	0.00001	0.0717933	0.0017	1.51	0.281983455	3E-05	6.810686031	1.043656565	1.69	0.019876898	1.79
112-68	1504	0.281929	0.000031	0.00129323	0.000021	0.068903	0.00012	1.51	0.281890808	6.2E-05	3.522924465	2.156191559	1.81	0.040749419	1.99
112-73	1504	0.281993	7.9E-06	0.00127996	0.000067	0.0541636	0.00066	1.51	0.2819552	1.58E-05	5.808014063	0.420264659	1.73	0.007585854	1.85
Garnet-biotite gneiss															
103-01	1492	0.281982	9.8E-06	0.000929296	0.000013	0.0470609	0.00077	1.49	0.281954925	1.96E-05	5.329891852	0.668636639	1.73	0.012512581	1.87
103-06	1492	0.281935	9.5E-06	0.000894864	0.000011	0.0445956	0.00085	1.49	0.281908928	1.9E-05	3.697668258	0.651480752	1.79	0.012159239	1.97
103-07	1492	0.281944	8.8E-06	0.000690485	0.000016	0.0365096	0.00094	1.49	0.281923883	1.76E-05	4.228338241	0.591462331	1.77	0.010944054	1.93
103-09	1492	0.281973	7.9E-06	0.000854218	0.000037	0.0389971	0.00067	1.49	0.281948113	1.58E-05	5.088142135	0.484166065	1.73	0.008852906	1.88
103-14	1492	0.281979	8.1E-06	0.00079748	0.000024	0.0412267	0.0015	1.49	0.281955766	1.62E-05	5.359714848	0.525240731	1.72	0.00970681	1.87
103-16	1492	0.282024	0.00001	0.00101906	0.000039	0.0528309	0.00093	1.49	0.28199431	2E-05	6.727481909	0.629069987	1.67	0.011688896	1.78
103-19	1492	0.282003	0.000012	0.00121145	0.000027	0.0634967	0.0015	1.49	0.281967705	2.4E-05	5.783380128	0.795824961	1.71	0.014941882	1.84
103-28	1492	0.281985	8.4E-06	0.000869011	0.000031	0.0454707	0.0015	1.49	0.281959682	1.68E-05	5.498674981	0.532057987	1.72	0.009812656	1.86
103-29	1492	0.28199	9.4E-06	0.000622985	0.000036	0.0324708	0.0012	1.49	0.281971849	1.88E-05	5.930459998	0.592690487	1.70	0.010869772	1.83
103-31	1492	0.28197	0.000013	0.000918874	0.00004	0.0501856	0.0019	1.49	0.281943229	2.6E-05	4.91483999	0.839915652	1.74	0.01553085	1.89
103-33	1492	0.282023	9.4E-06	0.00120395	0.000029	0.0679016	0.0019	1.49	0.281987923	1.88E-05	6.500845405	0.60716457	1.68	0.011374411	1.80
103-34	1492	0.28199	0.00001	0.000594762	3.1E-06	0.0353015	0.00027	1.49	0.281972672	2E-05	5.959638715	0.703301354	1.70	0.013123101	1.83
103-36	1492	0.281965	0.000011	0.00092624	0.000024	0.0449402	0.00078	1.49	0.281938014	2.2E-05	4.729796728	0.731057009	1.75	0.013593149	1.90
103-37	1492	0.281971	0.000013	0.00100944	0.000058	0.0439556	0.00098	1.49	0.28194159	2.6E-05	4.856692714	0.802696583	1.74	0.014732994	1.90
103-42	1492	0.281981	0.000012	0.00103708	0.00007	0.0415025	0.0016	1.49	0.281950785	2.4E-05	5.182972392	0.706912739	1.73	0.012877218	1.88
103-44	1492	0.282028	0.000013	0.00132712	0.000028	0.0666879	0.0013	1.49	0.281989335	2.6E-05	6.55093232	0.864728365	1.68	0.01632407	1.79
103-45	1492	0.281869	0.000013	0.00112917	0.000042	0.0440842	0.0005	1.49	0.281836102	2.6E-05	1.113380637	0.8357802	1.89	0.015319141	2.12
103-46	1492	0.282052	9.7E-06	0.00147062	0.000043	0.0636318	0.0013	1.49	0.282009154	1.94E-05	7.254226538	0.599507743	1.66	0.011270002	1.75
103-47	1492	0.282	0.000022	0.00120422	0.000038	0.0568742	0.001	1.49	0.281964915	4.4E-05	5.684398262	1.482791279	1.71	0.02789029	1.85
103-49	1492	0.282016	9.1E-06	0.00139106	0.000018	0.0625734	0.00067	1.49	0.281975472	1.82E-05	6.059000334	0.608618218	1.70	0.011508151	1.82
103-50	1492	0.28201	0.000017	0.00109254	9.2E-06	0.0579278	0.00064	1.49	0.281978169	3.4E-05	6.154715739	1.187486138	1.70	0.022428189	1.82
103-52	1492	0.281958	7.4E-06	0.000982433	0.000034	0.0454196	0.0011	1.49	0.281929377	1.48E-05	4.423301905	0.454883678	1.76	0.00832396	1.92

Sample															$^{176}Lu/^{177}Hf$ (0.015)
Analysis	Age(Ma)	$^{176}Hf/^{177}Hf$	1σ	$^{176}Lu/^{177}Hf$	1σ	$^{176}Yb/^{177}Hf$	1σ	t(Ga)	$^{176}Hf/^{177}Hf(t)$	2σ	$\varepsilon_{Hf}(t)$	2σ	t_{DM}	2σ	Protolith age
Alkali feldspar granite															
106-04	1542	0.282	0.000014	0.00135359	0.000019	0.0545247	0.0016	1.54	0.281959165	2.8E-05	6.698571065	0.953031622	1.72	0.018060482	1.83
106-08	1542	0.281981	0.000012	0.0011409	0.000014	0.0537201	0.00057	1.54	0.281946581	2.4E-05	6.251982481	0.821778705	1.74	0.01548759	1.85
106-10	1542	0.282033	0.000008	0.0015634	0.000044	0.0615396	0.0022	1.54	0.281985835	1.6E-05	7.645101559	0.473619857	1.69	0.008900182	1.77
106-22	1542	0.282018	9.6E-06	0.00117377	0.00002	0.0499829	0.0011	1.54	0.28198259	1.92E-05	7.529915574	0.638579301	1.69	0.012033101	1.78
106-28	1542	0.282062	0.000011	0.00168854	0.000067	0.0670687	0.00068	1.54	0.28201106	2.2E-05	8.54032552	0.637308688	1.65	0.012048076	1.71
106-30	1542	0.282046	0.000012	0.00203101	0.000037	0.0821561	0.0021	1.54	0.281984728	2.4E-05	7.605817495	0.772528221	1.69	0.014839945	1.77
106-32	1542	0.281981	0.000014	0.0011895	0.000029	0.0482971	0.0012	1.54	0.281945115	2.8E-05	6.199948274	0.931618368	1.74	0.017501494	1.86
106-37	1542	0.282027	7.8E-06	0.00118706	0.000026	0.0471218	0.00057	1.54	0.281991189	1.56E-05	7.83509544	0.497967759	1.68	0.009354314	1.76
106-42	1542	0.282021	0.00001	0.00103396	0.00002	0.0404712	0.00066	1.54	0.281989807	2E-05	7.786074582	0.666971209	1.68	0.012532524	1.76
106-45	1542	0.281892	0.000012	0.000730472	0.000012	0.0292636	0.00017	1.54	0.281869963	2.4E-05	3.532812586	0.826061356	1.84	0.01534905	2.02
106-47	1542	0.282009	8.1E-06	0.00135724	0.000041	0.0553056	0.0013	1.54	0.281968055	1.62E-05	7.014072118	0.48714181	1.71	0.009090988	1.81
106-49	1542	0.28198	9.9E-06	0.00129404	0.000012	0.0522075	0.0011	1.54	0.281940961	1.98E-05	6.052531311	0.677003835	1.75	0.012805504	1.86
106-51	1542	0.281993	9.9E-06	0.00150908	0.000068	0.0585283	0.0021	1.54	0.281947474	1.98E-05	6.283664522	0.557089614	1.74	0.010276695	1.85
106-55	1542	0.282008	7.3E-06	0.00141063	0.000016	0.0554595	0.001	1.54	0.281965444	1.46E-05	6.921419552	0.483891127	1.71	0.009159711	1.81
106-59	1542	0.281958	0.00001	0.00116945	0.000062	0.0456233	0.0016	1.54	0.28192272	2E-05	5.405147686	0.577035544	1.77	0.010535143	1.90
106-60	1542	0.282002	8.8E-06	0.00157858	0.000018	0.0637314	0.001	1.54	0.281954377	1.76E-05	6.528662438	0.586078134	1.73	0.011139093	1.84
106-62	1542	0.281983	0.000011	0.00144117	0.000027	0.0577922	0.0011	1.54	0.281939523	2.2E-05	6.001474367	0.722961704	1.75	0.013642309	1.87
106-63	1542	0.281948	9.2E-06	0.000920511	7.1E-06	0.038984	0.00045	1.54	0.28192023	1.84E-05	5.316778527	0.637810489	1.77	0.011957796	1.91
106-66	1542	0.281989	8.5E-06	0.000989769	0.000016	0.0401083	0.00048	1.54	0.281959141	1.7E-05	6.69771189	0.569066853	1.72	0.010659579	1.83
106-68	1542	0.281986	0.000012	0.000873365	0.000009	0.0364402	0.00021	1.54	0.281959652	2.4E-05	6.715871652	0.832485332	1.72	0.015616914	1.82
106-71	1542	0.282043	9.6E-06	0.00150076	0.000022	0.0583521	0.0017	1.54	0.281997725	1.92E-05	8.067066728	0.63429665	1.67	0.012065002	1.74
106-75	1542	0.282085	0.000013	0.00191551	0.00012	0.0781697	0.0058	1.54	0.282027213	2.6E-05	9.113584584	0.665777987	1.63	0.01256965	1.68
106-76	1542	0.282011	6.2E-06	0.00153418	0.00005	0.0649796	0.0024	1.54	0.281964717	1.24E-05	6.895608834	0.333008316	1.71	0.006134864	1.81
106-77	1542	0.281916	9.9E-06	0.00132432	0.000063	0.0464629	0.00098	1.54	0.281876048	1.98E-05	3.74875895	0.567796241	1.83	0.010275951	2.00
106-78	1542	0.281953	0.000011	0.0011004	0.00007	0.0418089	0.0017	1.54	0.281919803	2.2E-05	5.301627516	0.630884712	1.77	0.011473586	1.91
106-80	1542	0.282002	0.000011	0.0013634	0.0001	0.0474353	0.0021	1.54	0.281960869	2.2E-05	6.759047635	0.566644951	1.72	0.010294006	1.82
106-81	1542	0.281902	9.9E-06	0.00134394	0.000088	0.045557	0.0017	1.54	0.281861456	1.98E-05	3.230894146	0.514263107	1.85	0.009012165	2.03
Fine-grained granite															
EPB-04-03	1503	0.281959	0.000012	0.00101355	0.000048	0.041524	0.0011	1.50	0.281929168	2.4E-05	4.76712057	0.751413997	1.76	0.013833437	1.91
EPB-04-08	1503	0.282045	9.3E-06	0.00119581	0.000054	0.054749	0.0011	1.50	0.282009804	1.86E-05	7.628620555	0.547251534	1.65	0.010168219	1.74
EPB-04-13	1503	0.281997	0.000013	0.00107607	0.000031	0.0449096	0.0011	1.50	0.281965328	2.6E-05	6.050318898	0.857899722	1.71	0.016045438	1.84
EPB-04-18	1503	0.281975	0.000012	0.00118759	0.000023	0.056363	0.00071	1.50	0.281940046	2.4E-05	5.153129357	0.803637678	1.75	0.015081295	1.89
EPB-04-24	1503	0.282171	0.000015	0.00157347	0.000059	0.0552504	0.0017	1.50	0.282124688	3E-05	11.70550284	0.941356443	1.50	0.018105874	1.49
EPB-04-26	1503	0.282096	0.000013	0.00172695	0.000021	0.0846323	0.0014	1.50	0.282045171	2.6E-05	8.883686199	0.878789194	1.61	0.016887904	1.67
EPB-04-27	1503	0.281942	9.8E-06	0.00108155	0.000052	0.0425481	0.00092	1.50	0.281910167	1.96E-05	4.092820577	0.586916239	1.79	0.010682762	1.95
EPB-04-31	1503	0.281949	0.000019	0.00116518	0.000084	0.04407	0.0014	1.50	0.281914706	3.8E-05	4.253878925	1.173027251	1.78	0.021543575	1.94

Sample															$^{176}Lu/^{177}Hf$ (0.015)
Analysis	Age(Ma)	$^{176}Hf/^{177}Hf$	1σ	$^{176}Lu/^{177}Hf$	1σ	$^{176}Yb/^{177}Hf$	1σ	t(Ga)	$^{176}Hf/^{177}Hf(t)$	2σ	$\varepsilon_{Hf}(t)$	2σ	t_{DM}	2σ	Protolith age
Fine-grained granite (continued)															
EPB-04-33	1503	0.282033	9.9E-06	0.00114139	0.000029	0.0509282	0.0005	1.50	0.281999406	1.98E-05	7.259619078	0.642059388	1.67	0.012044159	1.76
EPB-04-36	1503	0.281967	0.000017	0.00117276	0.000029	0.0484727	0.0015	1.50	0.281932482	3.4E-05	4.884724413	1.145972105	1.76	0.021505051	1.91
EPB-04-38	1503	0.281979	0.000015	0.00166769	0.00011	0.0590807	0.0017	1.50	0.281929915	3E-05	4.793624817	0.834820134	1.76	0.015209305	1.91
EPB-04-39	1503	0.281982	0.000011	0.00104313	0.000036	0.0477296	0.0019	1.50	0.281951298	2.2E-05	5.552421694	0.705507742	1.73	0.013100893	1.87
EPB-04-42	1503	0.282009	0.000012	0.00100222	0.000026	0.0436341	0.0011	1.50	0.281979502	2.4E-05	6.553295007	0.797370836	1.69	0.014920845	1.81
EPB-04-43	1503	0.28197	0.000012	0.0011341	0.000014	0.0484466	0.0007	1.50	0.28193662	2.4E-05	5.031564196	0.822438203	1.75	0.015475006	1.90
EPB-04-49	1503	0.28197	0.000016	0.00144067	0.000032	0.0613756	0.0012	1.50	0.281927597	3.2E-05	4.711359919	1.068731641	1.77	0.020154933	1.92
EPB-04-53	1503	0.282013	0.000011	0.00139089	0.000013	0.0600235	0.0011	1.50	0.281972062	2.2E-05	6.289286689	0.753553528	1.70	0.014305617	1.82
EPB-04-54	1503	0.281991	6.6E-06	0.00131997	0.000011	0.0558186	0.00078	1.50	0.28195215	1.32E-05	5.582650916	0.445447486	1.73	0.00841105	1.86
EPB-04-56	1503	0.282029	0.000014	0.000777608	0.000012	0.0320469	0.0011	1.50	0.282006113	2.8E-05	7.497632536	0.968563342	1.66	0.01814535	1.75
EPB-04-61	1503	0.281962	0.00001	0.000765468	6.5E-06	0.0309465	0.00053	1.50	0.28193947	2E-05	5.132696107	0.696158063	1.74	0.013011371	1.89
EPB-04-62	1503	0.282101	0.000011	0.000912839	0.000037	0.0346624	0.00099	1.50	0.282074133	2.2E-05	9.911437717	0.703418794	1.57	0.013214426	1.60
EPB-04-63	1503	0.28198	8.3E-06	0.00110315	0.000037	0.0477737	0.0017	1.50	0.281947531	1.66E-05	5.418758765	0.511790015	1.74	0.009446375	1.87
EPB-04-67	1503	0.281979	0.000014	0.00111806	0.00005	0.0446431	0.0021	1.50	0.281946092	2.8E-05	5.367698852	0.889183346	1.74	0.016497524	1.88
EPB-04-71	1503	0.28196	0.000016	0.000711252	6.4E-06	0.0317644	0.00085	1.50	0.281939066	3.2E-05	5.118349667	1.12220869	1.75	0.020968642	1.89
EPB-04-75	1503	0.282082	9.2E-06	0.00158642	0.000041	0.0634103	0.00077	1.50	0.282035307	1.84E-05	8.533650722	0.567310486	1.62	0.010760941	1.69
EPB-04-82	1503	0.281998	0.000014	0.00113606	0.000043	0.0454907	0.0015	1.50	0.281964563	2.8E-05	6.023147736	0.903805977	1.71	0.016865756	1.84
EPB-04-83	1503	0.282054	0.000015	0.00153539	0.000059	0.0625182	0.0008	1.50	0.282008809	3E-05	7.593319503	0.941356443	1.66	0.017780161	1.74
Coarse-grained granite															
EPB-05-01	1537	0.281866	0.000019	0.00346215	0.000069	0.10184	0.0017	1.55	0.281761209	3.8E-05	-0.209709653	1.200391372	2.01	0.023150231	2.24
EPB-05-02	1537	0.281993	0.000011	0.00188193	0.000099	0.0624145	0.0019	1.55	0.281936039	2.2E-05	5.995036557	0.568094335	1.75	0.010380644	1.87
EPB-05-05	1537	0.282033	0.00002	0.00222001	0.00013	0.0749131	0.002	1.55	0.281965806	4E-05	7.051481889	1.140319144	1.72	0.021563836	1.81
EPB-05-07	1537	0.281917	0.000015	0.00242043	0.000081	0.115322	0.0043	1.55	0.28184374	3E-05	2.719315034	0.890688075	1.89	0.016618617	2.07
EPB-05-08	1537	0.281921	0.000012	0.00180459	0.000094	0.0649645	0.00074	1.55	0.28186638	2.4E-05	3.522813745	0.649816973	1.85	0.011695669	2.02
EPB-05-14	1591	0.282034	0.000024	0.00348774	0.0002	0.142178	0.004	1.59	0.281925243	4.8E-05	6.69084026	1.260998472	1.78	0.024275643	1.87
EPB-05-15	1537	0.28195	0.000018	0.00152438	0.000038	0.0649093	0.0025	1.55	0.281903861	3.6E-05	4.853035063	1.196011388	1.80	0.022581918	1.94
EPB-05-16	1537	0.281999	0.000017	0.00243926	0.00017	0.083056	0.0031	1.55	0.28192517	3.4E-05	5.60929251	0.841441052	1.77	0.015354302	1.90
EPB-05-17	1537	0.281896	0.000013	0.00156075	0.000081	0.0559087	0.0011	1.55	0.28184876	2.6E-05	2.897489995	0.748726868	1.87	0.013562267	2.06
EPB-05-20	1537	0.28197	0.000014	0.00147287	0.000078	0.0645119	0.0033	1.55	0.28192542	2.8E-05	5.618173318	0.826152693	1.77	0.015281337	1.89
EPB-05-26	1537	0.281994	0.00002	0.0017905	0.0001	0.0669342	0.0012	1.55	0.281939806	4E-05	6.128741287	1.204771356	1.75	0.022601537	1.86
EPB-05-28	1537	0.282016	0.000016	0.00146008	0.000064	0.065486	0.0018	1.55	0.281971807	3.2E-05	7.264466254	0.998191598	1.70	0.01877617	1.80
EPB-05-32	1537	0.281899	0.000024	0.00160723	0.000043	0.0541911	0.0015	1.55	0.281850353	4.8E-05	2.954031919	1.611152972	1.87	0.030409325	2.05
EPB-05-33	1537	0.281925	0.000017	0.00224689	0.00017	0.0872126	0.0032	1.55	0.281856992	3.4E-05	3.189654728	0.841441052	1.87	0.014810238	2.04
EPB-05-34	1537	0.281974	0.000009	0.00151522	0.000024	0.0664535	0.001	1.55	0.281928138	1.8E-05	5.714642005	0.587263659	1.76	0.011083035	1.89
EPB-05-35	1537	0.281919	0.000012	0.00168266	0.000098	0.0612644	0.0016	1.55	0.28186807	2.4E-05	3.582810778	0.641223345	1.85	0.011467833	2.02
EPB-05-36	1537	0.281873	0.000026	0.00582698	0.00029	0.222749	0.0064	1.55	0.281696632	5.2E-05	-2.501586286	1.222457632	2.15	0.020766983	2.38
EPB-05-37	1537	0.282015	0.000011	0.0025762	0.000035	0.12243	0.001	1.55	0.281937025	2.2E-05	6.030035904	0.705592387	1.76	0.013675662	1.87
EPB-05-40	1537	0.281983	0.000011	0.0011784	0.000066	0.0458517	0.001	1.55	0.281947333	2.2E-05	6.395867954	0.638991768	1.74	0.011758975	1.85
EPB-05-41	1537	0.281986	0.000014	0.00183813	0.00011	0.0611188	0.0018	1.55	0.281930364	2.8E-05	5.793654561	0.757403667	1.76	0.013919676	1.88
EPB-05-42	1591	0.282003	0.000011	0.00166313	0.000088	0.0638832	0.0015	1.59	0.281951139	2.2E-05	7.609999258	0.586074161	1.73	0.010899541	1.81

Sample															$^{176}Lu/^{177}Hf$ (0.015)
Analysis	Age(Ma)	$^{176}Hf/^{177}Hf$	1σ	$^{176}Lu/^{177}Hf$	1σ	$^{176}Yb/^{177}Hf$	1σ	t(Ga)	$^{176}Hf/^{177}Hf(t)$	2σ	$\varepsilon_{Hf}(t)$	2σ	t_{DM}	2σ	Protolith age
Coarse-grained granite (continued)															
EPB-05-44	1591	0.281944	9.7E-06	0.00142357	0.000034	0.0618924	0.0011	1.59	0.281899609	1.94E-05	5.780990499	0.613323746	1.80	0.011489784	1.92
EPB-05-50	1537	0.281973	0.000019	0.00226236	0.00011	0.0716295	0.0014	1.55	0.281904524	3.8E-05	4.876571275	1.112306682	1.80	0.020856574	1.94
EPB-05-51	1537	0.282022	0.000012	0.00185387	0.0001	0.0842592	0.0063	1.55	0.281965888	2.4E-05	7.054397454	0.636926531	1.71	0.011813261	1.81
EPB-05-52	1537	0.281967	0.000012	0.00168576	0.000046	0.0673758	0.0006	1.55	0.281915976	2.4E-05	5.283015223	0.752940513	1.78	0.014149593	1.91
EPB-05-54	1537	0.281985	0.000014	0.00256656	0.00029	0.0992751	0.0082	1.55	0.281907317	2.8E-05	4.975682178	0.370690394	1.80	0.00520089	1.93
EPB-05-55	1537	0.282021	0.000012	0.00166152	0.000025	0.0675684	0.0018	1.55	0.28197071	2.4E-05	7.225530202	0.798057061	1.71	0.015220934	1.80
EPB-05-58	1537	0.282013	0.000014	0.00151661	0.00009	0.0554557	0.0019	1.55	0.281967096	2.8E-05	7.097270623	0.800371808	1.71	0.014884046	1.81
EPB-05-62	1537	0.281944	8.7E-06	0.00175542	0.000059	0.0666876	0.0024	1.55	0.281890868	1.74E-05	4.391909269	0.49077523	1.82	0.008989471	1.97
EPB-05-68	1537	0.281996	0.000012	0.00197251	0.000057	0.0811731	0.0027	1.55	0.281936297	2.4E-05	6.004206105	0.729308035	1.76	0.013776446	1.87
EPB-05-72	1537	0.28195	0.000009	0.000971736	0.000024	0.036645	0.00094	1.55	0.281920588	1.8E-05	5.446687201	0.587263659	1.77	0.010916317	1.91
EPB-05-76	1537	0.28196	9.2E-06	0.00159124	0.00011	0.0539536	0.0022	1.55	0.281911837	1.84E-05	5.13611683	0.416696771	1.79	0.007242593	1.92
EPB-05-79	1537	0.281999	0.000013	0.00242705	0.000065	0.101475	0.0025	1.55	0.281925539	2.6E-05	5.622408536	0.783101382	1.77	0.01491678	1.89
EPB-05-81	1537	0.281975	0.000014	0.00186445	0.000083	0.0719928	0.004	1.55	0.281918568	2.8E-05	5.374988206	0.815410657	1.78	0.015175408	1.91
Tonalitic gneiss															
101-08	1495	0.281959	0.000013	0.00102347	0.000051	0.0371687	0.00058	1.50	0.281928978	2.6E-05	4.6432796	0.816470782	1.76	0.015034297	1.92
101-10	1495	0.281984	0.000011	0.00116352	0.000036	0.0452038	0.0014	1.50	0.28194987	2.2E-05	5.384656359	0.705753289	1.73	0.013139775	1.87
101-15	1495	0.281923	0.000017	0.00144849	0.000052	0.0554509	0.0024	1.50	0.281880511	3.4E-05	2.923350592	1.098280075	1.83	0.020448077	2.02
101-18	1495	0.281947	0.000021	0.00115914	0.000053	0.0432295	0.0008	1.50	0.281912998	4.2E-05	4.076219019	1.380089368	1.78	0.025691406	1.95
101-22	1495	0.281983	0.000018	0.000678825	7.8E-06	0.0278045	0.00066	1.50	0.281963088	3.6E-05	5.853706601	1.261271639	1.71	0.023561879	1.84
101-28	1495	0.282033	0.000017	0.00119828	0.000074	0.0410006	0.0021	1.50	0.28199785	3.4E-05	7.087306801	1.052478876	1.67	0.019616324	1.77
101-29	1495	0.281932	0.000017	0.00109299	0.000066	0.0335145	0.0012	1.50	0.281899939	3.4E-05	3.612781022	1.069133857	1.80	0.019635453	1.98
101-30	1495	0.281946	0.000015	0.00119717	0.000056	0.035529	0.00098	1.50	0.281910883	3E-05	4.001145814	0.948007001	1.79	0.017510525	1.96
101-32	1495	0.28196	0.000011	0.000924809	0.000056	0.0393067	0.0028	1.50	0.281932872	2.2E-05	4.781465816	0.664115836	1.75	0.012104236	1.91
101-33	1495	0.281944	0.000016	0.00076073	0.000018	0.0293944	0.0012	1.50	0.281921685	3.2E-05	4.384479278	1.098090954	1.77	0.020440784	1.93
101-34	1495	0.282003	0.000013	0.0009005	0.000036	0.0382597	0.0013	1.50	0.281976585	2.6E-05	6.332684953	0.847698872	1.70	0.015764068	1.82
101-35	1495	0.281985	0.000014	0.00150702	0.00016	0.0552882	0.0065	1.50	0.281940794	2.8E-05	5.062581122	0.660519452	1.75	0.011503331	1.89
101-37	1495	0.282011	0.000013	0.000907901	0.000047	0.0266593	0.00069	1.50	0.281984368	2.6E-05	6.608872148	0.824798273	1.69	0.015289727	1.80
101-38	1495	0.281989	0.000013	0.00145187	0.000047	0.0616214	0.0017	1.50	0.281946412	2.6E-05	5.261934344	0.824798273	1.74	0.015429402	1.88
101-40	1495	0.281935	0.000015	0.00119008	0.000038	0.0419978	0.00089	1.50	0.281900091	3E-05	3.6181757	0.985480709	1.80	0.018344033	1.98
101-43	1495	0.282012	0.000013	0.00133009	0.000091	0.0444227	0.0013	1.50	0.281972984	2.6E-05	6.204886672	0.733195875	1.70	0.013434289	1.82
101-45	1495	0.281937	0.000025	0.00113262	0.000068	0.043093	0.0028	1.50	0.281903776	5E-05	3.748960693	1.632752443	1.80	0.030290118	1.97
101-45	1495	0.281939	0.000011	0.00109899	0.000075	0.0398153	0.002	1.50	0.281906763	2.2E-05	3.854940174	0.624560255	1.79	0.011196957	1.96
101-49	1495	0.282065	0.000019	0.00146266	0.000065	0.0598202	0.003	1.50	0.282022095	3.8E-05	7.947668714	1.213161313	1.64	0.022940953	1.72
101-52	1495	0.281976	0.000014	0.000793915	0.000018	0.0340658	0.001	1.50	0.281952712	2.8E-05	5.485500468	0.956145372	1.73	0.017831729	1.87
101-53	1495	0.281943	8.2E-06	0.000815286	0.000012	0.032793	0.0012	1.50	0.281919085	1.64E-05	4.292203559	0.556994417	1.77	0.010363465	1.94
101-54	1495	0.282003	0.000017	0.000957605	0.000077	0.042737	0.0035	1.50	0.28197491	3.4E-05	6.273242283	1.046233258	1.70	0.019285818	1.82
101-58	1495	0.281973	0.000017	0.000910503	0.000034	0.0353685	0.00098	1.50	0.281946292	3.4E-05	5.257680595	1.135753783	1.74	0.021148227	1.88
101-72	1495	0.281971	0.000019	0.00153085	0.000075	0.0689664	0.0034	1.50	0.281926095	3.8E-05	4.540966069	1.192342586	1.77	0.022219039	1.92
101-74	1495	0.282017	9.4E-06	0.000606221	0.000028	0.0257012	0.0016	1.50	0.281999217	1.88E-05	7.135820197	0.608851804	1.66	0.011256194	1.77
101-78	1495	0.281934	8.1E-06	0.00112595	0.000037	0.0481396	0.0016	1.50	0.281900972	1.62E-05	3.649444551	0.497850321	1.80	0.00911021	1.98

Ages: LA-MC-ICPMS U-Pb ages from the present study

8.6 Whole-rock Pb isotope data

Table 6. Whole-rock Pb isotope data

Sample	$^{206}Pb/^{204}Pb$	$^{207}Pb/^{204}Pb$	$^{208}Pb/^{204}Pb$
101-23-10	18.9257	15.6124	39.2967
102-23-10	17.2819	15.4873	36.9009
103-23-10	19.7573	15.7149	39.3976
105-23-10	19.3578	15.6769	39.2795
106-23-10	25.3106	16.2181	42.7189
112-23-10	29.5864	16.414	38.615
EPB-06-04	20.3783	15.7737	40.4107
EPB-06-05	24.2591	16.0743	42.4075
EPB-06-06	25.4773	16.2192	45.9115